Thesis for the Master's degree in chemistry

Lianglin Qi

Supramolecular synthesis of porous crystalline networks from DNA-based building units

60 study points

DEPARTMENT OF CHEMISTRY
Faculty of mathematics and natural sciences

UNIVERSITY OF OSLO 05/2015

Acknowledgements

To my supervisor, Professor Carl Henrik Gørbitz, thank you for your continuous feedback and constant availability. I greatly appreciate the skills and knowledge I have learnt from you, and your guidance throughout this project.

To my co-supervisor, Professor Lise-Lotte Gundersen, thank you so much for all your advice and suggestions for the whole year of organic synthesis task.

To Håkon Gulbrandsen, thank you for providing me help in the lab, teaching me the microwave reaction and taking time to give comments on my writing.

To Thomas Aarhus, thank you for helping me a lot when I first got started.

To Martin Hennum, thank you a lot for your aid with my laboratory work and all tips for solving problems. I got to know many new things from you.

To Britt and Jakob, thank you for all your help with the laboratory routines.

To Kim Fredriksen, it was so nice to have those conversations and leisure time with you. I missed the open-air barbecue.

To Tushar, Ngan and Jan, thank you for all the enjoyable moments and for your company when working late.

Thanks to Frode Rise and Dirk Petersen for the help related to NMR experiments. Thank you for your patience and friendliness.

Thanks to Osamu Sekiguchi for running the MS service.

Thanks to everyone I met here. It has been a special and amazing experience to work and live here.

Finally, I would like to thank my family for their understanding and support. I would not be where I am, if not for you. I miss all of you.

Lianglin Qi

Oslo, May 2015

Abstract

Porous organic networks, prepared by supramolecular assembly of carefully selected building units, have potential biological applications as drug carrier, molecular sensors and more. In these materials two types of molecules, called nodes and linkers, are connected by hydrogen bonds to form open 3-dimensional networks.

In the current project the selection of linker and node compounds was inspired by hydrogen bonding between the DNA nucleobases adenine and thymine. Linkers with an aliphatic chain of variable length (I) and node molecules derived from tetraphenylmethane (II) were successfully synthesized. Synthesis of other node compounds derived from adamantane (III) and tetraethylmethane (IV) proved to be challenging.

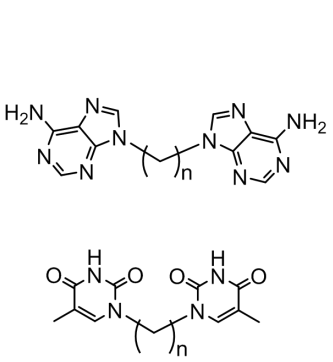

I

n = 2 or 3

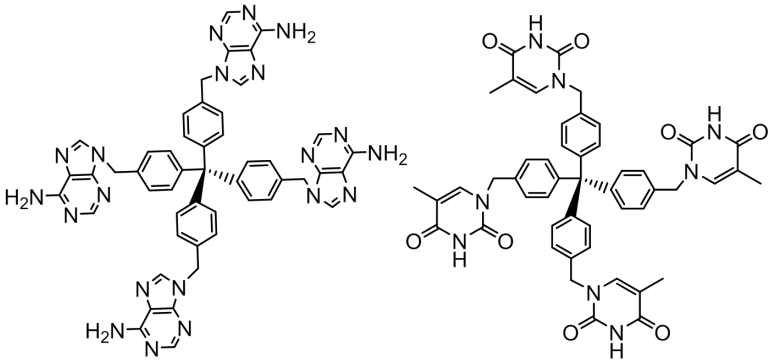

II

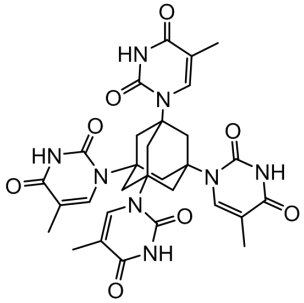

III

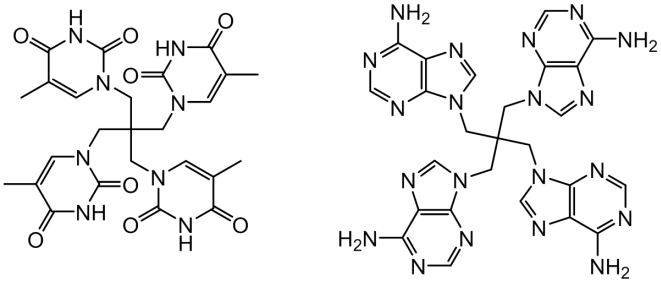

IV

X-ray diffraction data were collected for three different types of crystals. 9,9'-dimethylene-bis(adenine) was obtained as a remarkably stable tetrahexafluoro-2-propanol solvate. Two modifications of tetrakis(4-thyminylmethylphenyl)methane,

grown with methanol or 2-propanol as precipitating solvent in vapor diffusion experiments, also have exceptionally high solvent content for a molecular crystal, with either 2-dimensional or 3-dimensional solvent regions calculated to account for 35 or 47 % of the unit cell volume. Both types of crystals decayed instantly when removed from the mother liquor, and had to be flash frozen in liquid nitrogen before being transferred to the X-ray diffractometer. In the crystals investigated hydrogen bonds are formed between adenine moieties (linker molecule) or thymine moieties (node molecules). The intended formation of interactions between adenine and thymine in a co-crystallized linker-node complex did not take place, probably due to a mismatch in the solubilities of the linker and node substances in various solvents.

Abbreviations and acronyms

1. General

A	Adenine
Aq.	Aqueous
COSY	Correlation spectroscopy
COF	Covalent organic framework
d	dublet (NMR)
DCM	Dichloromethane
DMF	Dimethylformamide
DMSO	Dimethyl sulfoxide
DNA	Deoxyribonucleic acid
EI	Electron impact
ESI	Electrospray mass
Et_3N	Triethylamine
EtOAc	Ethyl acetate
h	hour(s)
HFP	1,1,1,3,3,3-Hexafluoro-2-propanol
HMBC	Heteronuclear multiple bond correlation experiment
HRMS	High resolution mass spectrometry
HSQC	Heteronuclear single-quantum coherence
Hz	Hertz
IPA	Iso-propanol
J	Coupling constant (NMR)
m	multiplet (NMR)
M^+	Molecular ion peak (MS)
Me	Methyl
MEK	Methyl ethyl ketone
MHz	Megahertz
MOF	Metal-organic framework
MS	Mass spectrometry
M.p.	Melting point
m/z	Mass to charge ratio
Ph	**r. t.**
PXRD	Phenyl

Hertz

Iso-propanol

J

Coupling constant (NMR)

m

multiplet (NMR)

M^+

Molecular ion peak (MS)

Me

MEK

Methyl

Methyl ethyl ketone

MHz

MOF

Megahertz

Metal-organic framework

MS

Mass spectrometry

M.p.

Melting point

m/z

Mass to charge ratio

Ph

PXRD

r. t.

Phenyl

Powder X-ray diffraction

Room temperature

s

singlet (NMR)

sat.

Saturated

t

Temp.

T

triplet (NMR)

Thymine

Temperature

TFA

Triflouroacetic acid

TLC

Thin layer chromatography

XRD

X-ray diffractions

2. For this project

AdC2Ad

9,9’-Dimethylene-bis(adenine)

AdC3Ad

9,9’-Trimethylene-bis(adenine)

ThC2Th

1,1’- Bimethylene-bis(thymine)

ThC3Th

1,1’- Trimethylene-bis(thymine)

Th4

Tetrakis(4-thyminylmethylphenyl)methane

Ad4

Tetrakis(4-adeninylmethylphenyl)methane

CONTENTS

Part I

Introduction

1. Supramolecular materials

Supramolecular chemistry is a branch of chemistry describing chemical systems generated from a number of self-assembled molecular components. [1] Supermolecule is the complex of molecules held together by noncovalent bonds under control of thermodynamics, molecular environment and solvent influence using one or more types of functional building units. [2-4] Supramolecular assemblies utilize the weak and reversible noncovalent interactions, including hydrogen bonding, metal coordination, dipole-dipole interactions, van der Waals forces, π-π interplay and electrostatic interaction, while traditional chemistry mainly focuses on formation of covalent bonds.[1, 2]

The primary building units used to construct the molecular framework are the nodes serving as joint points and the linkers connecting them. The linkers may be linear, while the nodes have planar or three-dimensional configurations. The composite unit of linker and node molecules is a secondary building unit (**Figure 1**).

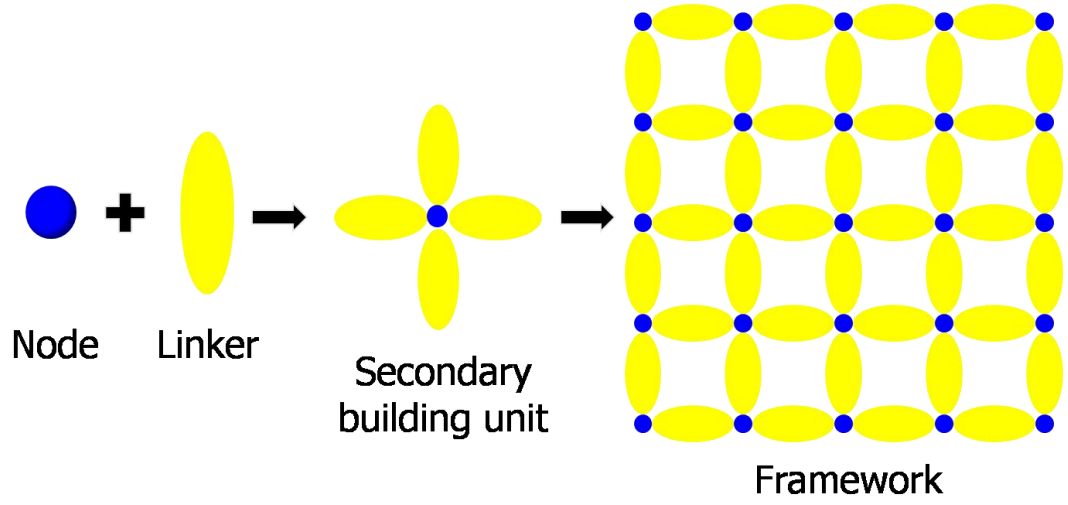

Figure 1: A general construction of framework from node and linker materials.

Commonly used linkers are functionalized polyether chains, biphenyls or triphenyls, and simple alkyl chains.[5] Well studied nodes are metal ions or clusters of metal ions and 3D organic materials as shown in **Figure 2**.

2. Crystal engineering

The aim of crystal engineering is the design and synthesis of new solids with desired physical and chemical properties, based on the understanding of intermolecular interactions in the context of crystal packing.[6] Unlike the traditional organic chemistry, which concerns the formation and cleavage of covalent bonds, crystal engineering focuses on hydrogen bonding and coordination complexation of networks. An important step forward in the understanding of the organization of molecular crystals is to introduce a concept called the supramolecular synthon defined as a structural unit within a supermolecule that can be formed and/or assembled by known or conceivable synthetic operations involving intermolecular interactions (**Figure 3, 4**).[7-9]

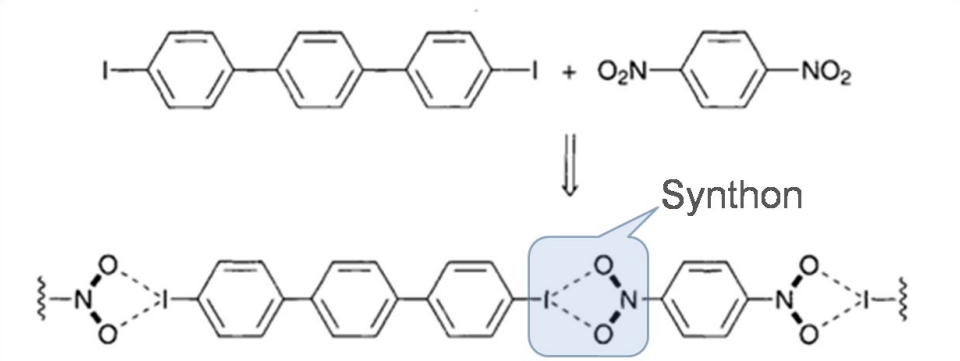

Figure 3: An example of supramolecular synthon. The synthon duplicates to form a chain of starting materials.[9]

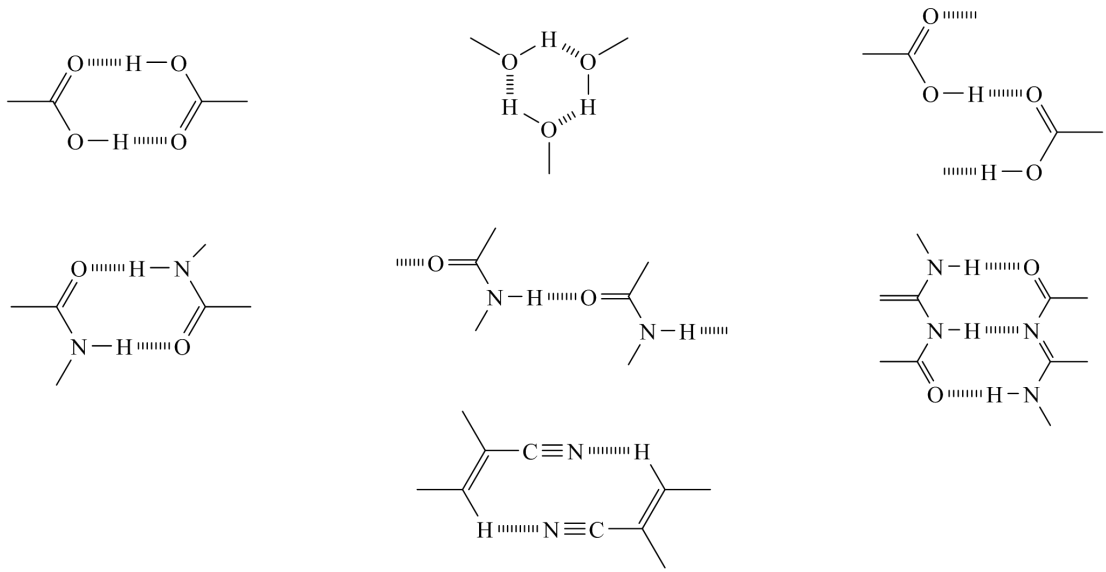

Figure 4: Examples of some common supramolecular synthons found in organic and biological systems. A synthon can be formed through single or multiple hydrogen bonds.

Synthons recur in several crystal structures and can be regarded to play the same role as functional groups do in traditional organic synthesis (**Figure 5**). Recognition of supramolecular synthons is based on the determination of specific intermolecular interactions like hydrogen or halogen bonds, stacking interactions and so on. Hence they provide a degree of predictability when constructing crystals.

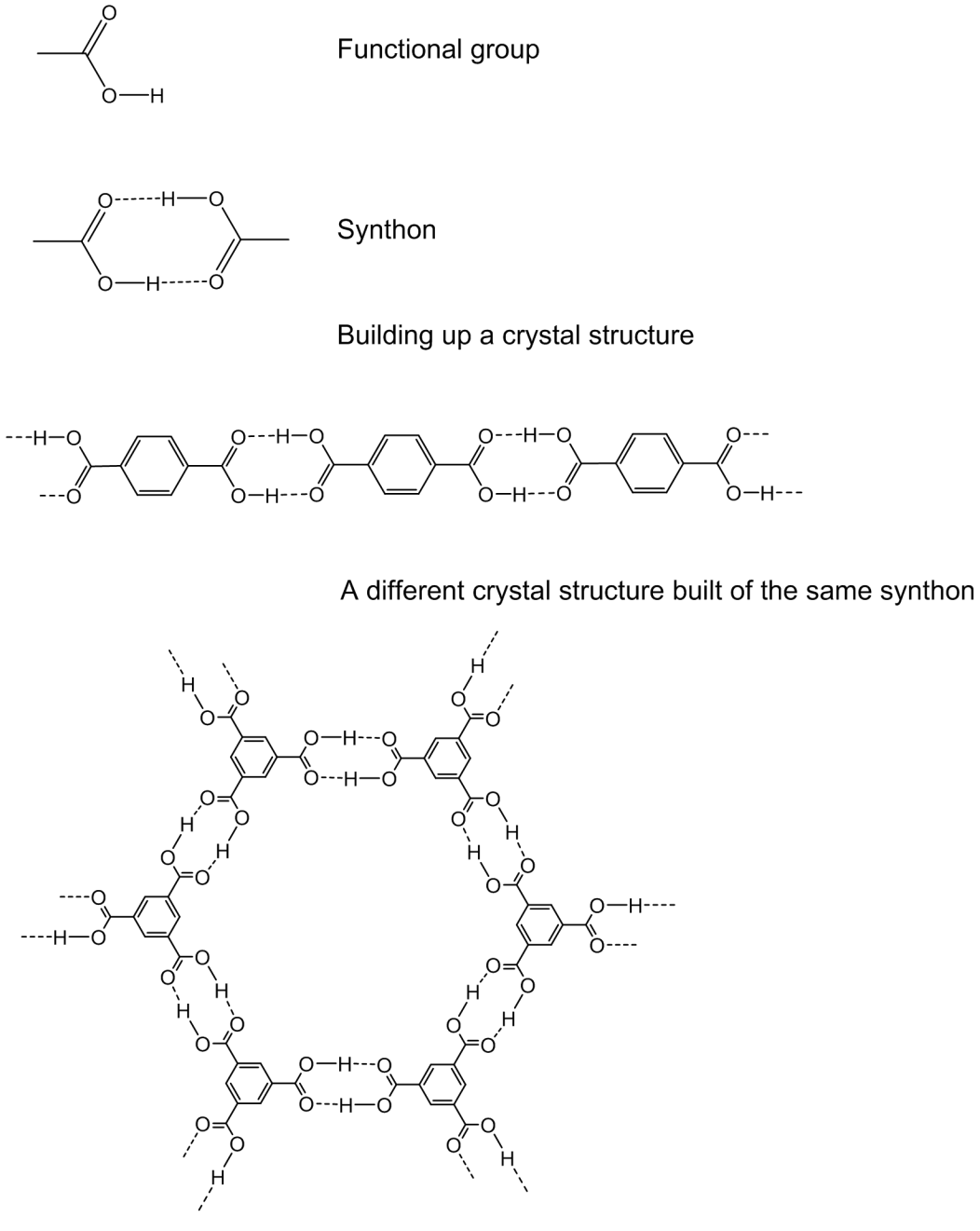

Figure 5: Self-assembly of supramolecular synthons via hydrogen bonds.
[10] Based on a synthon, different crystal structures can be designed.[8]

During the past two decades, supramolecular chemistry and crystal engineering have made significant achievements in areas of catalysis,[11] separation,[12] pharmaceutics, [13] and energy storage. [14] Nowadays, the study of supramolecular chemistry and crystal engineering contributes to both structural and functional materials and helps to understand many biological processes. In turn, biological systems often serve to inspire the effort.[10] The success of crystal engineering relays on the synthesis, crystallization, crystal structure analysis, and computational methods.[15]

3. Porous organic networks

A porous organic framework consists of numerous building units assembling to form a periodic and uniform pore structure leading to unique physical and chemical properties.[16] For such a porous framework, the pore size is the most important parameter. Hence, organic porous materials have attracted considerable attention due to their adjustable pore sizes and stabilities, which ultimately depends on the structures and nature of the linker and node compounds. For instance, the length of phenyl ring systems or carbon chains in the linker molecules determine the pore sizes when forming distinct frameworks (**Figure 6**). [17]

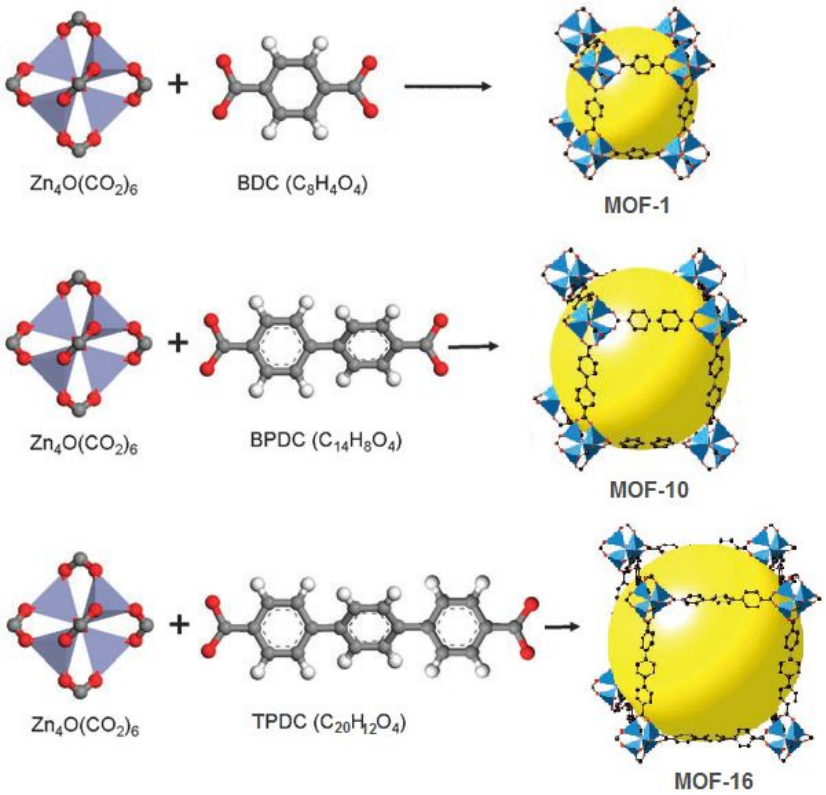

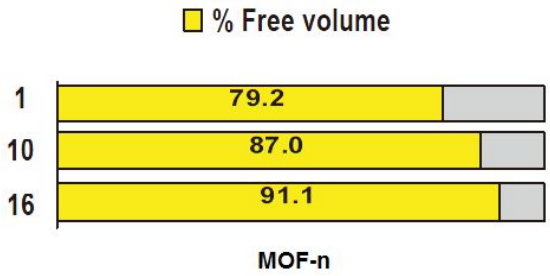

Figure 6: A series of metal-organic frameworks (MOFs). Blue polyhedral: metal cluster; gray spheres: C; red spheres: O; white spheres: H; large yellow spheres: pore space. Longer linker material gives larger free volume. [18, 19]

3.1. Classification of porous network

Based on the composition and interaction of building units, porous organic frameworks can be mainly classified into three classes: covalent organic frameworks (COFs), [20-22] metal–organic frameworks (MOFs), [23-25]and hydrogen-bonded organic frameworks. [26, 27]

COFs are constructed by formation of covalent bonds between starting materials containing only light elements (H, B, C, N, and O), such as COF-1 (**Figure 7**).[28-31]

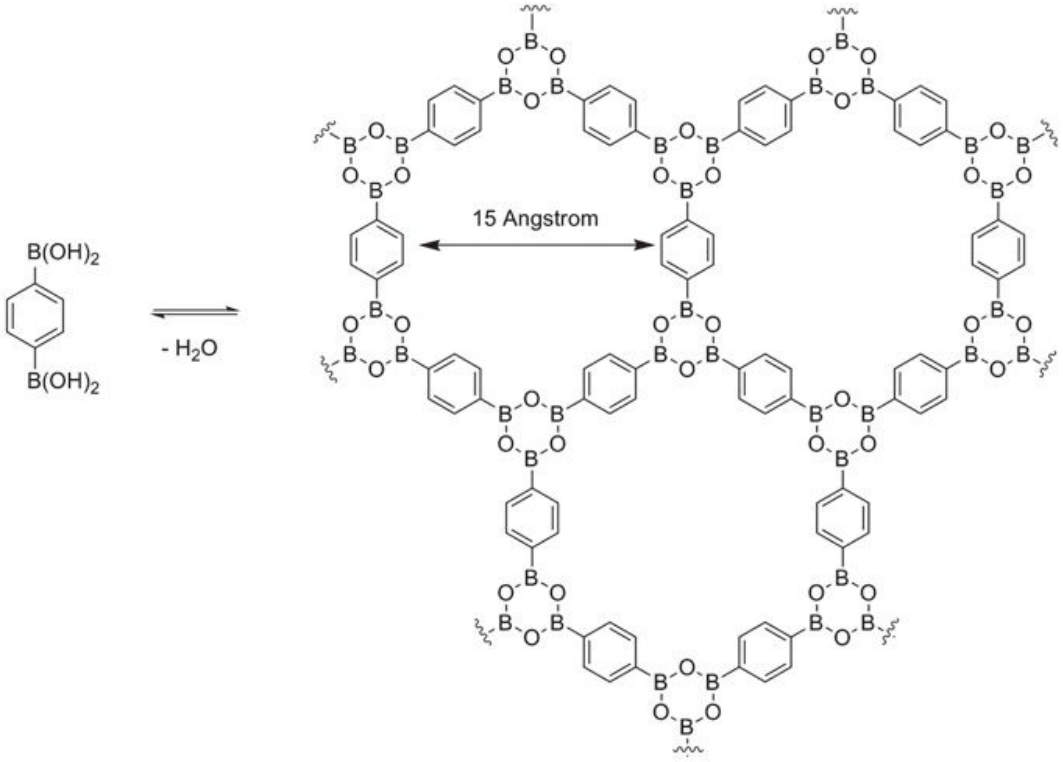

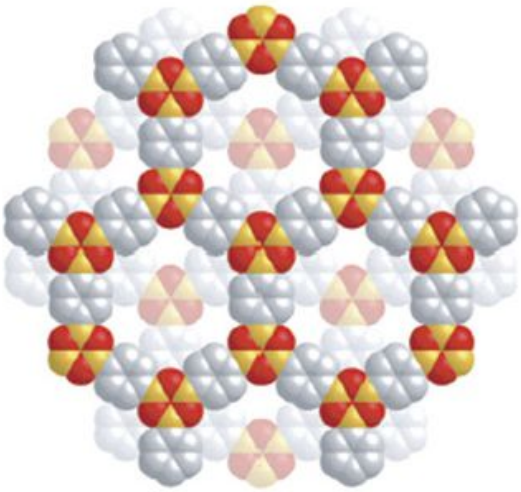

Figure 7: Schematic representation of assembly of COF-1. Condensation reaction of benzene-1,4-diboronic acid gives 2D supermolecular layers, which stack to form 3D porous framework. [32] Red: oxygen; yellow: boron; gray: carbon.

MOFs are crystalline networks consisting of metal ions or clusters (as nodes) coordinated to rigid organic molecules (as linkers) to form 3D frameworks by stacking layers (**Figure 8**).[20, 33-36]

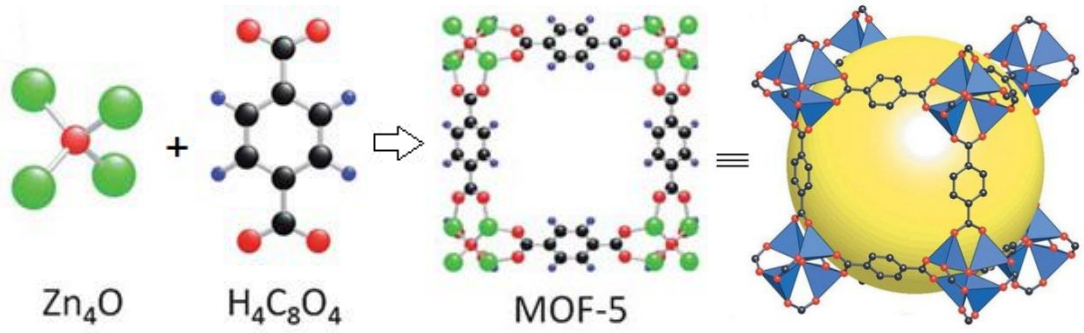

Figure 8: Construction of MOF-5. Zn: green spheres or blue tetrahedrons, O: red spheres, C: black or gray spheres, H: blue spheres. The large yellow spheres represent the largest molecule that could fit in the cavities. [21, 37]

Hydrogen-bonded organic frameworks are directly self-assembled from purely organic building blocks only via hydrogen-bonding interactions between node and linker molecules or only one type of molecules (**Figure 9**). [38-41]

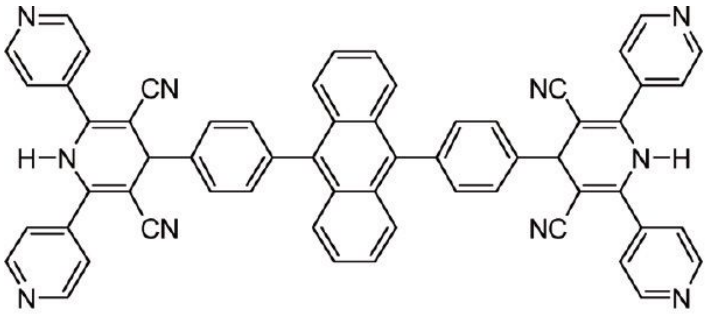

L^1

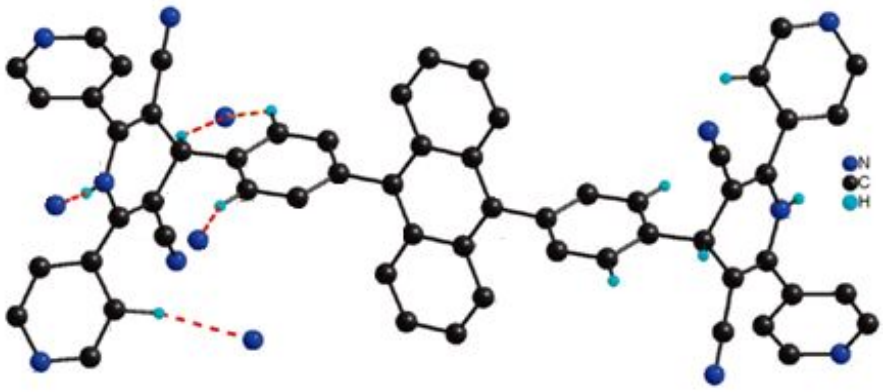

(a)

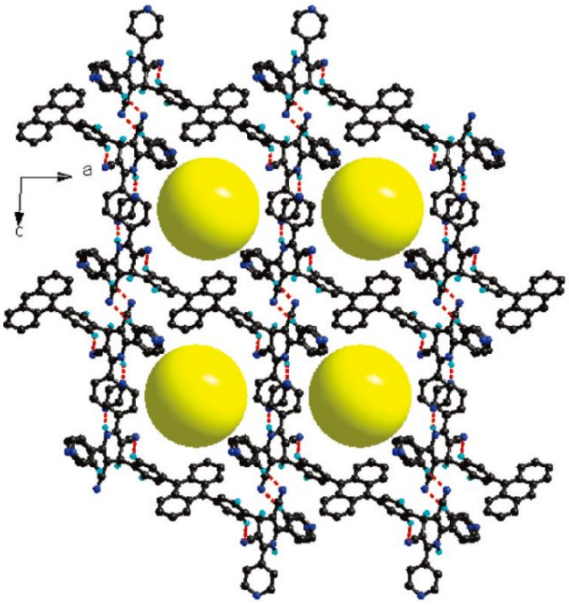

(b)

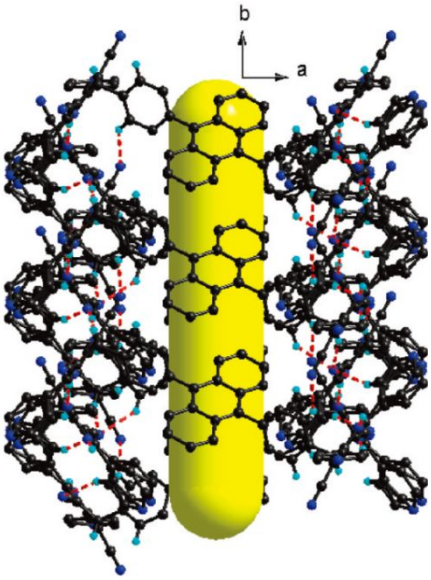

(c)

Figure 9: Crystal structure of a hydrogen-bonded framework SOF-1. L^1 is the building unit molecule. (a) View of the molecular structure and hydrogen bonding for the symmetric unit. (b) View of 3D porous organic framework. (c) Side view of the channel. The channels are shown in yellow. C: black spheres; H: light blue; N: dark blue; hydrogen bonds: red dashed lines.[26]

3.2. Functions and principles of porous organic network

Organic porous networks have shown potential applications in gas storage, [14, 42,43] separation,[12, 44] catalysis,[11, 45]drug delivery and sensing[13, 46] due to their easy-accessible high surface area, tunable pore functionality and structural flexibility. [47, 48] The functional principle of these materials rely on the tunable pore or channel volume and the interaction between host and guest molecules to allow target guest molecules to fit into the pore under required dynamic control.[30, 49, 50]

Additionally, a high surface area allows the exposure of numerous active sites binding to more guest molecules adsorbed in the framework. [51] Another interesting and unique principle has been described as 'breathing' or 'gate opening'.[44] This phenomenon occurs in the presence of structural flexibility of the frameworks. The thermal control or the change of the molecular environment allows the pore to deform so that the guest molecules can be released or adsorbed (**Figure 10**).[52, 53]

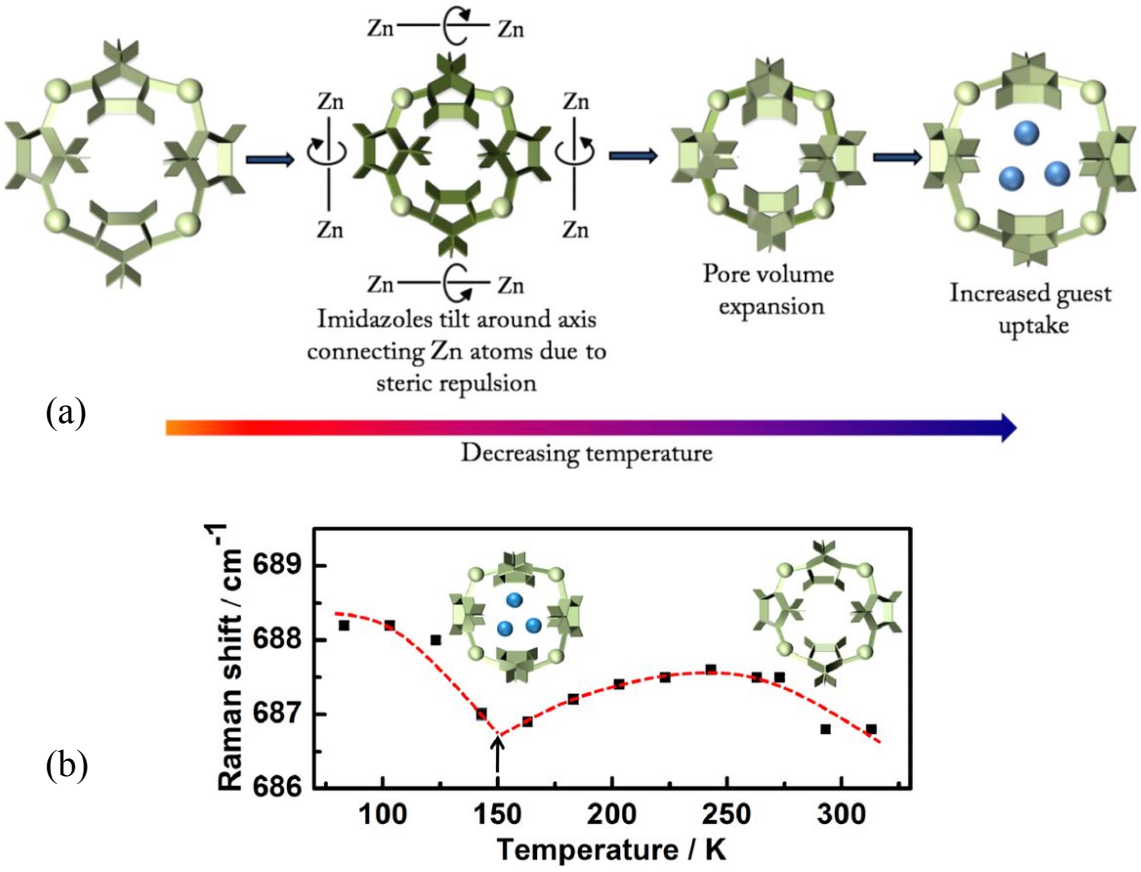

Figure 10: The functional principle of zeolitic imidazolate framework ZIF-8. (a)Scheme shows the form transition upon guest molecule adsorption under the thermal control. (b) Relation between transition and temperature. Bule sphere: guest molecules.[53]

3.3. Study of porous organic network

Because of the applications mentioned above, many novel organic porous frameworks have been successfully designed and synthesized in the last decade. [54-57]Classic porous materials, like MOFs and COFs have been developed to a large extent with various void volume and internal surface area.

When comparing the three main types of porous organic frameworks, COFs have rigid structures with large surface areas and high thermal stability due to the strong covalent interactions, but the formations of these bonds have to undergo specific reactions such as condensation reaction.[31, 52] It means that the selection of reaction conditions plays an essential role for establishing the framework. Most of the well-studied starting materials of COFs have planar configurations (**Figure 11**), so the open networks are usually obtained by stacking of numerous 2D layers.

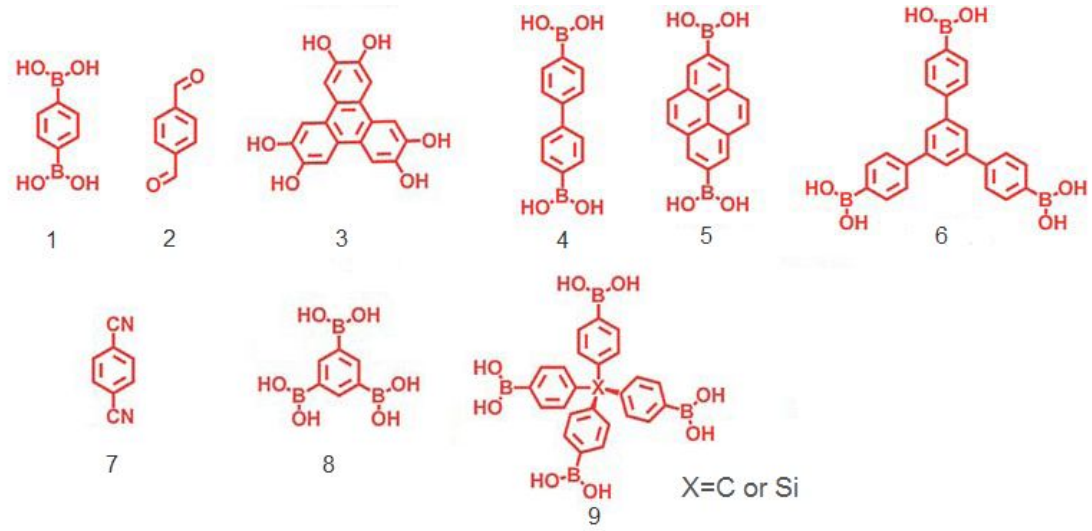

Figure 11: Some commonly used building blocks for COFs. 9 is a 3D structure, while 1-8 have planar configurations.[37]

By contrast, MOFs and hydrogen-bonded organic frameworks are the candidates assembling through noncovalent interactions. These types of frameworks usually provide high-symmetry 3D structures described as 'cages'.[58] MOFs require mild synthetic conditions even at room temperature.[59] Abundant organic linker materials and metal ions or clusters are readily designed and studied, so there are many options of building units and combinations for predictable frameworks.[59]

Hydrogen-bonding organic frameworks are usually not robust enough to exhibit permanent porosity in the absence of guest molecules. [32] It is known that in many frameworks the pores are filled with some solvent molecules as guests, and they will collapse upon the removal of those molecules, because the hydrogen-bonding interactions are so weak that they are easy to split, once the pores lose the support of solvent molecules. [41, 60-64]

4. DNA base pairs

Naturally occurring DNA is an essential self-assembling structure.[65] The DNA double helix structure is constructed by two coiled hydrogen-bonded strands, which are composed of sugar-phosphate backbones and nucleobases To keep the distance between two antiparallel strands, each type of bicyclic nucleobase guanine (G) or adenine (A) bonds with just one type of single ring nucleobase cytosine (C) or thymine (T) (**Figure 12**). This is called complementary base pairing.[66] Hence, adenine bonds only to thymine with two hydrogen bonds, and cytosine bonds only to guanine with three hydrogen bonds. [67]

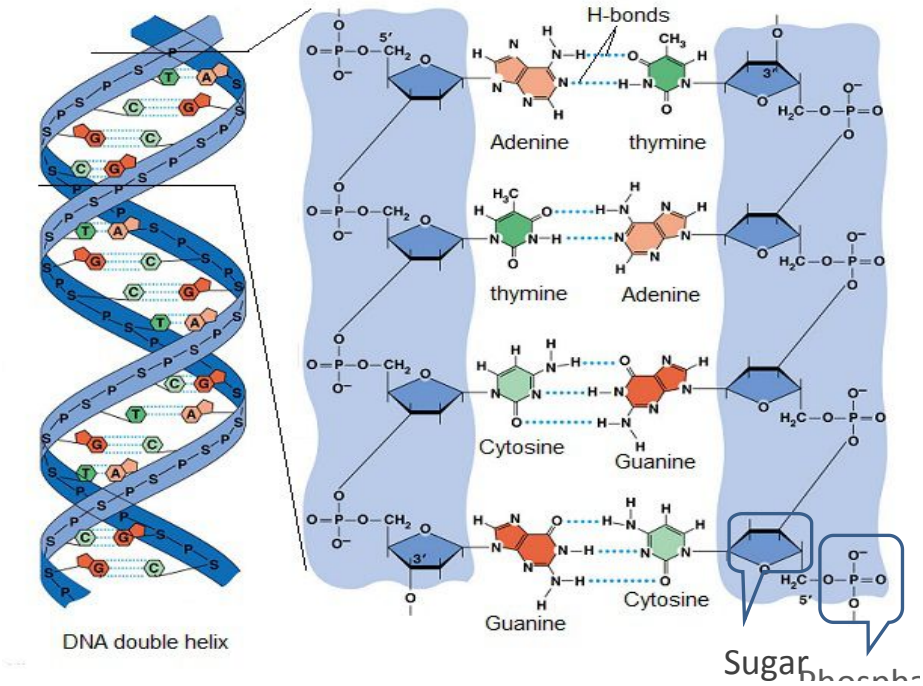

Figure 12: A fragment of DNA double helix. Noncovalent hydrogen bonds between the nucleobase pairs are shown as dashed lines. Two hydrogen bonds exist between adenine and thymine, while three between guanine and cytosine.[67]

In the organism, the sequence of these base pairs in DNA expresses and controls the genetic information. It is worth noting that the hydrogen bonds of each base pair are decisive for the construction and stability of DNA double helix.[68]

According to the property of highly controlled molecular recognition between two matching nucleobases, DNA based materials have been probed in many cases. A new type of porous solids making use of bioinspired molecular fragments of nucleobases or nucleobase derivatives as functional groups has been developed. [69] DNA base molecules could act as part of building blocks for assembling nano materials and molecular devices.[70] Nucleobase Zn(II) complexes with nuclease activity and cytotoxicity has been synthesized and investigated based on DNA binding property. [72]DNA base pairs can be regarded as a type of supramolecular synthons due to their complementary multiple hydrogen bonding donor and acceptor sites. [73]

5. The aim of the project

In this program, considering all functions, principles, merits and shortcomings of MOF, COF and hydrogen-bonded organic framework, we aim to build a series of porous crystalline frameworks using DNA bases as a part of the building blocks. Our target molecules were aimed to self-assemble into 3D networks via intermolecular hydrogen bonds between DNA base pairs instead of using metal clusters or covalent bonds. To obtain the 3D structure, the node molecule should extend towards three dimensions. This means that the organic node cannot be planar, but must have a polyhedral molecular structure. Since the carbon atom forms maximum four single bonds, the obvious 3D node structure is tetrahedral.

Due to the high reactivities of C-6 carbonyl group and C-2 amino group in guanine, protecting ans deprotecting reactions at these positions are always required to undergo *N9*-alkylation.[74, 75] Therefore, more complicated synthetic routes may be needed. Concerning this complexity, we selected the DNA base pair A-T rather than C-G as the option for synthesizing the building units of the self-assembling frameworks. When not incorporated into double helix, adenine can interact with itself, and the same for thymine.[70] Therefore, there are three predicted binding motifs (**Figure 13**).

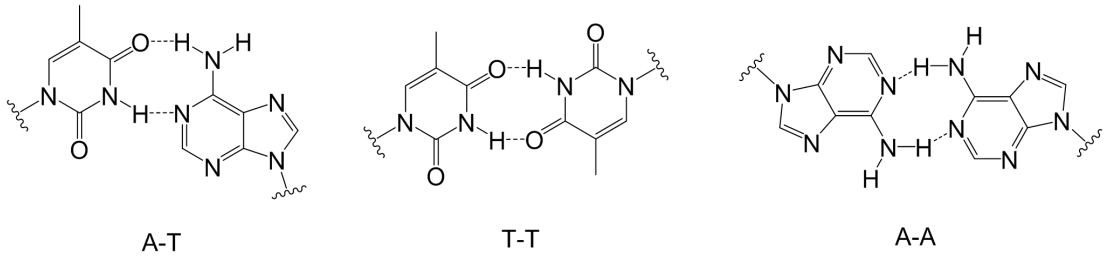

Figure 13: Three possible bonding types of adenine (A) and thymine (T): A-T, T-T, A-A.

Two target classes of networks are designed (**Figure 14**). In class A, both node and linker are used. Each linker connects to two nodes, while each node attaches four linkers. In class B, only one or two node compounds are involved, and the ratio between two different nodes should be 1:1.

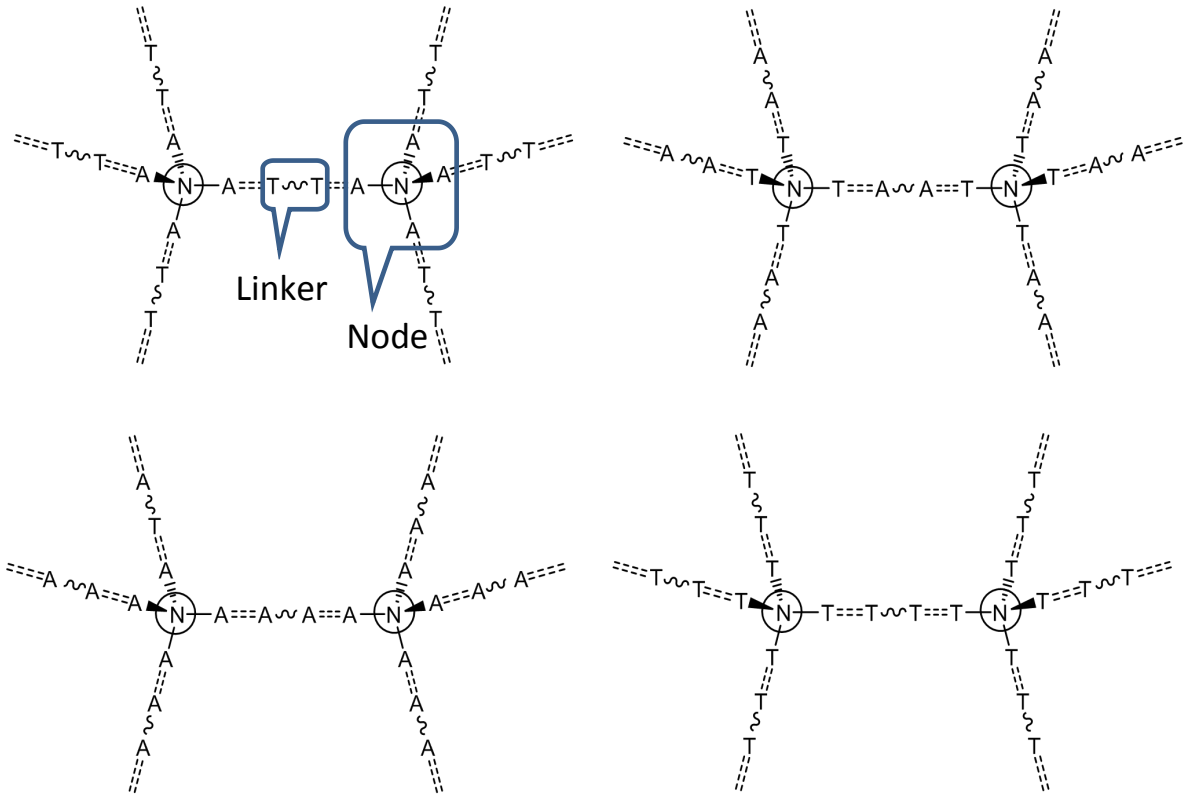

class A

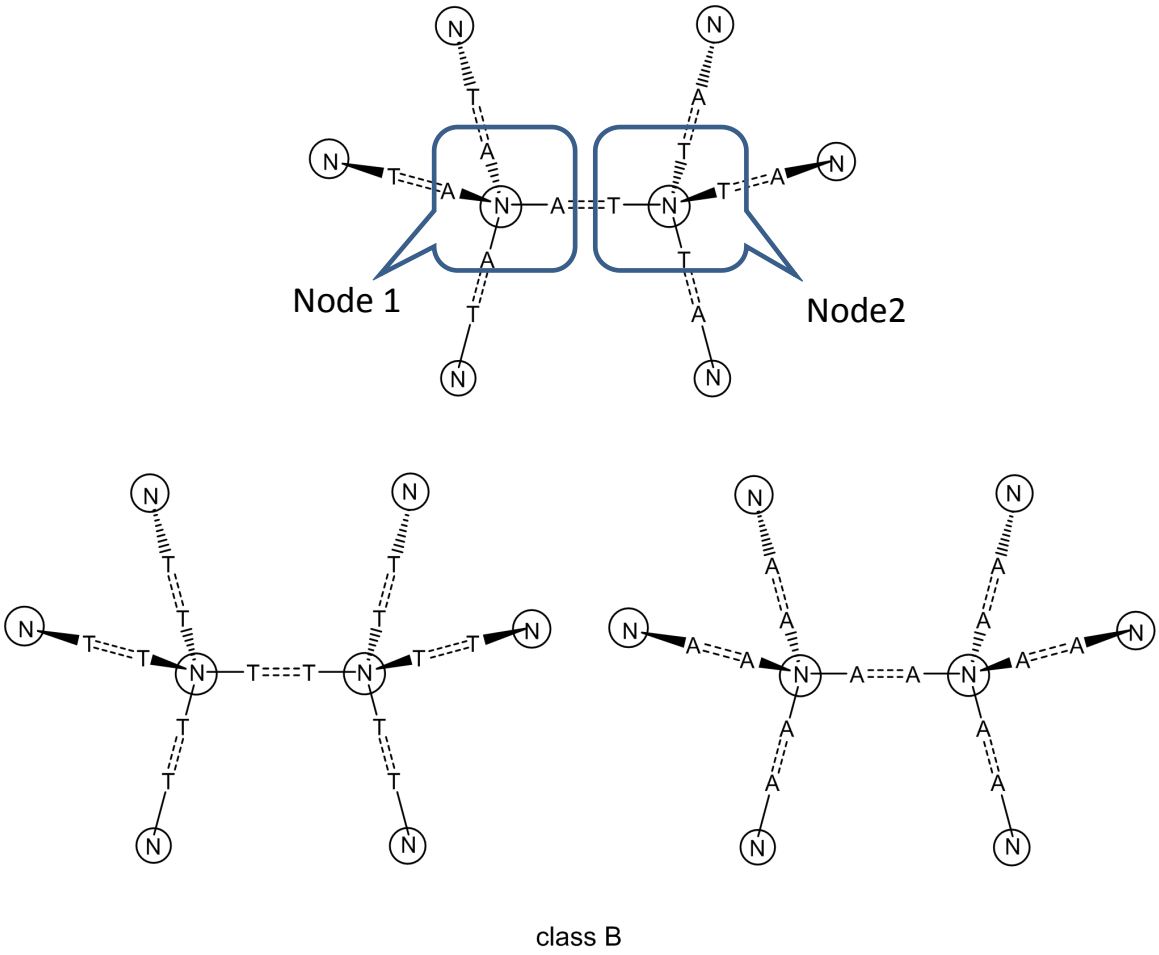

Figure 14: Two target classes of networks. Circled N: core of node molecule; A: adenine; T: thymine; Dashed line: hydrogen bonds; curved line: two or three carbon chain of linker molecule.

Serving this goal, we planned to synthesize two distinct series of materials, which are linear linkers and tetrahedral nodes. The target compounds to be synthesized are specified in **Table 1.**

Table 1: **Target compounds for synthesis**

	Adenine derivatives	Thymine derivatives
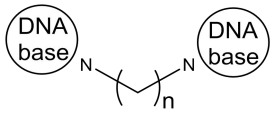	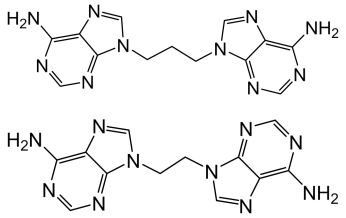	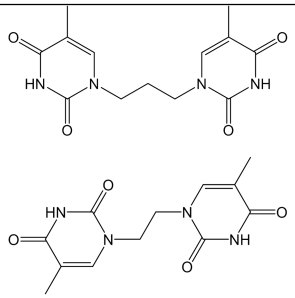
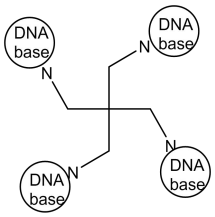	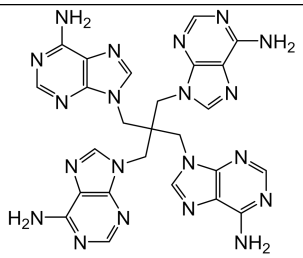	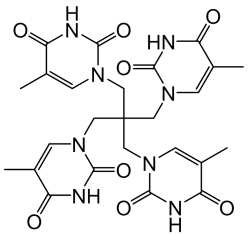
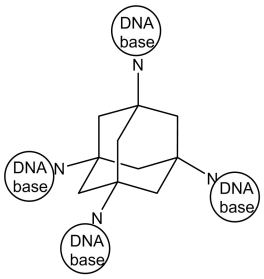	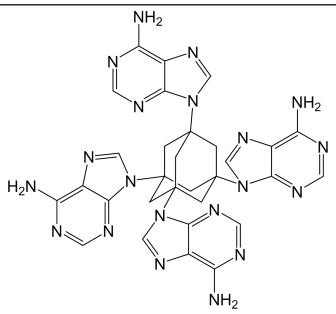	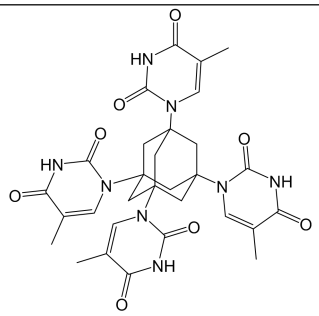
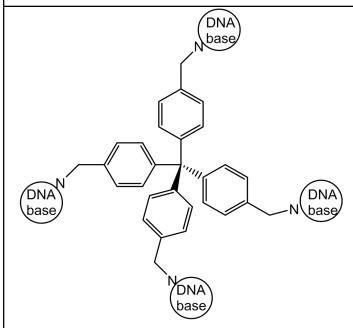	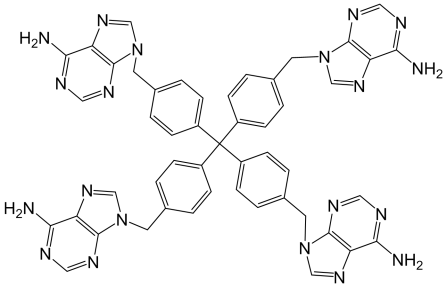	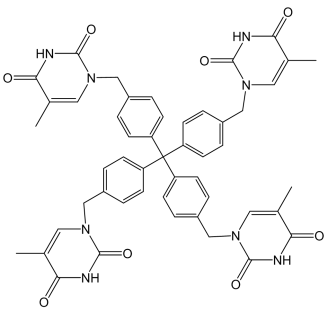

Syntheses of these compounds in **Table 1** could be possibly realized through *N*-alkylation reactions of heteroaromatic adenine or thymine.[75-80] The syntheses of linker compounds have been reported, [81-83] while the node compounds have not been prepared yet.

6. Challenge

Although some DNA base, such as adenine, have already been investigated in metal-organic framework or complex and the new solid materials,[84, 85] the potential of nucleobases as tools in supramolecular chemistry has not yet been fully exhausted. Two main reasons are the low solubility of the nucleobase derivatives in common organic solvents and the synthetic challenges due to their chemical properties. Specifically, due to the low solubility of the adenine and thymine derivatives in common low or moderate polar organic solvents, the achievement of crystals that can be used for structural analysis is hampered.[69] Both adenine and thymine have several sites susceptible to alkylation. It was therefore necessary to employ procedures that gave alkylation at the desired site, and in some cases protecting groups have to be introduced.[77]

Part II

Strategies and methods

7. Synthetic methods

7.1. *N*-alkylation of adenine and thymine

7.1.1. N-alkylation of adenine

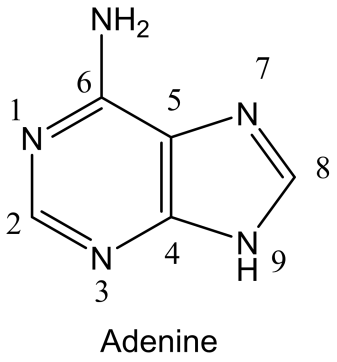

Figure 15: The structure of adenine and the accepted numbering system.

Adenine is also known as *9H*-purin-6-amine (**Figure 15**). The NH proton in adenine is acidic and can be easily abstracted by a base, and this property mainly leads to the *N*-alkylation of adenine.[86] Adenine, as a derivative of purine, has four *NH*-tautomers (**Scheme 1**). Under the specific conditions, *N-3, N7*- and *N9*- substituted products may be obtained from reactions. *N9*- and *N7*-alkylations are always achieved under basic conditions, and *N9*-alkylation is observed more often as the major product. [87, 88]

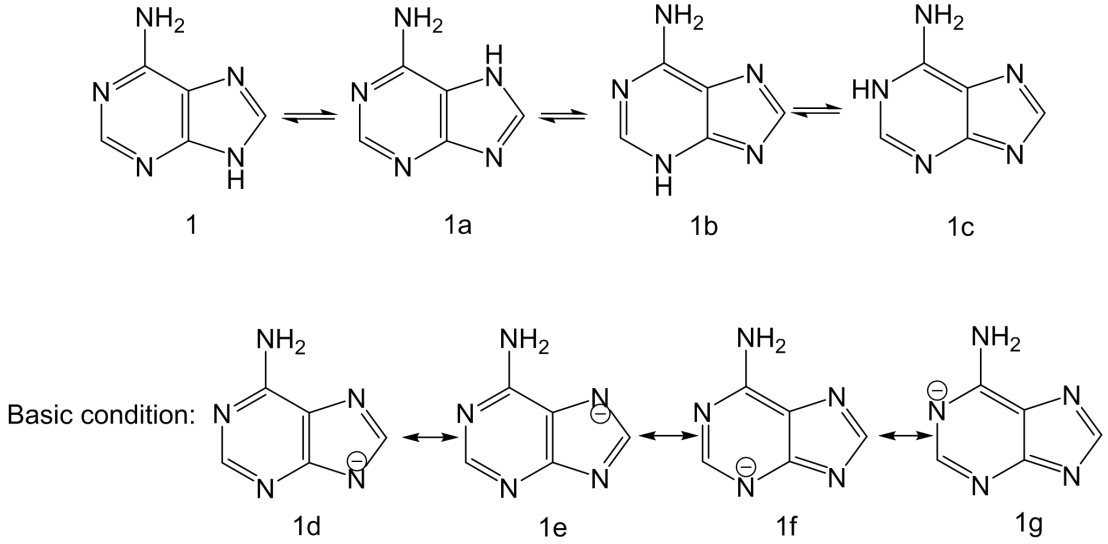

Scheme 1: Adenine tautomers, and the resonance forms of its anion in basic condition.

Base-induced coupling is the most known general method of the alkylation reactions. It consist of generating a anion in the presence of a base such as alkali metal carbonates such as K_2CO_3, or hydride (NaH) in a polar solvent.[77, 79, 89] The use of K_2CO_3 and NaH as bases, stimulate the deprotonation at N9 position of adenine. Then alkylation reagent as an electrophile attacks the N9 position. In some cases, the *N7* isomer or *N3* isomer may be obtained as a side product of the *N9*-alkylation reaction, especially when protected or modified adenine is used. [90- 93] The aim of this project is to obtain the *N9*- substituted product (**Scheme 2**).

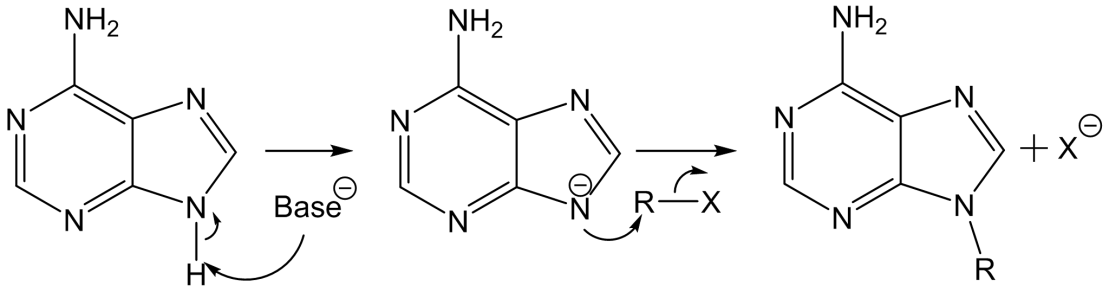

Scheme 2: *N*9-Alkylation mechanism of adenine.

7.1.2. N-alkylation of thymine

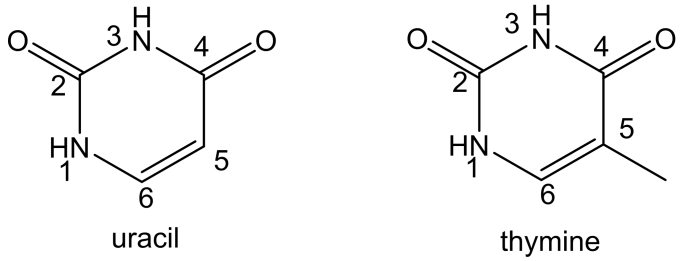

Figure 16: Molecular structures of uracil and thymine.

Thymine known as 5-methyluracil, is found in DNA, while in RNA, uracil replaces thymine as the nucleobase (**Figure 16**). Based on their molecular structures, they have similar chemical properties.

Monoalkylation of uracil or thymine generally has low selectivity. Therefore the *N1,N3*-dialkylated or *N1,O2*-alkylated derivatives are usually obtained as side products. Alkylation of the unprotected uracil with ethyl iodide was reported to give both *N1*-ethyl and *N1,N3*-diethyl derivatives. [94, 95] *N1*-alkylated uracil with allyl

bromide and potassium carbonate in DMF solution was isolated, but in a low yield.[96] Under Mitsunobu conditions *N1*- and *O2*-alkylation have been observed. In this project, *N1*-alkylated compounds are desired. Hence the protecting groups should be introduced at *N3*- or *O2*- position. Several protection strategies have been reported. [44, 96, 97]

7.2. Short methylene chain

Due to the wanted shape of our linker molecules, and to avoid the formation of intramolecular hydrogen bonds, we choose di- and tri-methylene chain halide reagents as the starting materials for syntheses of linker compounds (**Figure 17**).[77] Dimethylene chain allow the target molecule having a straight structure and a symmetric center, while trimethylene chain bends at central carbon, so it has a symmetric axis. Both of their compact molecular structures can restrict the flexibility of the aimed framework. These simple alkyl halide reagents are commercially available. In general, primary alkyl halides are great substrates in the S_N2 reaction. The aimed linker compounds have been synthesized following literature routes.[77, 78]

Figure 17: Molecular structures of starting materials, 1,2-dibromoethane (2) and 1,3-dibromopropane (3).

7.3. Pentaerythrityl adenine or thymine materials

The central carbon of pentaerythrityl is tetrahedral (**Figure 18**). The designed node compounds based on this structure have potential to lead the formation of 3D frameworks when connecting with linker molecules. The fixed bond angle (109.5°) of central carbon atom and the steric hindrance of large functional groups will restrict the bending at the CH_2 groups. In this case, there should be little flexibility in the pentaerythrityl derivatives. The syntheses of pentaerythrityl tetrabromide and pentaerythrityl tetraiodide have been reported.[76, 98] Using these tetrahalides as alkylation reagents for adenine or thymine, the reaction prefer to undergo a S_N1 mechanism (**Figure 19**).

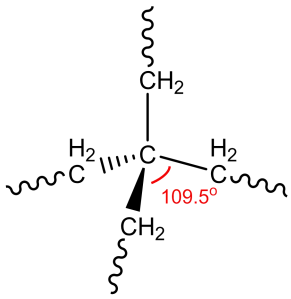

Figure 18: Structure of pentaerythrityl. Central tetrahedral carbon atom is shown. Curved line: connection of functional group.

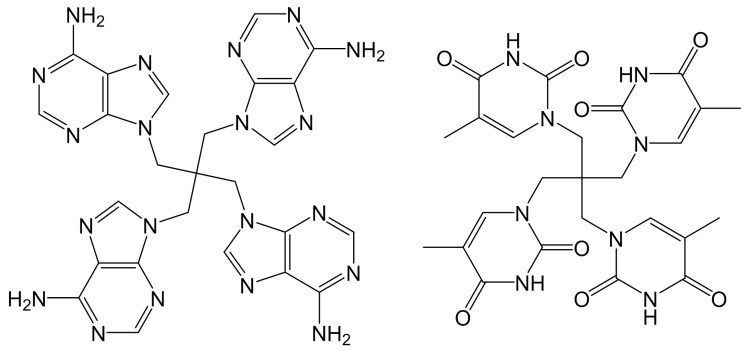

Figure 19: Designed node molecules: pentaerythrityl tetra adenine and pentaerythrityl tetra thymine.

7.4. 1,3,5,7-Bromoadamantane

Due to its rigid cage structure, adamantane is a candidate tetrahedral building block, which has potential to form 3D structure framework.[99-101] Many bridgehead substituted adamantane derivatives, including *N*-adamantylated products, have been synthesized by nucleophilic substitution in the presence of a Lewis acid.[102,103] Tetra bridgehead functionalized derivatives are less common, because they are often more difficult to synthesize (**Scheme 3**).[104] Substitution of adamantane at the bridgehead positions requires the activation of a tertiary C–H bond, so it means the requirement of harsher reaction conditions. Due to the strain of the cage structure of adamantane, the bridgehead carbon cannot form a planar configuration, so the backside attack is impossible at bridgehead positions. Hence the haloadamantanes cannot participate in S_N2 reactions. S_N1 reactions on bridgehead halides may also be difficult since the carbocation intermediate is not planar.[105]

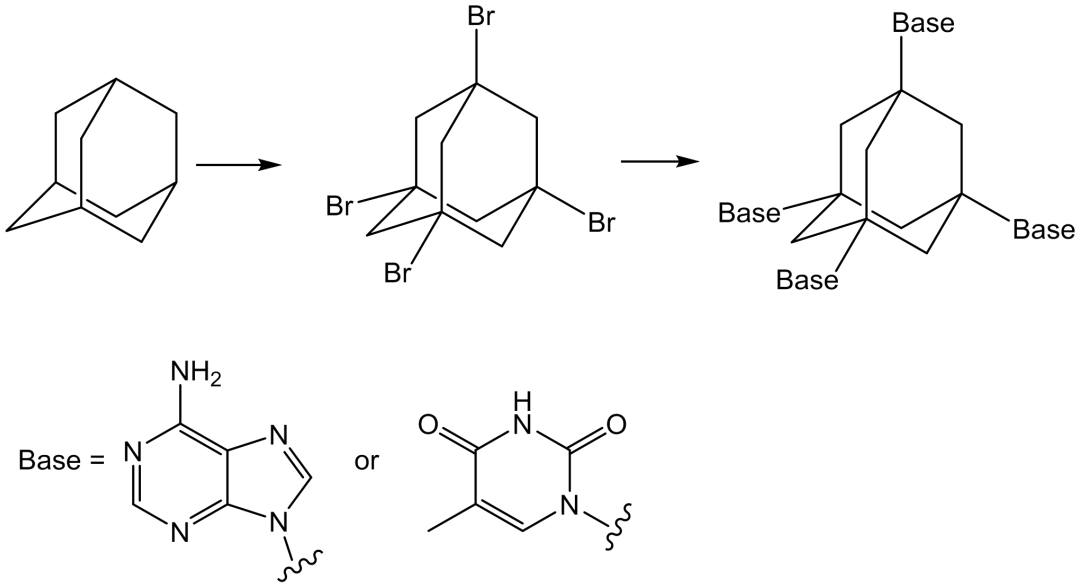

Scheme 3: From adamantane to tetra-bromoadamantane, then to tetra DNA-base adamantane.

Compared with pentaerythrityl adenine or thymine derivatives, the distance between each bridgehead carbon in adamantane structure theoretically reduces the steric hindrance of adenine or thymine substituents when polysubstitution occurs. Therefore, the adamantane derivatives were designed as a series of alternative node compounds.

7.5. Tetrakis(4-(bromomethyl)phenyl)methane

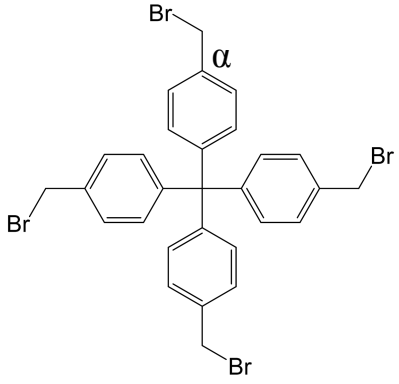

Figure 20: Molecular structure of tetrakis(4 (bromomethyl)phenyl)methane.

According to this molecular structure, there is a relatively bulky connecting group on α-carbon, so the nucleophilic substitution prefers to follow the S_N1 mechanism (**Figure 20**). Although the CH_2 groups in this structure will provide the node molecules with higher flexibility while forming network, this kind of compounds

should also be easier to synthesize. In comparison, the carbocation (b) can be stabilized by resonance of benzene ring system, while the carbocation (a) would be more difficult to form due to the breaking of the aromatic electron system (**Scheme 4**). Hence, as a candidate, tetrakis(4-(bromomethyl)phenyl)methane was more reliable. Compared to pentaerythrityl bromide, 1,3,5,7-bromoadamantane and tetra p-bromophenyl methane, tetra (*p*-bromomethylphenyl) methane is more reactive for S_N1 substitution reaction, because of the formation of more stable carbocation

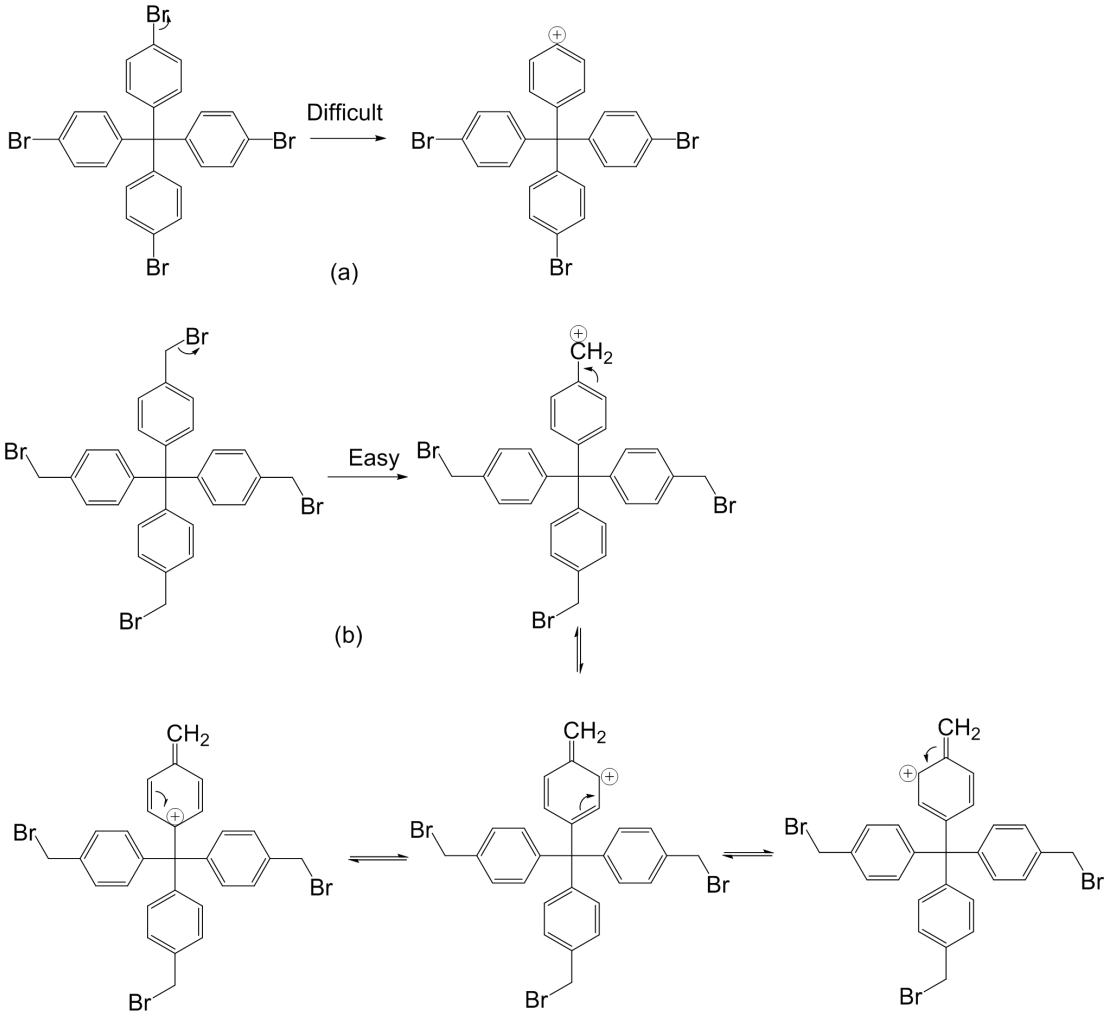

Scheme 4: (a) The carbocation of tetra *p*-bromophenyl methane is difficult to form. (b) The promising carbocation formed from tetrakis(4-(bromomethyl)phenyl)methane could be stabilized by four resonance forms.

8. X-ray crystallography

X-ray diffraction (XRD) is the most powerful method for providing structural information for crystalline networks. The results from processed and refined diffraction patterns provide reliable and required parameters for 3-dimensional molecular structures and determination of the absolute configuration of the molecules.[88, 92] In the past decades, X-ray diffraction methods have improved rapidly, especially for the diffraction data collection procedures. The usage of area detectors as an electronic version of photographic film reduced the data collection time by recording many reflections simultaneously. [106, 107] Impressive advances in computer hardware and software development shorten the time to solve and refine a structure from days or weeks to hours.[107] The application of constant low temperature obtained from a cold gas stream by evaporation of liquid nitrogen makes it possible to slow the radiation damage of X-ray beams for crystals, and reduce the thermal vibrations, which give a more well-defined electron density and more accurate structure determination.[94]

A powder X-ray diffraction (PXRD) pattern is the 'fingerprint' for a compound, and both the positions and the relative intensity of the peaks in a diffraction pattern are indicative of a particular phase and material. A database is available for such 'fingerprints' of most chemical compounds, for which a crystal structure has been solved. Once two compounds interact via any interaction, including H-bond, a new pattern will form for the complex with characteristic signals belonging to neither of them.

Single crystal X-ray diffraction effectively provides reliable information about the parameters of the unit cell and lattice. This method can be employed to determine the configurations and disorder of molecules, since the electron density map indicates the real atomistic locations (**Figure 21**). [108-110]

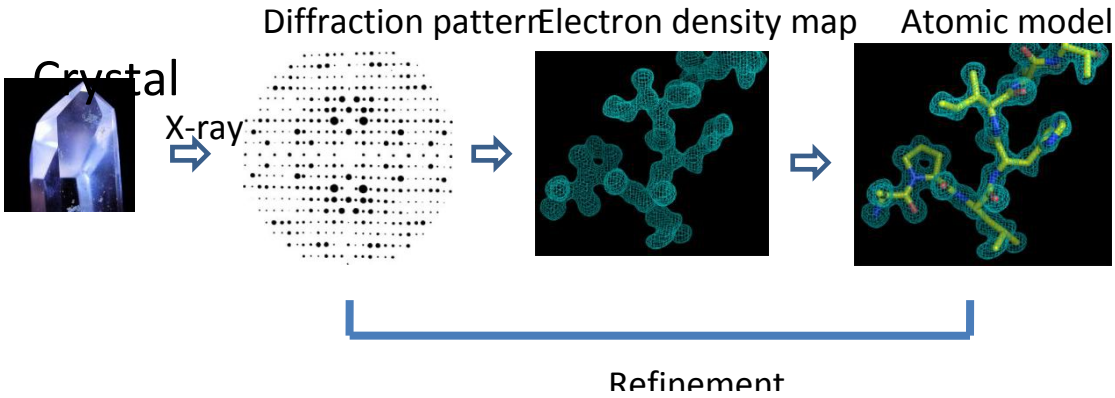

Figure 21: Four main steps of single crystal X-ray diffraction analysis.[109]

9. Crystal growth

All strategies for crystallization are aimed at bringing a concentrated solution of a homogeneous population of molecules very slowly towards a state of minimum solubility.[106] The size and shape of the obtained crystals vary tremendously on the chemical natures of the compounds,[111] as does the solubility in different solvents. The selection of solvent and precipitating reagent is consequently important for the crystal quality.

9.1. Slow evaporation

Slow evaporation is the quickest and easiest crystallization process depending on the choice of solvents and sometimes it is combined with temperature control. The evaporation of solvent leads to a rise of the concentration of the solute until crystals form (**Figure 22**).[109]

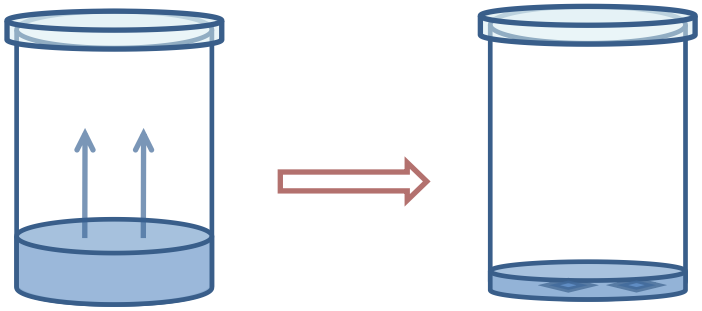

Figure 22: Crystal growth: slow evaporation.

This method is aimed at bringing a concentrated solution of homogeneous compounds very slowly toward a state of super-saturation, from which the crystals grow. It is undesirable to let a solvent evaporate to dryness as this will allow crystals to become encrusted, grow into an aggregate or be contaminated by impurities.[108, 109] The crystals may be degraded by loss of co-crystallized solvent, and sticked on the walls of container furthermore cause the problem when harvesting the crystals.

9.2. Solvent layering

Another commonly used technique is solvent layering (**Figure 23**). One solvent should be carefully layered over top of a second solvent. These two solvents should be miscible in one another.[107] The compound should be soluble in one of them, but not the other one. The compound precipitates along with the diffusion of two solvents. Rate of crystal growth depends on the concentration and solubility of the compound in the resulting mixed solvent system.

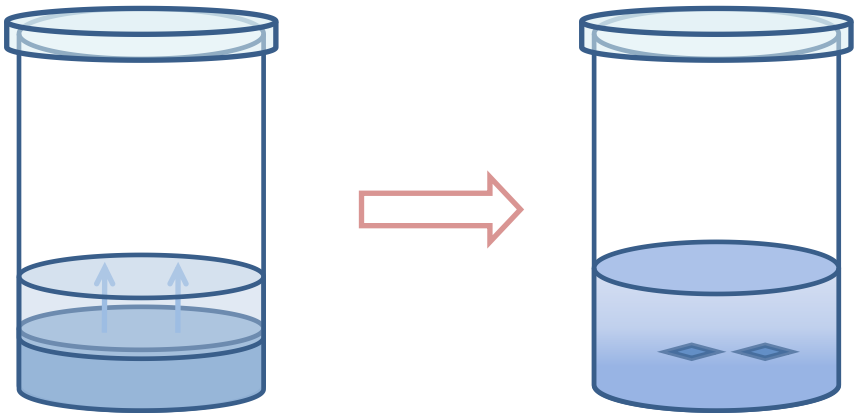

Figure 23: Crystal growth: solvent layering. Light blue: precipitating reagent; dark blue: solution of compound.

9.3. Vapor diffusion

Vapor diffusion may succeed when other crystallization techniques fail.[107] With this method, the suitable solvent and precipitating reagent are isolated. The vapor of the precipitating reagent diffuses into the solution so that the solubility of target compounds decreases. The crystals ultimately precipitate from a saturated solution.

This technique is easier to handle, and there are more options of solvents (**Figure 24**).[95]

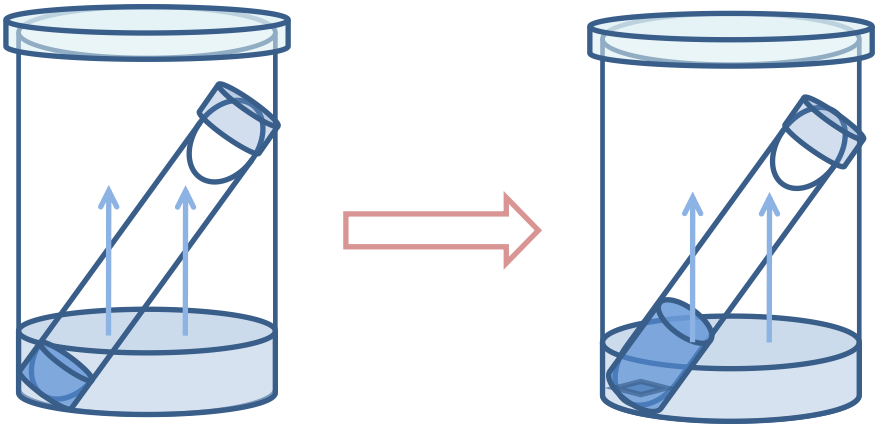

Figure 24: Crystal growth: vapor diffusion. Light blue: precipitating reagent; dark blue: solution of compound.

In order to harvest the crystals easily out of the containers, small vials with straight walls are always used to allow crystals floating out without obstacle.[109] All the crystal growth experiments should be conducted without disturbance to the setups containing crystal mother liquor.

Part III

Result and discussion

10. Syntheses

10.1. Synthesis of 9,9'-dimethylene-bis(adenine) **2** (AdC2Ad)

Adenine **1** was *N*-alkylated with 1,2-dibromoethane in the presence of NaH or K_2CO_3 using DMF as the solvent to give compound **2** (**Scheme 5**).[81,82]

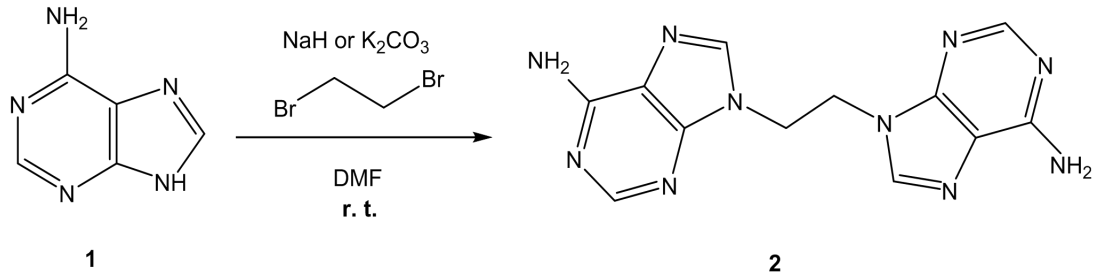

1 **2**

Scheme 5

The reaction ran for 48 hours at ambient temperature, but the conversion was low. Compound **2** was purified by recrystallization from acetic acid-methanol (1:1). The yield was 15 % with NaH. In contrast, the yield reached 27 % when K_2CO_3 was applied. In the literature there was no reported yield of final pure compound because the crude product was split into portions for different purification methods. [81, 82] Based on the experimental result, K_2CO_3 was a better base than NaH for the deprotonation of N9 position of adenine in this reaction.

For adenine *N9*-alkylation with 1,2-dibromoethane, under basic condition and in solvent DMF,[77, 79] the reaction is likely to follow S_N2 substitution mechanism. The adenine anion, as the nucleophile, attack from the backside of the target carbon (**Scheme 6**). However, during the second step, because of the steric hindrance of the attached adenine group, the approach of the second adenine might be very difficult.

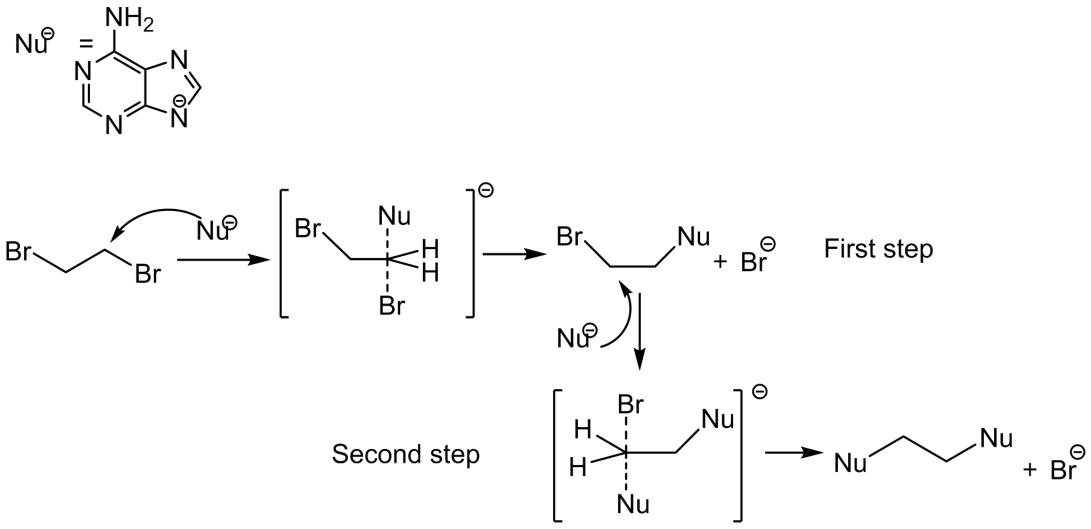

Scheme 6: Supposed mechanism of the synthesis of *9,9'*-dimethylene-bis(adenine) **2**.

10.2. Synthesis of 9,9 '-trimethylene-bis(adenine) **3** (AdC3Ad)

Adenine **1** was *N*-alkylated with 1,3-dibromopropane in the presence of NaH in DMF to form compound **3** (**Scheme 7**).[81]

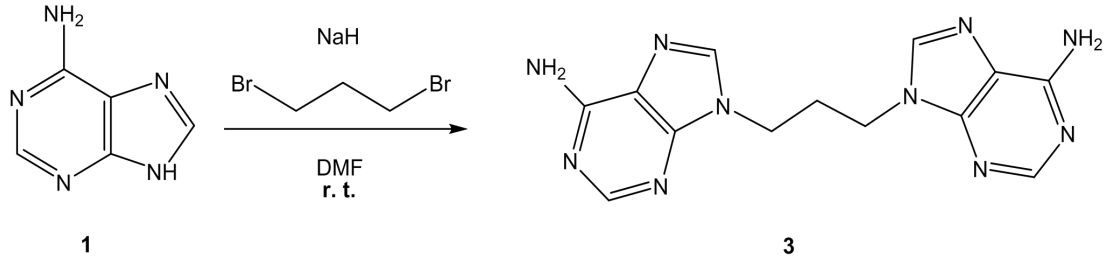

Scheme 7

The reaction ran for six days at room temperature, and the conversion was still low. The final yield of **3** was 26 % by recrystallization from acetic acid-methanol (1:1). No literature yield of pure product was reported.[81] The yield was better than that of compound **2** which was obtained through the same route following the same mechanism, but with a one carbon atom shorter alkyl bromide. Longer carbon chain might reduce the steric effect of the adenine group attached in first step when the second one approaching. The S_N2 reaction is more favorable.

10.3. Synthesis of pentaerythrityl bromide **6**

The tetraol **4** was reacted with benzenesulfonyl chloride in pyridine in an esterification reaction, and then the resulting compound **5** was reacted with NaBr to give the final product **6** (**Scheme 8**). [112]

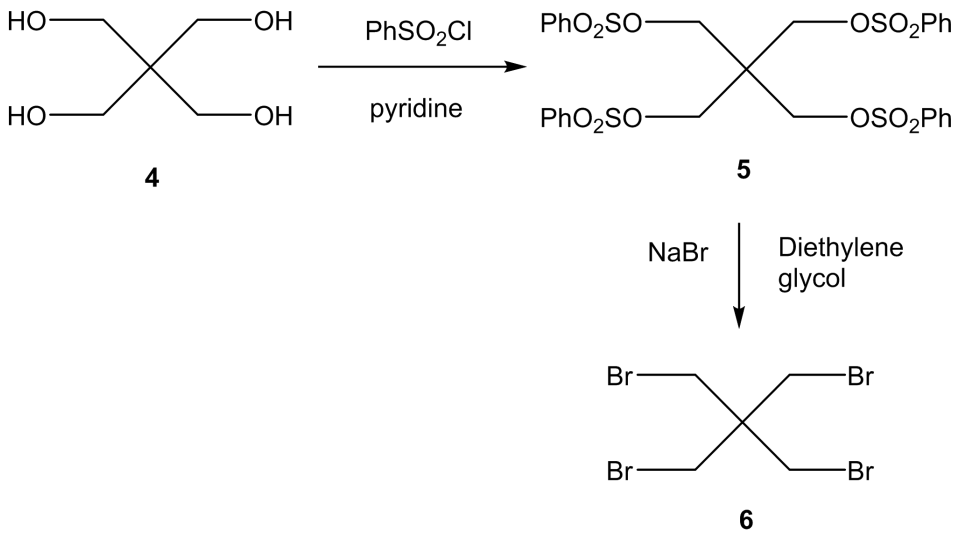

Scheme 8

The first step completed after 4.5 hours at 40 °C. Compound **5** was not stable enough for storage at room temperature, so it should be freshly prepared as an intermediate reagent for the next step. The second step finished after 19 hours at 130 °C. The yield of product over two steps **6** was 84 % calculated from the starting tetraol **4,** and the pure compound was obtained after washing with water and methanol.

10.4. Synthesis of pentaerythrityl iodide **7**

Pentaerythrityl iodide **7** was converted from pentaerythrityl bromide **6** in a halogen replacement reaction in the presence of NaI and methyl ethyl ketone as the solvent (**Scheme 9**).[113]

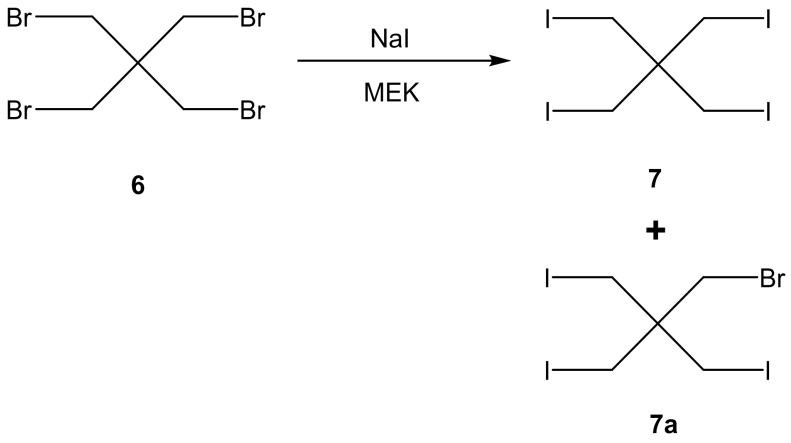

Scheme 9

This reaction was refluxed for four days, and the starting material was completely consumed, but there was still incompletely substituted by-product **7a** (ca. 15 % from ^{1}H NMR spectrum of crude product). The crude product, a mixture of **7** and **7a**, had low solubility in chloroform, EtOAc, DMSO, benzene and toluene, and as both compounds **7** and **7a** have the quite similar chemical properties and polarities, it turned out to be very difficult to separate them by recrystallization and flash chromatography. When taking the crude mixture into a cycle as starting material to react with excess sodium iodide for three times, the pure compound **7** was obtained with an overall yield of 91 %.

10.5. Attempted synthesis of tetrakis(9-adeninylmethyl)methane **8**

Adenine **1** reacted with pentaerythrityl tetrabromide **6** in the presence of potassium carbonate, and DMF was used as solvent (**Scheme 10**). This reaction did not give the target compound **8**. Instead, monosubstituted compound **8a** was detected by ^{1}H NMR and MS, and the conversion of adenine was very low even with heating and using of long reaction time (**Table 2**).

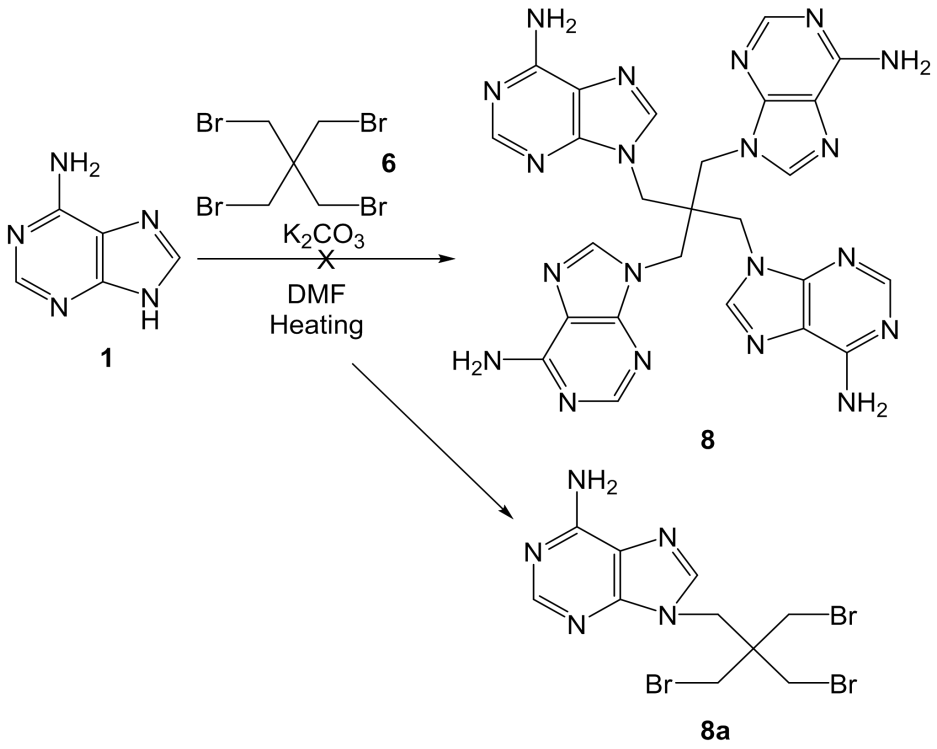

Scheme 10

Compared with neopentyl bromide, the structure of pentaerythrityl tetrabromide is even more crowded (**Figure 25**). It is well known that primary alkyl halides usually undergo the S_N2 reaction, and S_N2 reaction is sensitive to steric hindrance. Neopentyl halide, because of its steric bulk on α-carbon, is inert towards the S_N2 mechanism, but is moderately reactive under conditions favorable to the S_N1 mechanism.[114] In comparison, compound **6** is more likely followed the S_N1 substitution mechanism (**Scheme 11**).

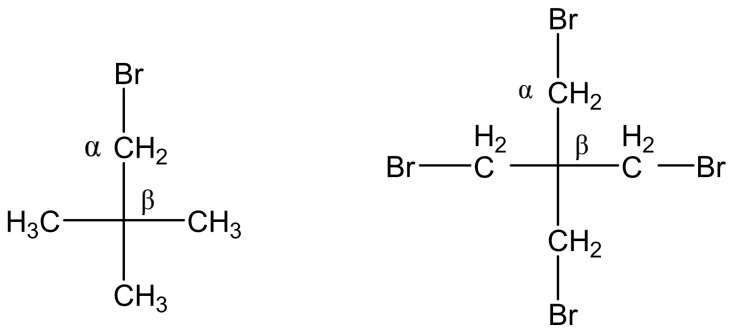

Neopentyl bromide Pentaerythrityl tetrabromide

Figure 25: Molecular structures of neopentyl bromide and pentaerythrityl tetrabromide indicate the reaction centre α carbon and the steric effect from *β* position.

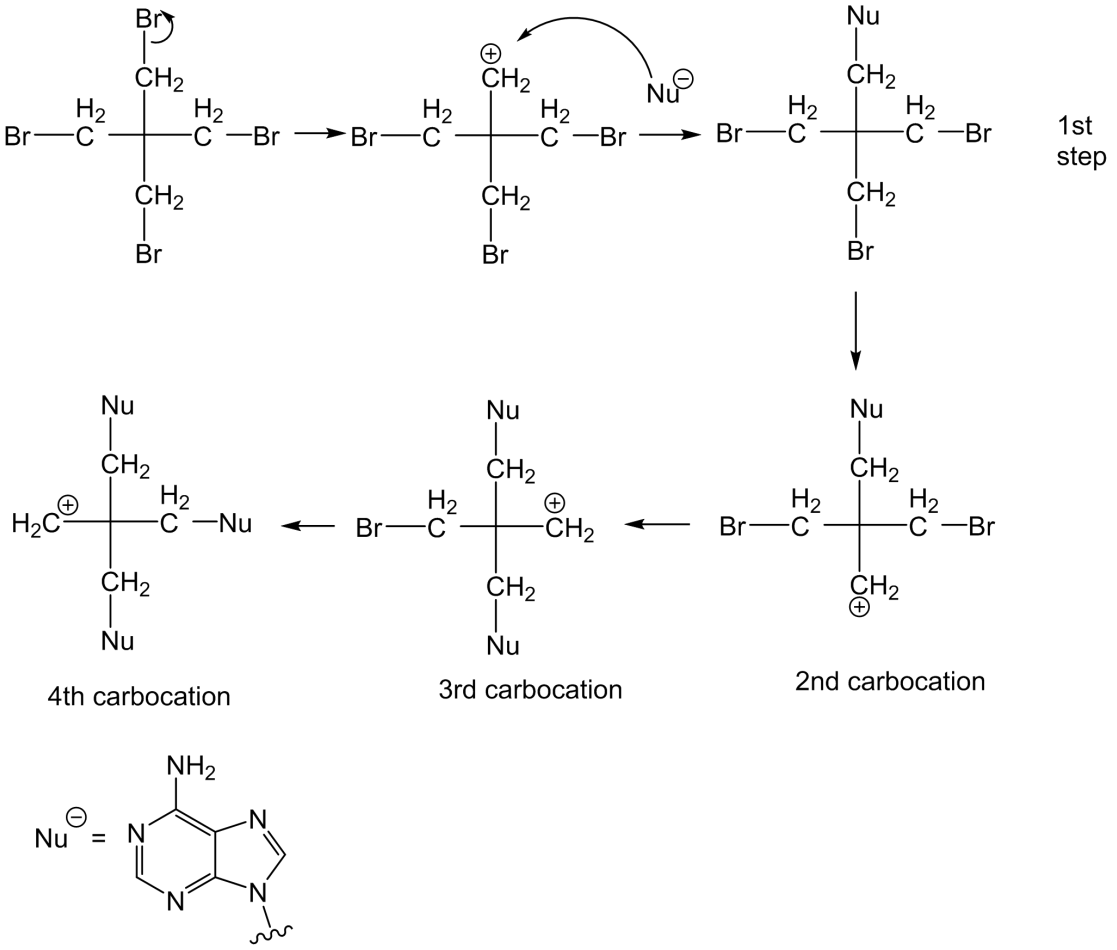

Scheme 11: A supposed four-step procedure of tetra substitution from compound **6** to **8**. The carbocation formed in each step.

For S_N1 reactions, I^- is a better leaving group than Br^-, so pentaerythrityl iodide **7** was attempted for this synthetic route while heating up to 70 °C, 100 °C and 130 °C for two or three weeks (**Table 2**). Unfortunately, none of the reactions give the target tetrasubstituted product. Signals of monosubstituted product were observed in ^1H NMR and MS (EI) spectra.

Table 2: various conditions for synthesis of tetrakis(9-adeninylmethyl)methane

Base	Temp.	Time	Result
12 eq. K_2CO_3 1 eq. 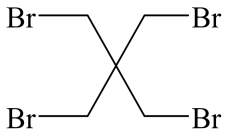 **6** 6 eq. 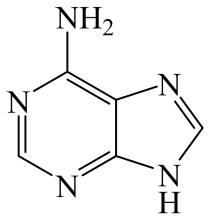 **1**	r.t.	2 weeks	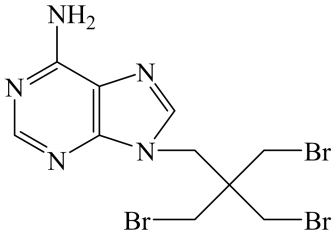 **8a**
	70 °C	3 weeks	**8a** + unknown
12 eq. K_2CO_3 1 eq. 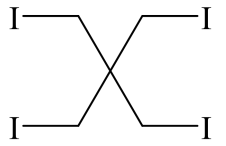 **7** 6 eq. 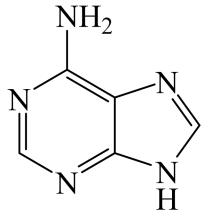 **1**	70 °C	7 days	5 spots shown on TLC plate. No corresponding signal of target product in ^1H NMR and MS (EI) spectra.
	100 °C	7 days	
	130 °C	12 days	

With continuous heating, DMF seemed to decompose with release of dimethylamine and CO as inferred by the smell of amine from the reaction mixture. There was no pure product recovered from the decomposed solvent.

To modify the reaction conditions, a synthesis reactor Monowave 300 was used for microwave reaction, and DMF was changed to degassed acetonitrile to fit microwave condition (**Scheme 12**). Microwave condition can provide rapid and uniform heating for a reaction.

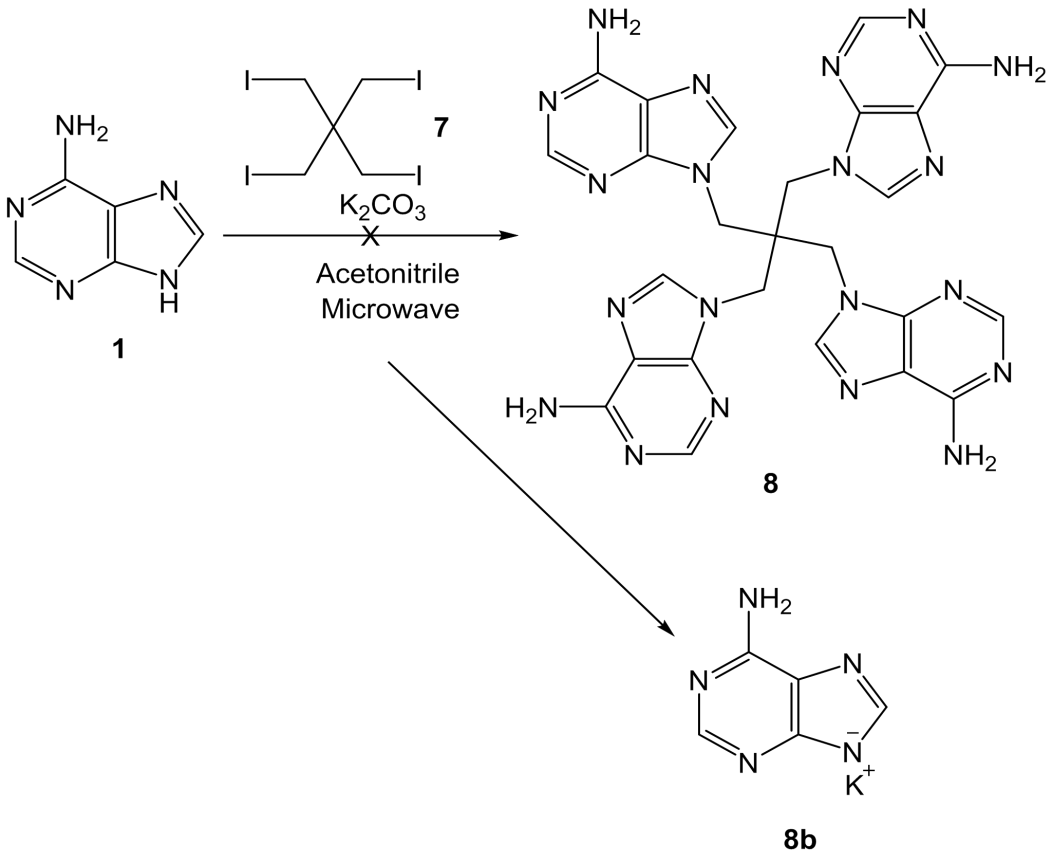

Scheme 12

Under microwave condition, only potassium adenine salt **8b** might be formed according to ^{1}H NMR and MS data after heating up to 175^{o}C for six hours (**Table 3**). This might be because the solubility of tetra iodide **7** in acetonitrile is too low to permit the reaction at a measurable rate.

Table 3: Microwave reactions

Base	Temp.	Heating time	Result
12 eq. K_2CO_3 6 eq. 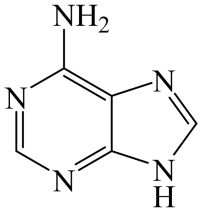 **1**	Microwave 175 ^{o}C	3 h	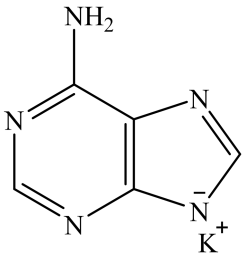 **8b**
		5 h	
		6 h	

From these two synthetic methods we assumed that harsher conditions might be needed for this transformation. Since similar *N*-alkylation with imidazole has been reported, this literature route was attempted for adenine (**Scheme 13**).[112] Strong base NaOH and solvent mixture of DMSO and toluene were applied. The ratio between DMSO and toluene was adjusted to 2:1 in order to completely dissolve adenine.

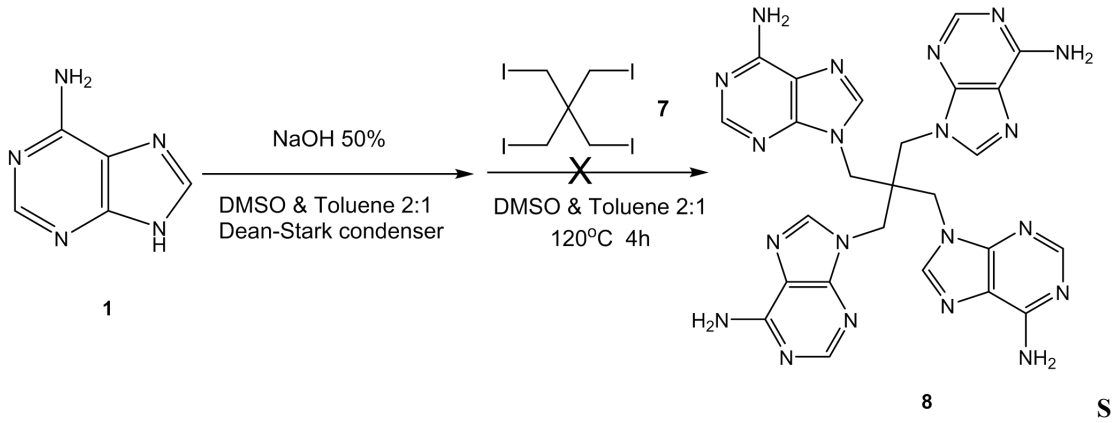

cheme 13

The reaction was run for 4 h at 120 °C, but the conversion was low and no formation of target product **8** was observed.

10.6. Synthesis of 1,1'- trimethylene-bis(thymine) **11** (ThC3Th)

Thymine **9** was reacted with TMS-Cl and triethylamine in toluene to introduce protecting groups at thymine O2 and O4 positions. This protecting reaction gave intermediate *O,O*'-bis(trimethylsilyl)thymine **10**, which is not stable at room temperature, so it was freshly prepared and used in the next step (**Scheme 14**).[83]

Compound **10** was converted to 1,1'-trimethylene-bis(thymine) **11** when supplied with 1,3-dibromopropane in DMF. The reaction was run for 24 h at 170 °C (**Scheme 14**). [83]

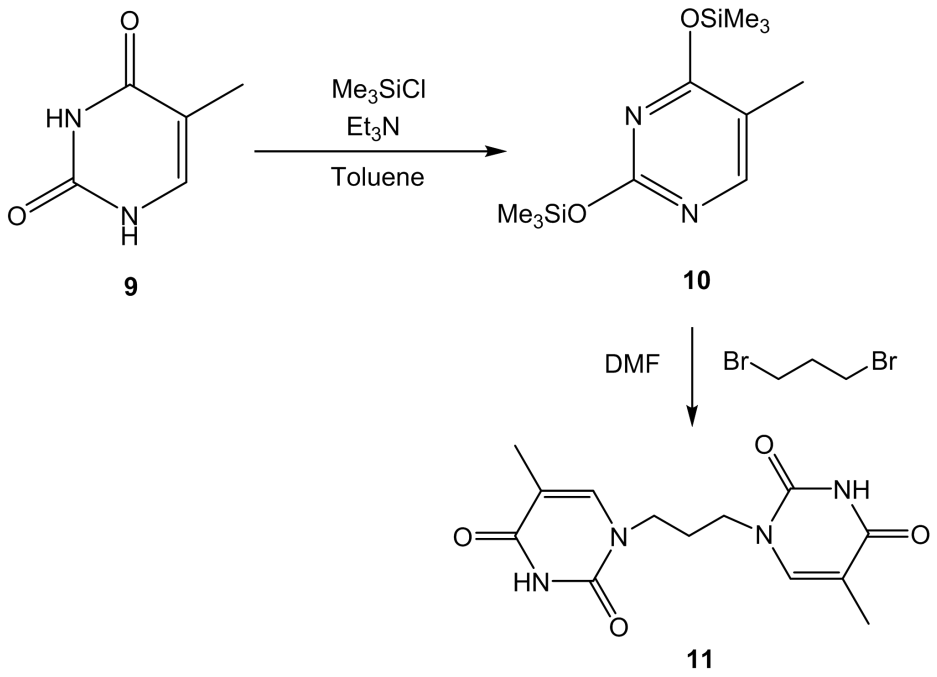

Scheme 14

Pure product **11** was obtained after filtration and washing with chloroform-methanol (1:1, 100 mL). Calculated from thymine **9**, the overall yield was 38 % less than the literature yield of 75%. The loss might occur in first step. TMS-Cl was considerably not freshly distilled, so the overall yield might be influenced. The literature reaction time of second step was 'overnight'. However, in our lab environment, the reaction did not reach the full conversion even after 24 h.

10.7. Synthesis of 1,1'- dimethylene-bis(thymine) **12** (ThC2Th)

Similar to the synthesis of 1,1'- trimethylene-bis(thymine), thymine was first converted to intermediate **10**. Then 1,2-dibromoethane was added to the solution of compound **10** in anhydrous DMF to give 1,1'- dimethylene-bis(thymine) **12** (**Scheme 15**).[83] This reaction was run for 36 hours at 170 °C. This *N1*-alkylation of thymine prefered to follow the S_N2 mechanism, so it was sensetive to steric effects. For the same reason as the *N9*-alkylation of adenine, short alkane chain allowed severer steric hindrance from the attached thymine group. Hence the disubstitution rate of 1,2-dibromoethane was lower than that of 1,3-dibromopropane.

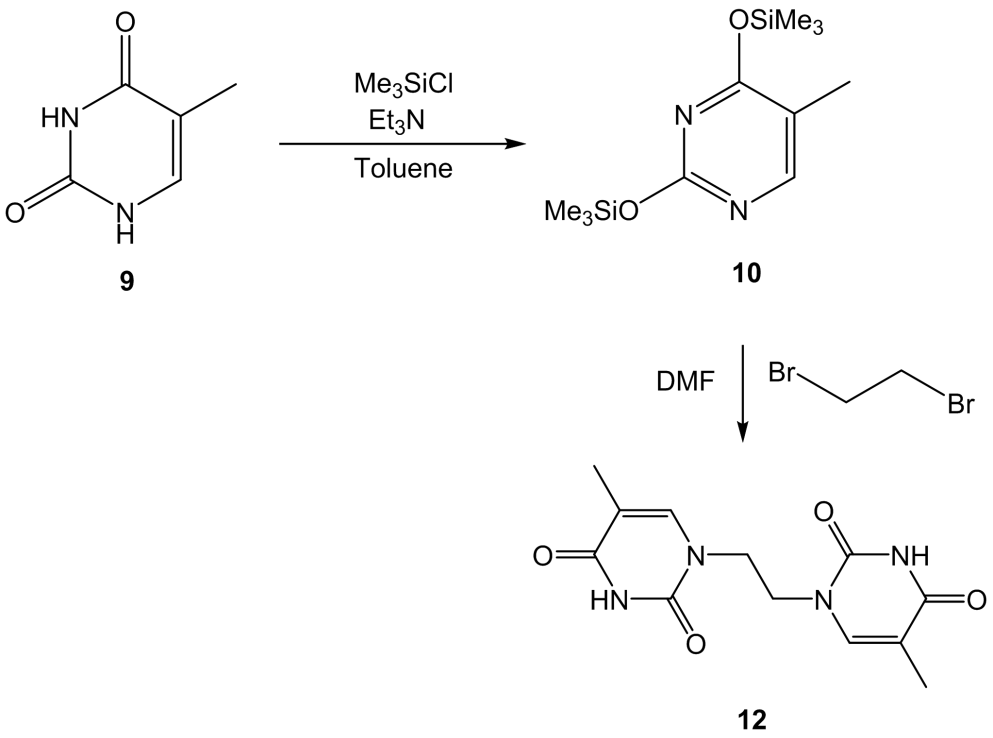

Scheme 15

The same purification method as for compound **11** worked well here. Based on the amount of thymine, the overall yield of product **12** was 50 %.

10.8. Attempted synthesis of tetrakis(1-thyminylmethyl)methane **13**

According to the syntheses of 1,1'- trimethylene-bis(thymine) and tetrakis(9-adeninylmethyl)methane, thymine was firstly protected with triethylamine and TMS-Cl to form the intermediate *O,O*'-bis(trimethylsilyl)thymine **10**, which was treated with reagent **7** in anhydrous DMF for *N*-alkylation (**Scheme 16**).[83] For the same reason as for adenine, this reaction was considered to follow the S_N1 mechanism with low reactivity. [42]

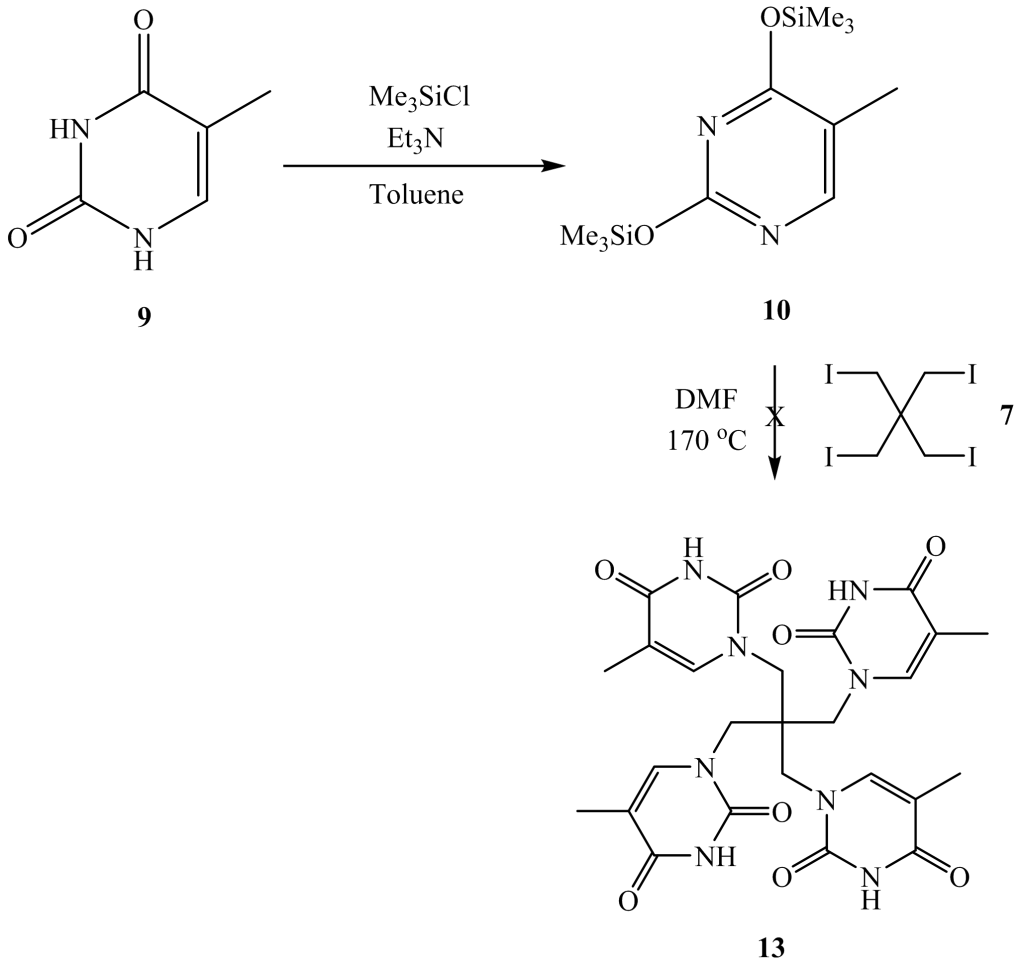

9 **10** **13**

Scheme 16

The reaction was run for eight days, but the conversion was still low. Four products were observed from TLC plate, and the crude product (68 mg) was applied to flash chromatography. The major fraction eluting from the column was iodine, and it partly sublimated into the rotavapor. The other fractions containing only one spot were too small for the structures to be confirmed (**Table 4**). From the ^{1}H NMR spectrum of the crude product, there was no corresponding signal of target compound **13**.

Table 4: result of flash chromatography

68 mg of material was applied onto the column

Eluent : MeOH in DCM	Fractions	# of spots on TLC plate	Weight
1 %	1-26	No UV visible spot	21 mg*
	28-34	1	<1 mg
	35-41	2	<1 mg
3 %	42-47	3	<1 mg
	50-55	2	<1 mg
	57-61	1	<1 mg
5 %	63-70	2	ca.2 mg
	71-74	-	-
10 %	75-78	-	-
	79-87	1	<1 mg
	88-93	-	-

* 21 mg iodine collected after the column.

10.9. Synthesis of 1,3,5,7-tetrabromoadamantane **15**

Both $AlCl_3$ and $AlBr_3$ can be used as Lewis acid in the halogenation reaction of adamantane **14** and bromine (**Scheme 17**).[115] When using $AlCl_3$, there was always around 5 % of 1-chloro-3,5,7-tribromoadamantane **15a** in the main product 1,3,5,7-tetrabromoadamantane **15**. When $AlBr_3$ was applied, compound **15** was the only product, and the yield reached 91 %.

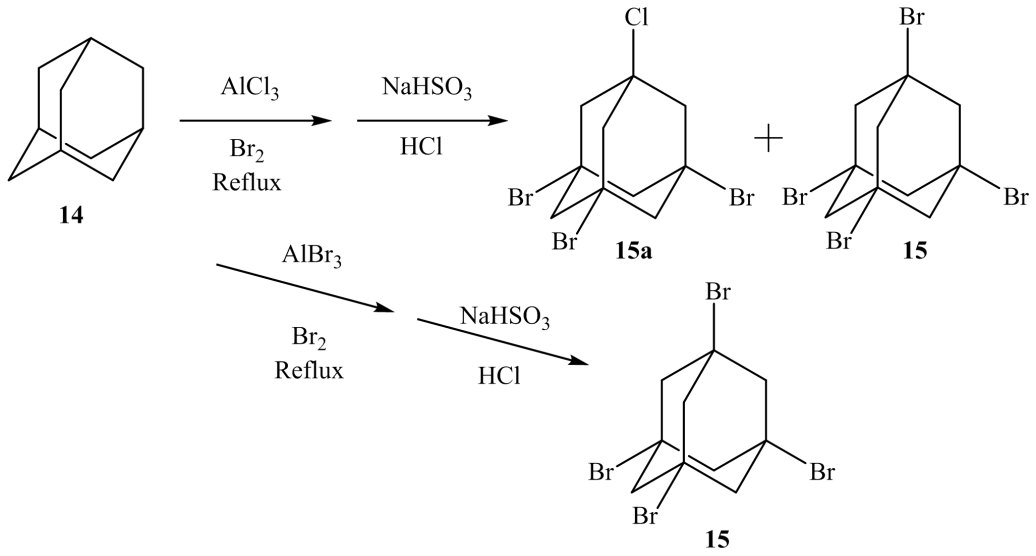

Scheme 17

10.10. Attempted synthesis of 1,3,5,7-tetraiodoadamantane **16**

The halogen replacement reaction from bromide **15** to iodide **16** was reported (**Scheme 18**).[115]

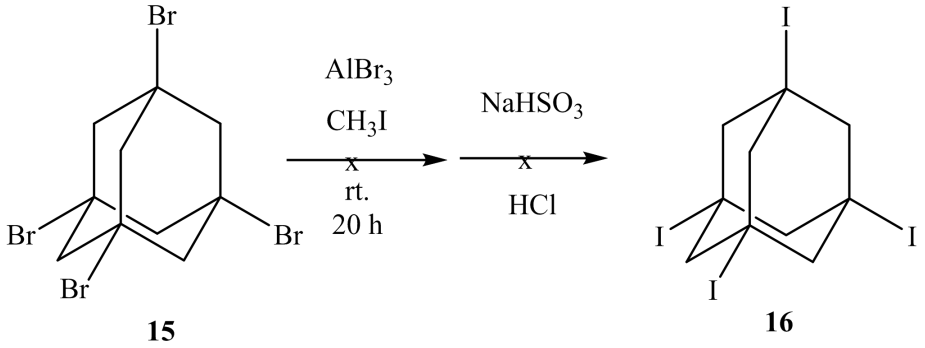

Scheme 18

In practice this reaction did not occur. One possible reason was that $AlBr_3$ was too sensitive to the moisture, so that the visible orange smoke was immediately observed while opening the reagent bottle. As a Lewis acid, $AlBr_3$ reduced the reactivity once it absorbed moisture, especially when used in a small scale. To avoid the exposure to the air, $AlBr_3$ can be handled in glove box.

10.11. Attempted synthesis of 1,3,5,7-tetrathymineadamantane **17**

The synthesis of 1,3,5,7-tetrauraciladamantane has been reported.[116] Since thymine **9** and uracil have similar molecular structures and chemical properties for *N*-alkylation, we applied this route to thymine (**Scheme 19**). Unfortunately, in the original paper there was some conflicting information regarding the reaction temperature, which was stated to be both 60 °C and 160 °C. Both temperatures were tried independently.

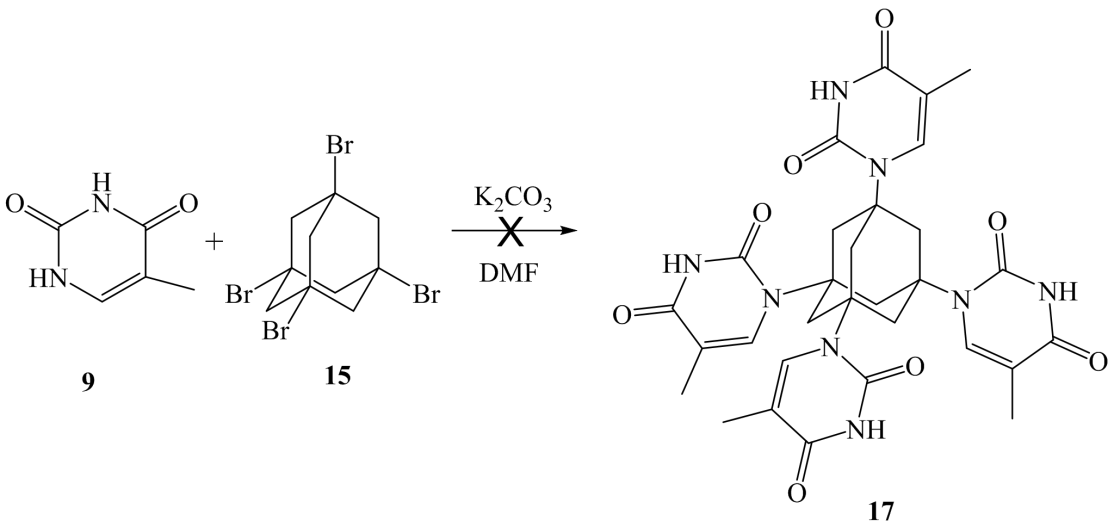

Scheme 19

This reaction was run for 48 hours at 60 °C and 24 h at 160 °C, but did not reach full conversion. From the ^{1}H NMR and MS spectra of the crude product, there was no signal or fragment that indicates the target compound **17**. Because of the three-dimensional structure of adamantane, the substituent cannot attack from the backside of bromine. In a S_N1 reaction, the strain at bridgehead carbon of adamantane restrains the formation of the planar carbocation intermediate at bridgehead position, so it makes this alkylation reaction difficult to realize.[117]

10.12. Synthesis of 1,3,5,7-tetrauraciladamantane **19**

Aiming at finding out any reason why the reported route failed when applied to thymine, we repeated the exact literature reaction with uracil **18** (**Scheme 20**).[116]

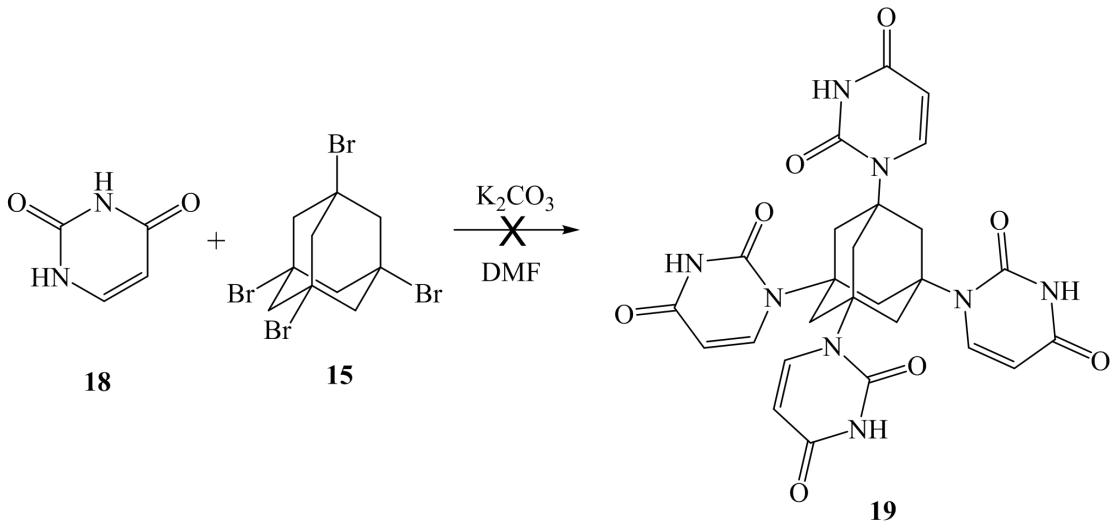

Scheme 20

Attempts were made at both 60°C and 160°C for 24 h, but neither reaction reached full conversion, nor gave the target product **19** compared to the literature data. We could not establish why the literature reaction was failed to work, but it was obvious that this alkylation with adamantane is difficult.

Regarding the structure of adamantane, this substitution should follow the S_N1 mechanism. As mentioned above, due to the rigid molecular structure, even S_N1 is difficult to realize. Based on the other *N*-alkylation reactions with adenine **1** and thymine **9**, thymine appeared to be more reactive than adenine.

Since the thymine *N*-alkylation with halogenated adamantane proved to be difficult, an alternative tetrahedral molecule, tetrakis(4-(bromomethyl)phenyl)methane **21** was attempted for *N*-alkylation of adenine and thymine to give node materials.

10.13. Synthesis of tetrakis(4-(bromomethyl)phenyl)methane **21**

The halogenations of the commercially available starting material tetraphenylmethane **20** has been realized with bromomethoxymethane and $TiBr_4$ as the Lewis acid to give the target compound tetrakis(4-(bromomethyl)phenyl)methane **21** with a reported yield of 60 % (**Scheme 22**).[118] The product was purified by column chromatography. In our case, the purification was simplified by recrystallization from dichloromethane, although the yield was a little lower as 58 %.

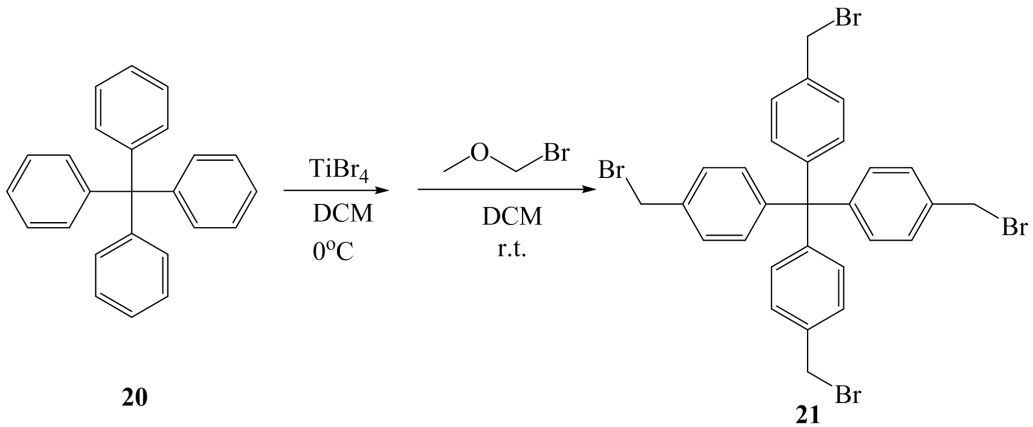

20 **21** **Schem e 22**

Similar to $AlBr_3$, the Lewis acid $TiBr_4$ is also very sensitive to moisture. The emitted orange smoke can be observed once the reagent bottle is opened. To avoid the loss of reactivity, the reaction should be carried out in a relatively large scale and with substantial excess of $TiBr_4$. Alternatively, a glove box could be used to handle this chemical. In our case, the reaction was in a large scale.

10.14. Synthesis of tetrakis(4-thyminylmethylphenyl)methane **22** (Th4)

From previous reactions it turned out that silylated thymine **10** could be completely dissolved in DMF, while unprotected thymine **9** existed in suspension form in the same amount of DMF. Considering their solubility, we designed the synthetic strategy described in **Scheme 23** according to the route for synthesis of 1,1'- dimethylene-bis(thymine) **12** using protected thymine.

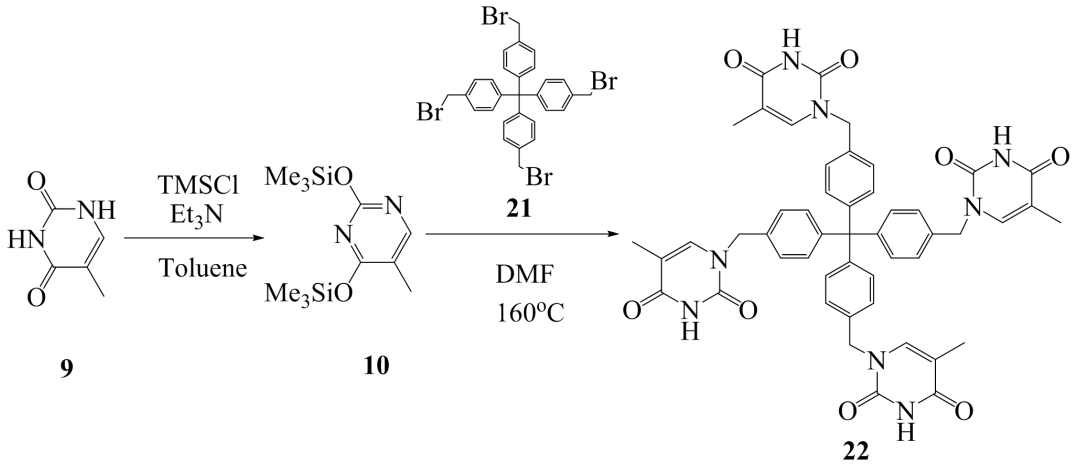

Scheme 23

Since the aromatic ring system helped to stabilize the carbocation as described above, this reaction provided a promising result. The structure of novel compound **22** was confirmed by ^{1}H NMR, ^{13}C NMR, MS (ESI) and single crystal X-ray diffraction. Although the yield (49 %) was not high, it was acceptable. The crowded molecular structure indicated a reason why this reaction required much heating and long time. This compound has high polarity and poor solubility. Hence the purification was reasonably challenging.

10.15. Synthesis of tetrakis(4-adeninylmethylphenyl)methane **23** (Ad4)

The strategy for synthesis of tetrakis(4-adeninylmethylphenyl)methane **23** was proposed in the light of route for 9,9'- dimethylene-bis(adenine) **2** synthesis (**Scheme 24**).

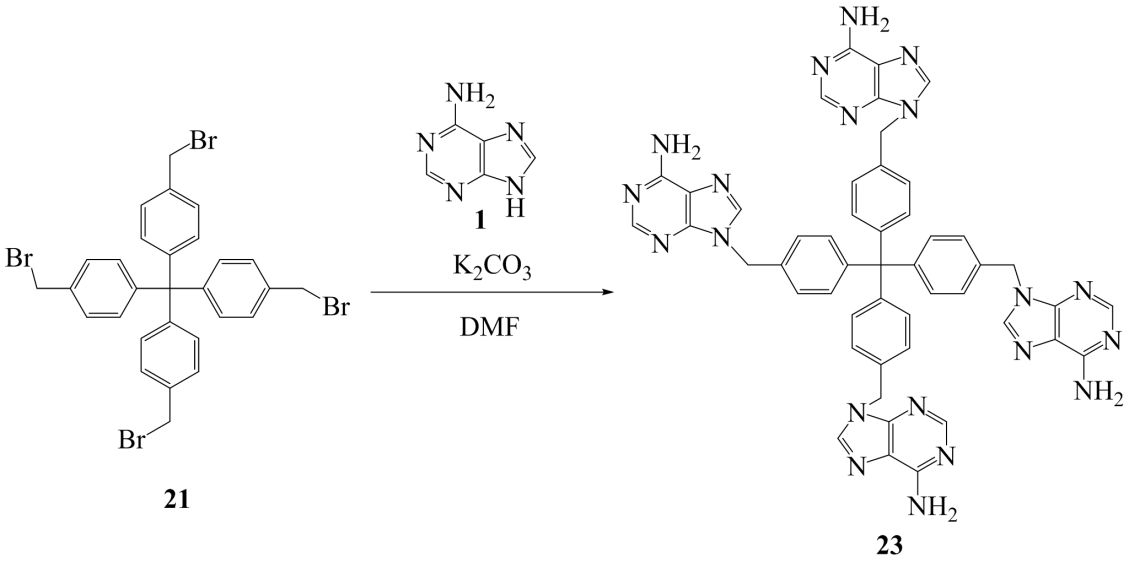

Scheme 24

This novel compound was confirmed by ^{1}H NMR, ^{13}C NMR and MS (ESI). Due to the poor solubility and high polarity of each component in the crude product, the purification turned out to be challenging. Based on the TLC plate, there was a serious trailing phenomenon. Flash chromatography was utilized with an eluent system of 5 % MeOH saturated with NH_3 in DCM. The use of NH_3 aimed to improve the trailing. After twice of flash chromatography, the purity was enhanced to 93%.

Unfortunately, during the third time of purification, a large amount of silicone grease was introduced from external environment by mistake, so the product was contaminated.

11. Crystal growth

11.1. Choice of solvent and precipitating reagent

For all the linker materials, AdC2Ad (**2)**, AdC3Ad (**3**), ThC2Th (**11**) and ThC3Th (**12**), and the node compound Th4 (**22**), considerable effort was put into the testing of solubilities in common solvents ranging from organic to inorganic, from low polarity to high polarity. DMSO, DMF, MeOH, MeCN, H_2O, 2-propanol (IPA), 1,1,1,3,3,3-hexafluoro-2-propanol (HFP) and DCM were tried. HFP was the only one which could dissolve all the compounds at room temperature, even though it took about 10 minutes before the solution of AdC2Ad (**2)** became clear. In DMSO, much heating was needed to achieve limited solubility. Linker compounds AdC2Ad (**2)** and AdC3Ad (**3**) had lower but little different solubility than linker ThC2Th (**11**) and ThC3Th (**12**), but much lower solubility than node compound Th4 (**22**) under the same conditions. For the other solvents, the solubility of all the compounds was extremely low. Interestingly, the Th4 node compound could be completely dissolved in a solvent mixture of MeOH-DCM, but not any of the linker compounds. For crystal growth experiments with vapor diffusion technique, a range of precipitating reagents, including DCM, MeOH, MeCN, H_2O, EtOAc and IPA, were attempted with the linker and node compounds.

11.2. Crystal formation

The crystal growing procedures showed that in most of setups containing mixed materials, two compounds always precipitated from the solution separately and in different shapes (**Table 5**). The solvent system of MeOH-DCM was tested for Th4 crystal growth.

Table 5: Results of crystallization experiments

Materials	Methods	Results
Th4	HFP Slow evaporation	Long needle-shaped crystals
Th4	DMSO Slow evaporation	Needle-shaped crystals
Th4	MeOH&DCM-MeCN Vapor diffusion	Amorphous powder
Th4-AdC2Ad	HFP Slow evaporation	Needle-shaped crystals
Th4-AdC2Ad	HFP-EtOAc Vapor diffusion	Beads
Th4-AdC2Ad	HFP-MeOH Vapor diffusion	Needle-shaped crystals and beads*
Th4-AdC2Ad	HFP-DCM Vapor diffusion	Plate-shaped crystals*
Th4-AdC2Ad	HFP-MeCN Vapor diffusion	Beads
Th4-AdC2Ad	HFP-H_2O Vapor diffusion	Tiny crystals and beads
Th4-AdC3Ad	HFP-MeOH Vapor diffusion	Needle-shaped crystals and beads
Th4-AdC3Ad	HFP-DCM Vapor diffusion	Plate crystals
Th4-AdC3Ad	HFP-IPA Vapor diffusion	Needle-shaped crystals and beads*
Th4-AdC3Ad	HFP-H_2O Vapor diffusion	Tiny crystals and beads
Th4-AdC3Ad	HFP-MeCN Vapor diffusion	Beads

Note: 1) * From this experiment, crystal was picked for single crystal XRD data collection. 2) Beads indicate the ball-shaped non-crystalline powder with the size < 0.1mm.

The node compound Th4 (**22**) was crystallized from both DMSO and HFP separately. Long, thin needle-shaped colorless crystals were observed from HFP (**Picture 1**), while small needle-shaped crystals formed from DMSO.

Picture 1: Long, thin needle-shaped crystals sticked to the wall of the vial.

For most of the experiments containing two compounds, crystals and beads forming in different rates were visible. A general appearance is shown as **Picture 2**.

Picture 2: Small beads stick on the wall and the crystals lie at the bottom of the vial.

A possible explanation for this phenomenon was based on the solubility. When two compounds have quite different solubilities in a solvent, the less soluble one reached the saturation concentration earlier than the other one, so they precipitated after quite different periods. In this occasion it was not prospective to form complex of these two compounds, and this was confirmed by single crystal XRD tests.

11.3. Stability

As indicated in **Table 5**, we managed to harvest some promising crystals for single crystal XRD experiments. The needle-shaped crystals from Th4-AdC3Ad in HFP-MeOH system were unstable after being removed from the mother liquor evidently due to the loss of co-crystallized solvent as were the crystals from Th4-AdC3Ad in HFP-IPA system. Hence, flash freezing in liquid nitrogen was used to stabilize the crystals before being transferred to the cold stream on the diffract meter for data collection at 100K. The plate crystal from Th4-AdC2Ad in HFP-DCM system was stable enough at room temperature without any special treatment.

12. X-ray diffraction experiments

12.1. Powder XRD attempts with linker materials only

To explore any possibility of combination between two types of linker molecules, ThC2Th **12** and AdC2Ad **2,** several treatment methods were tried as in **Table 6**.

Table 6: Attempts for forming the complex of ThC2Th and AdC2Ad

Material	Treatment	Result
ThC2Th	-	Reference (**Figure A1**)
AdC2Ad	-	Reference (**Figure A2**)
ThC2Th~AdC2Ad	HFP-MeOH Vapor diffusion	No complex (**Figure A3**)
ThC2Th~AdC2Ad	Grind in H_2O	No complex (**Figure A4**)
ThC2Th~AdC2Ad	Grind in DMSO	No complex (**Figure A5**)
ThC2Th~AdC2Ad	Grind in toluene	No complex (**Figure A6**)
ThC2Th~AdC2Ad	Grind in acetic acid	No complex (**Figure A7**)
ThC2Th~AdC2Ad	Ultrasonic, 5h, DMSO	No complex (**Figure A8**)
ThC2Th~AdC2Ad	Ultrasonic, 5h,H_2O	No complex (**Figure A9**)
ThC2Th~AdC2Ad	Ultrasonic, 5h, toluene	No complex (**Figure A10**)
ThC2Th~AdC2Ad	210 ^oC, 5 min	No complex (**Figure A11**)
ThC2Th~AdC2Ad	250 ^oC	No complex (**Figure A12**)
ThC2Th~AdC2Ad	300 ^oC	No complex (**Figure A13**)
ThC2Th~AdC2Ad	350 ^oC	Color change Decomposed (**Figure A14**)

Note: **Figure A1-A14** corresponding to powder XRD patterns are shown in Appendix.

Compared to the PXRD spectra of ThC2Th (**12)** AdC2Ad (**2),** in **Figure A3- A14** there was no any new signal indicating the formation of aimed complex of ThC2Th and AdC2Ad. It might because the intermolecular H-bonds of each compound might be so strong that they could not be broken even with molecular environment or thermodynamics intervention. Since ThC3Th has similar structure and solubility with ThC2Th, and AdC3Ad is similar to AdC2Ad, it was not essential to try the same experiments for them.

12.2. Single crystal XRD

12.2.1. Crystal from Th4-AdC3Ad in HFP-MeOH system

The structure was solved and refined with SHELXL-2013 to give the information in **Table 7**. The diffuse electron density from unidentified, disordered solvent molecules was initially refined to an *R*-factor of 0.1503. All solvent atoms were subsequently removed from the model, with electron density within the resulting void being efficiently removed by the SQEEZE routine of the PLATON program. Based on the new, corrected diffraction data file output from SQEEZE, further structural refinement brought the final *R*-factor down to 0.0727.

The XRD data defined this crystal as a crystalline framework of node compound Th4 (**Figure 26**). The framework was assembled via H-bonds. An asymmetric unit contains two Th4 molecules and one methanol molecule.

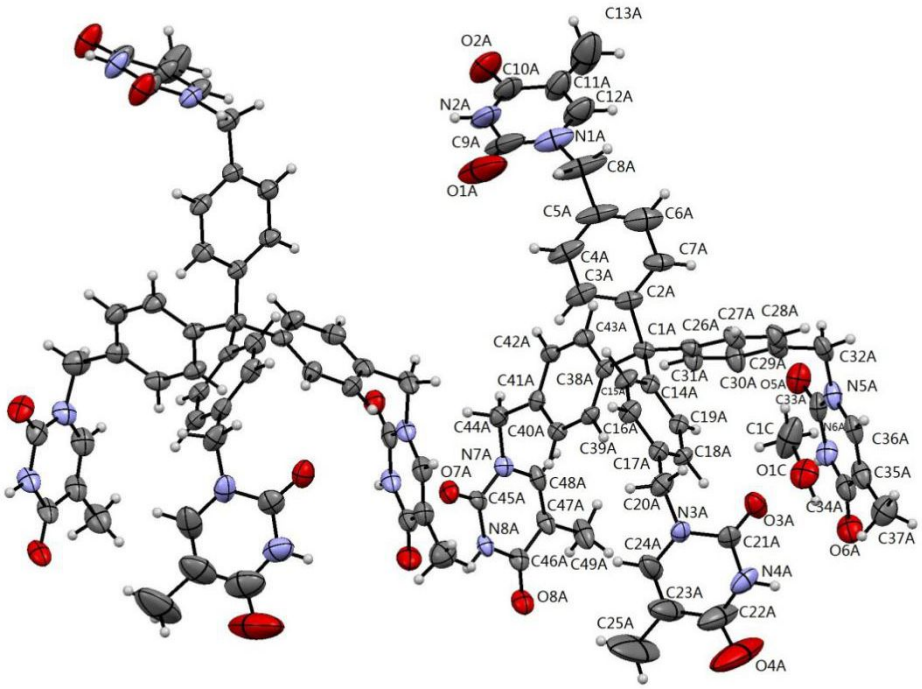

Figure 26: Two independent Th4 (**22**) molecules and one MeOH molecule in the asymmitric unit of *–x,-y,-z*. Thermal displacement ellipsoids are shown at the 50 % probability level.

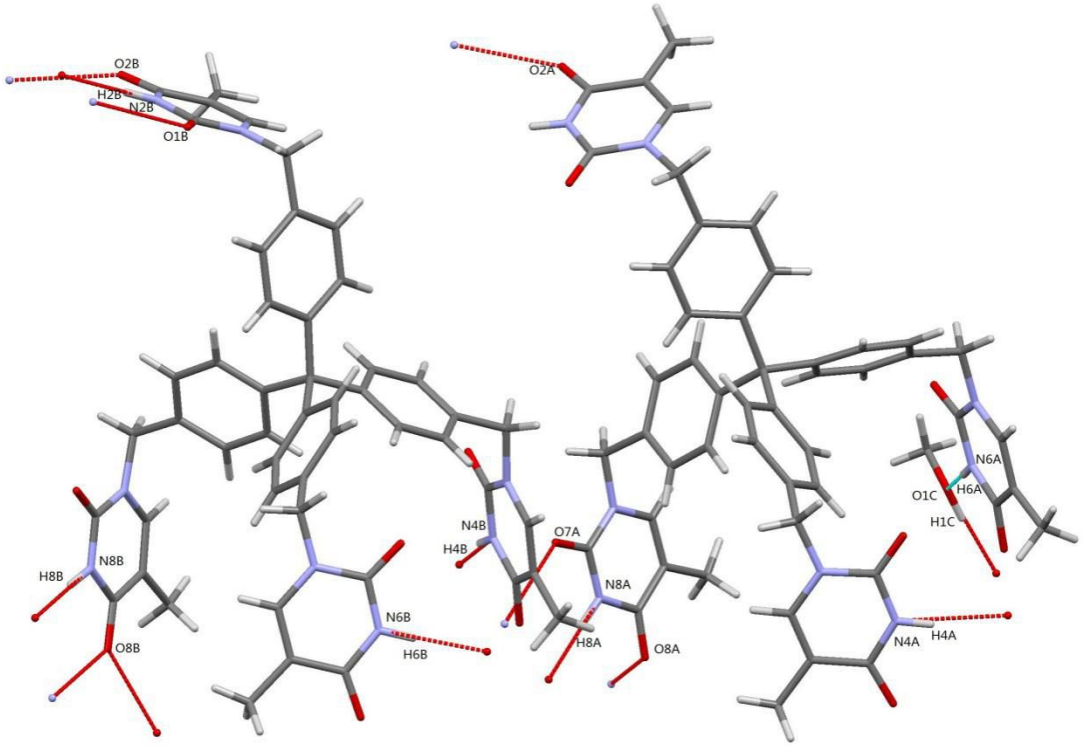

Figure 27: The hydrogen bonding sites of each Th4 (**22**) molecule are labeled. Hydrogen bonds are shown as dashed lines.

In a hydrogen bonding pattern (**Figure 27**), molecule A (right) bonds to this MeOH molecule via one hydrogen bond. Three side-chains of this molecule connect to adjacent one through one hydrogen bond, while the other side-chain forms three hydrogen bonds. In molecule B (left), two of its side-chains have three binding site and the other two have only one. It is noticeable that O8B as an acceptor forms two hydrogen bonds at one site. The crystal packing form of Th4 is shown in **Figure 28**.

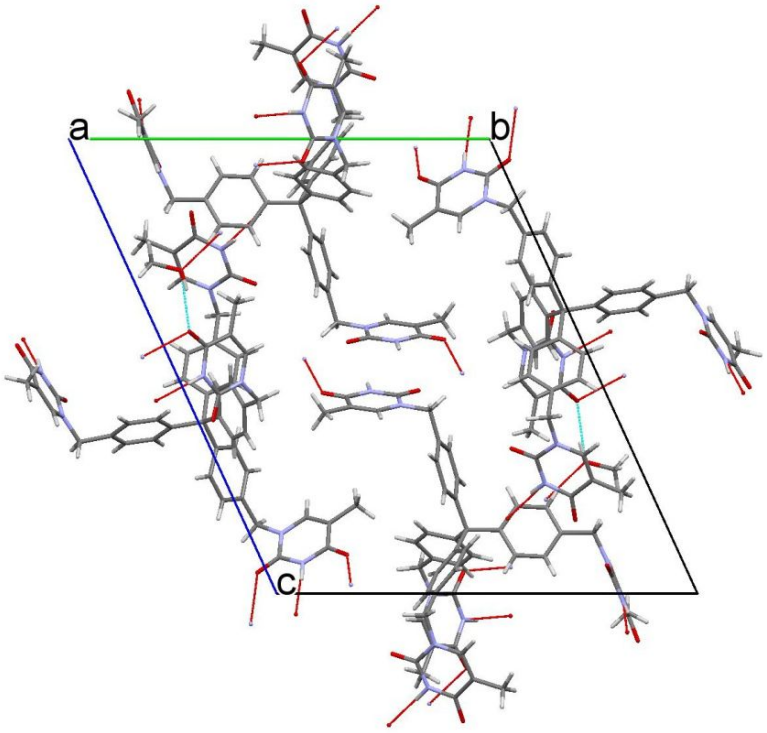

Figure 28: Crystal packing form of Th4 (**22**) viewed along the *a* axis. Hydrogen bonds are shown as dashed lines.

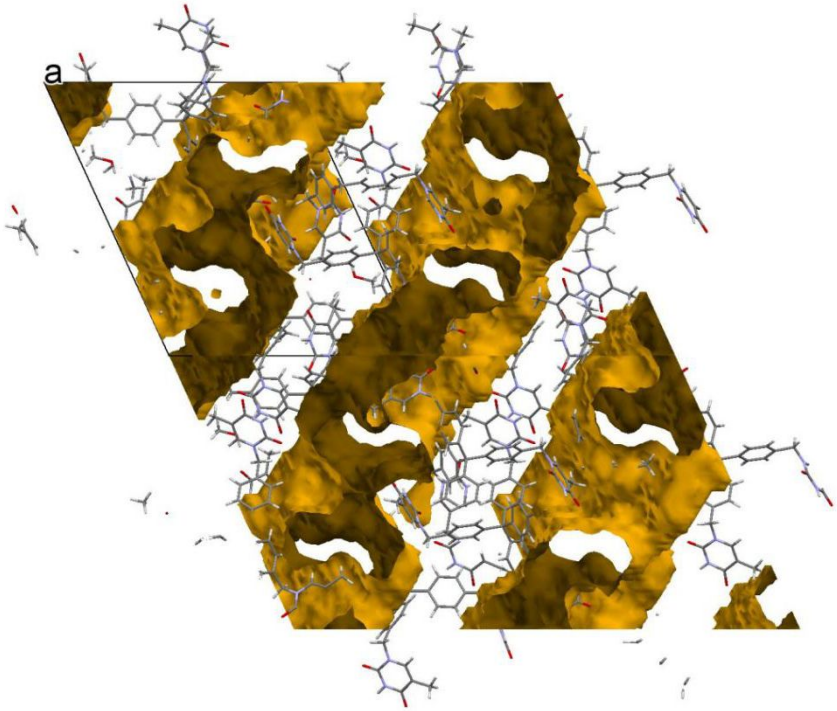

Figure 29: Crystal packing form of Th4 (**22**) viewed along the *a* axis. The void space after removing all the disordered solvent molecules was calculated by Mercury using a 1.2 Å probe radius and 0.5 Å grid spacing. The void surface is colored yellow

Channel system in this type of framework is two-dimensional, and the void volume after removal of disordered solvent molecules was calculated to 2086 $Å^3$ by SQEEZE, accounting for 35 % of the unit cell volume (**Figure 29**). When rotating the crystal packing form along the axis vertical to *bc* plane, we can see how the 2D channels exist (**Figure 30**).

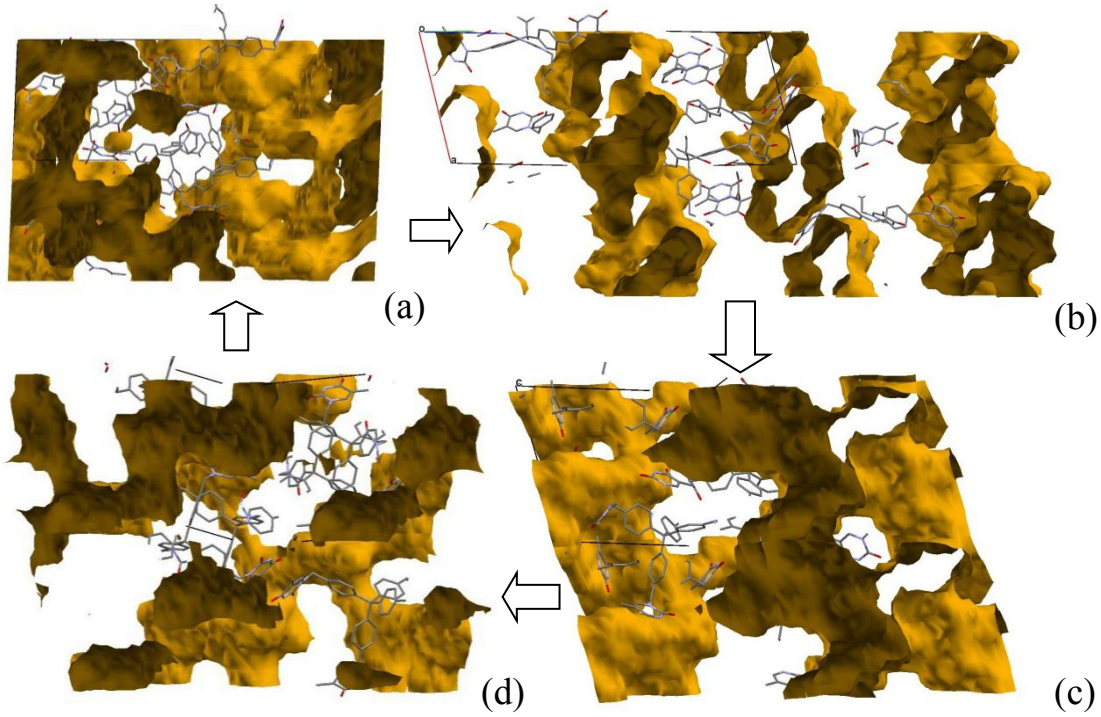

Figure 30: Rotation of crystal packing form of Th4 (**22**) from (a) viewed along *b* axis, to (b) paralleled 2D channels, to (c) opposite view of (a), to (d)

Table 7: XRD data of Th4 crystal from HFP-MeOH

Crystal data	
Chemical formula	$C_{49}H_{44}N_8O_8$
Mr	872.94
Space group	Triclinic *P*-1
Cell	*a* = 14.4613(17) Å α = 65.194(3) *b* = 20.326(2) Å β = 85.341(3) *c* = 23.303(2) Å γ = 73.765(3)
V (Å$^{3)}$	5964.7(12)
Solvent Accessible Volume (Å$^{3)}$	2085.3
Z	8
Radiation	Mo *Kα*
wavelength	0.71073
μ (mm^{-1})	0.069
Temperature (K)	100
Data collection	
T_{min}, T_{max}	0.742, 0.998
Measured reflections	88019
Independent reflections	16010
Reflections with $I > 2\sigma(I)$	10446
R_{int}	0.0727
Refinement	
$R[F^2 > 2\sigma(F^2)]$	0.0727
$wR(F^2)$	0.1814
No. of reflections	16010
No. of parameters	1201
$\Delta\rho_{max,}$ $\Delta\rho_{min}$	0.597 -0.279

12.2.2. Crystal from Th4-AdC3Ad in HFP-DCM system

The structure was solved and refined with SHELXL-2014 to give the information in **Table 8**. This crystal was confirmed as a crystalline framework of linker compound AdC2Ad with participation of four times of solvent (HFP) molecules (**Figure 31**). The framework was assembled via H-bonds described in **List 2.**

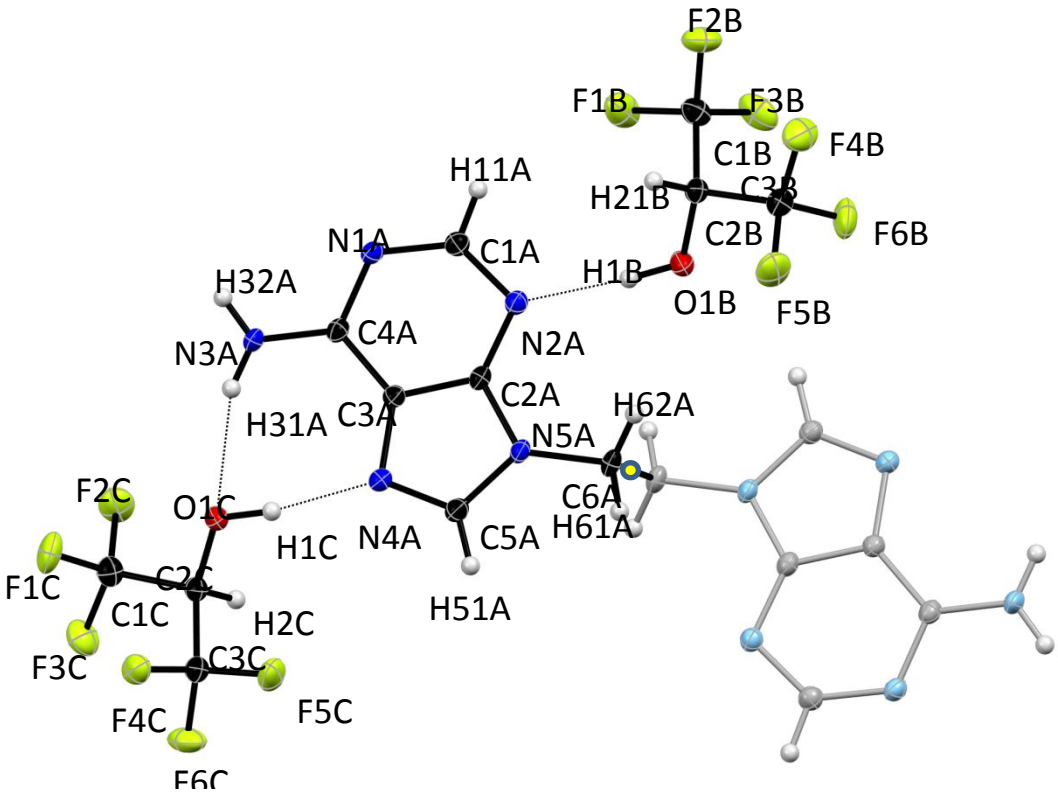

Figure 31: The molecular structure of AdC2Ad tetrahexafluoro -2-propanol solvate. Thermal displacement ellipsoids are shown at the 50 % probability level. The right half of the AdC2Ad molecule (atoms in lighter color) is generated from the left part by center-of-symmetry (small circle with yellow fill) with code $-x+1, y, -z+1$.

The symmetric molecules assembled into a crystal network via hydrogen bonds with HFP solvent molecules as a part of building unit (**Figure 32**).

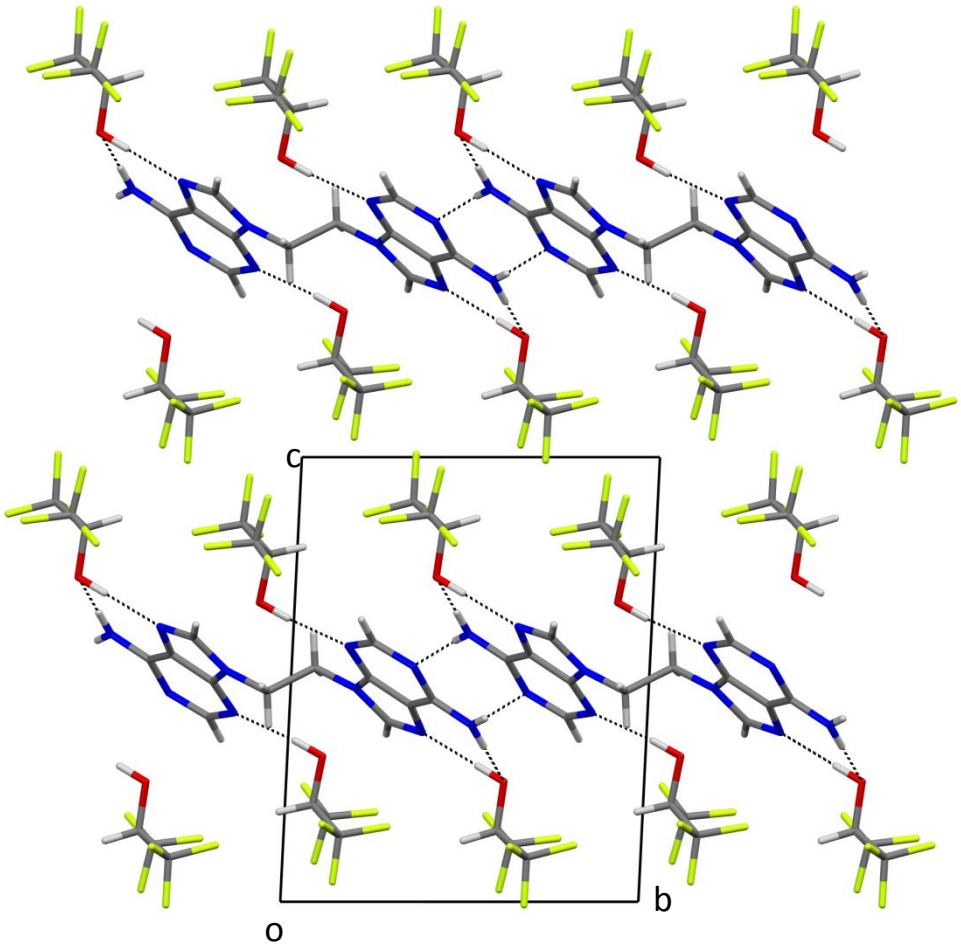

Figure 32: Crystal packing viewed along the *a* axis. Dashed lines: hydrogen bondS.

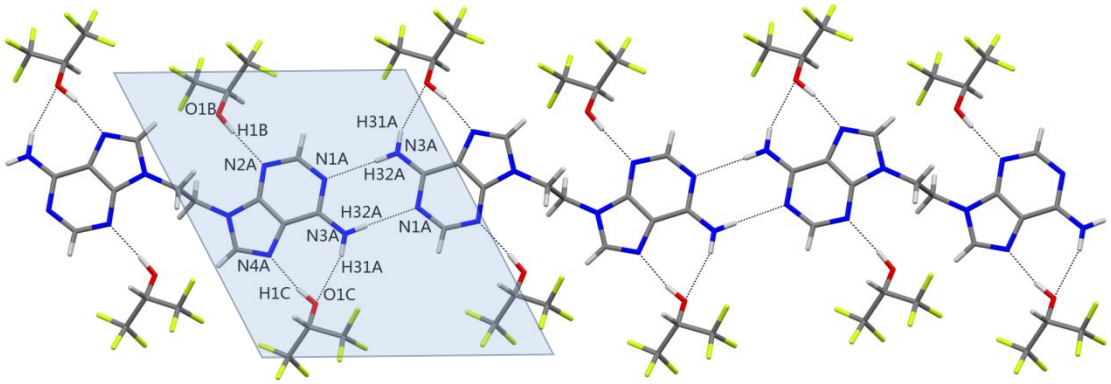

Figure 33: Hydrogen-bonded tape motif of AdC2Ad molecules supported by the solvent molecules. O1C acts as both a donor and an acceptor, while O1B is less tightly bound and acts only as a donor to N2A.

The AdC2Ad molecules are connected by a N1A···H32A-N3A (–*x* +1, *y*, –*z* + 1) hydrogen bonded tape (**Figure 33**). HFP molecules paticipate a N1A···H32A-N3A-H31A···O1C hydrogen donded chain in this framework. Considering the high solvent content in these crystals, it is remarkable that they are stable at room temperature. This framework is a densely packed structure of stacked layers, and there is no a channel or pore through this network. The layer can be described as a sandwich form, for which the solvent molecules act as 'bread' and AdC2Ad molecules is the filling.

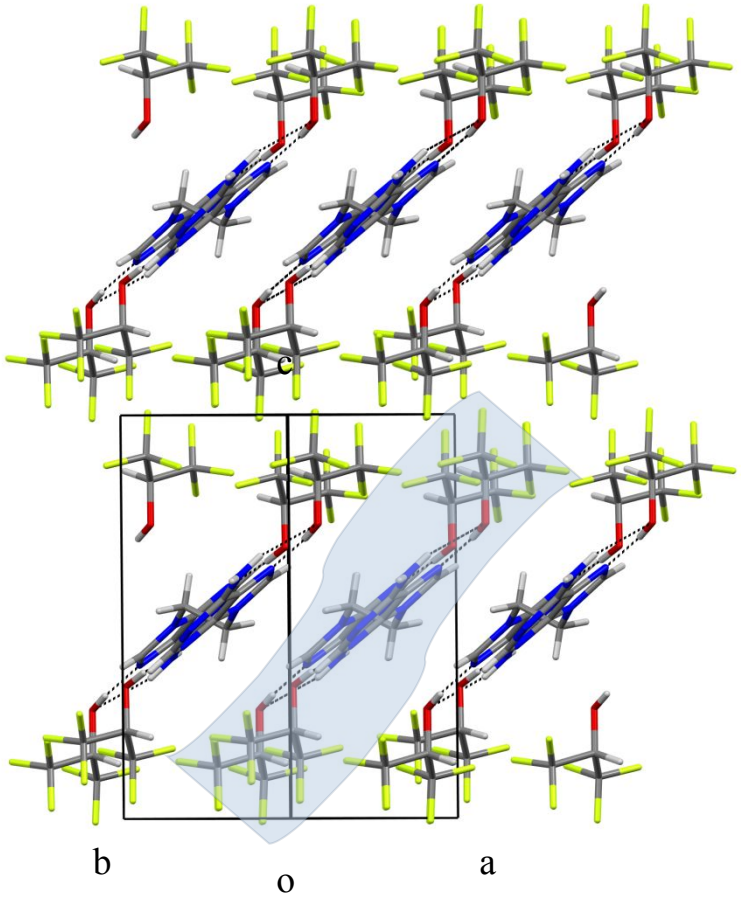

Figure 34: Stacking of hydrogen-bonded tapes along the *ab*-diagonal.

Table 8: XRD data of type AdC2Ad crystalline network

Crystal data	
Chemical formula	$C_{12}H_{12}N_{10}$
Mr	296.30
Space group	Triclinic *P*-1
Cell	*a* = 7.1752(7) Å *α* = 86.613(2) *b* = 10.3078(10) Å *β* = 87.488(2) *c* = 12.3995(12) Å *γ* = 71.906(2)
V (Å$^{3)}$	869.89(15)
Solvent Accessible Volume (Å$^{3)}$	1
Z	Mo *Kα*
Radiation	0.71073
wavelength	0.213
μ (mm^{-1})	100
Temperature (K)	
Data collection	0.994, 0.997
T_{min}, T_{max}	21096
Measured reflections	4878
Independent reflections	3936
Reflections with $I > 2\sigma(I)$	0.0281
R_{int}	
Refinement	0.0365
$R[F^2 > 2\sigma(F^2)]$	0.0818
$wR(F^2)$	4878
No. of reflections	319
No. of parameters	
$\Delta\rho_{max}$, $\Delta\rho_{min}$	

12.2.3. Crystal from Th4-AdC2Ad in HFP- IPA system

The structure was solved and refined with SHELXL-2013 to give the information in List 3. Electron density from disordered solvent molecules was first refined to an *R*-factor of 0.1335. All solvent atoms were subsequently removed from the model by the SQEEZE routine of the PLATON program. Based on the new, corrected diffraction data file output from SQEEZE, further structural refinement brought the final *R*-factor down to 0.0796.

The result showed this crystal was also a crystalline framework of node compound Th4 with presence of solvent molecules (**Figure 35**). The framework was assembled via H-bonds described in **Table 9.**

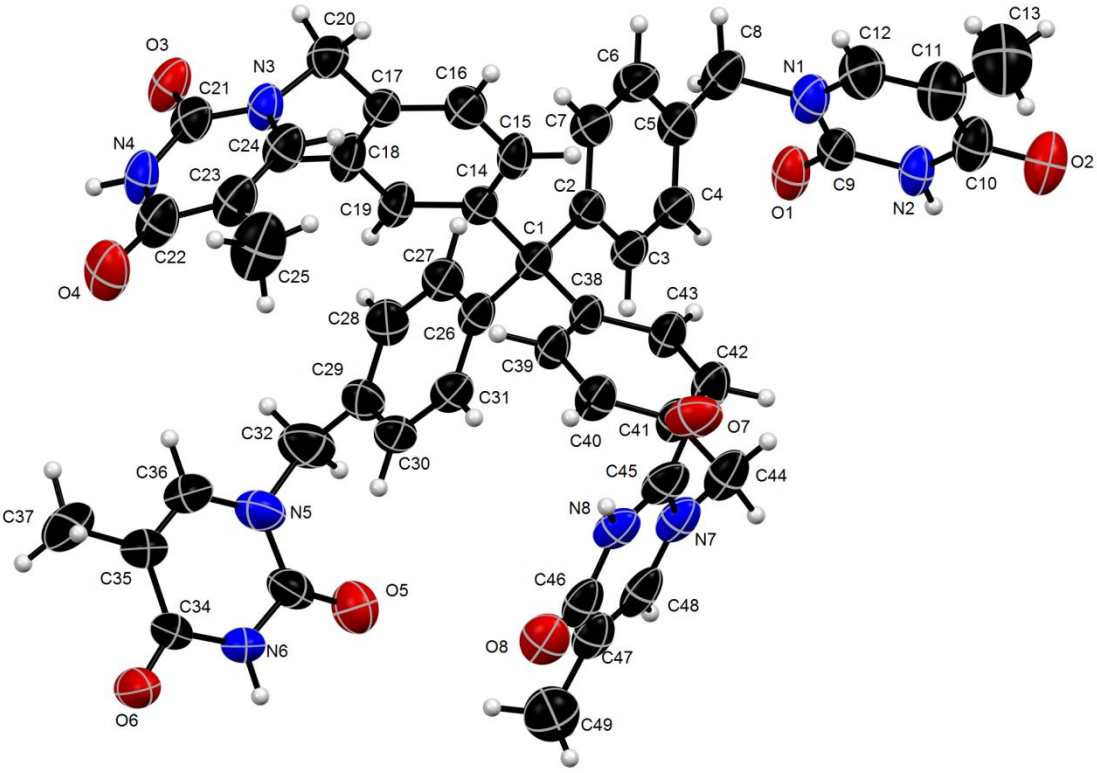

Figure 35: The molecular structure of Th4 (**22**) with the atomic numbering. Thermal displacement ellipsoids are shown at the 50 % probability level.

This compound forms the framework by intermolecular hydrogen bonds (**Figure 36**). Due to the overlay of atoms in one side-chain, a rotated view of this part is provided to the top right.

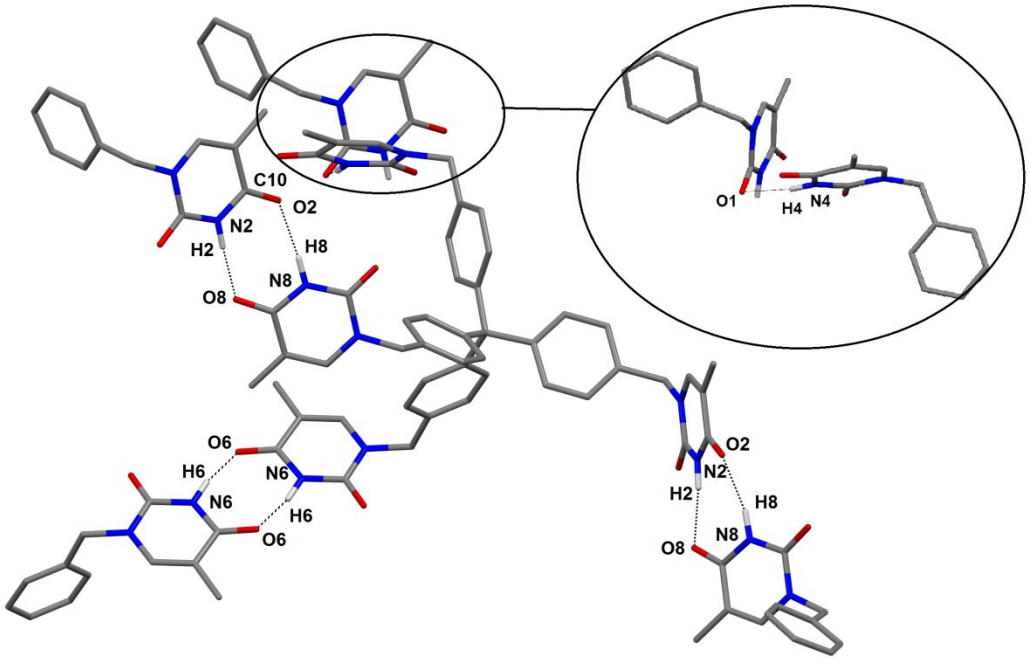

Figure 36: The hydrogen bonding sites of Th4 (**22**) molecule are labeled. Hydrogen bonds are shown as dashed lines.

Each Th4 molecule connects to the adjacent one via hydrogen bonds. In three side-chains, two hydrogen bonds present into a tape for each of them, while for the fourth arm, only one hydrogen bond forms to link two molecules. The two hydrogen bonds establish an eight number ring system with less flexibility than single bond. In this way, the molecules pack into a 3D framework with an unusual large void, which stabilized by numerous solvent molecules (**Figure 37, 38**).

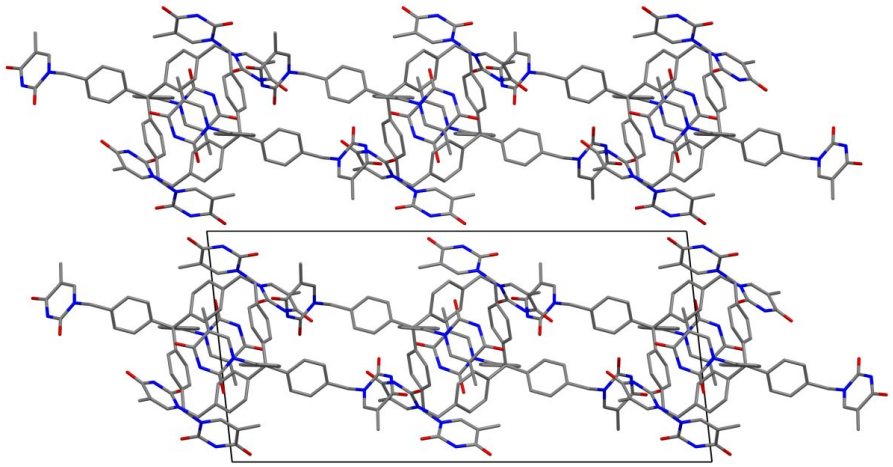

Figure 37: Crystal packing form of Th4 (**22**) viewed along the *b* axis without showing thehydrogen bonds.

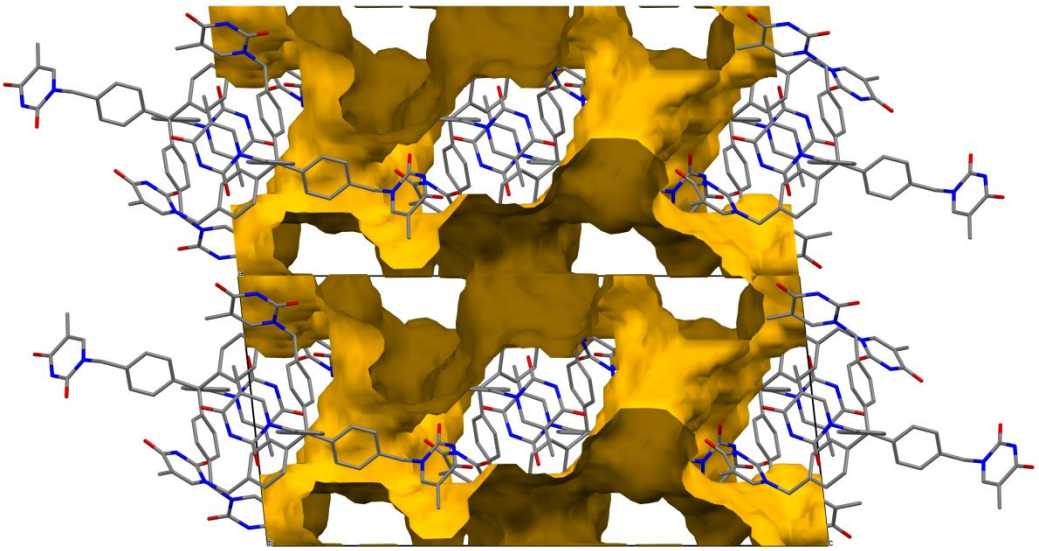

Figure 38: Crystal packing of Th4 (**22**) viewed along the b axis showing the void volume after removal of solvent molecules, as calculated by Mercury using a 1.2 Å probe radius and 0.5 Å grid spacing.

To view observe the three dimensional structure of the channels, an illustration shows the slices of a channel (**Figure 39**). Cuts was made at 3 Å intervals. The *c* axis is approximately 15 Å, so after five steps the cycle repeated as shown. From above figures three-dimensional channel can been seen extending throughout the whole network. According to the calculation by Mercury, channels account for 46 % of unit cell volume was channel.

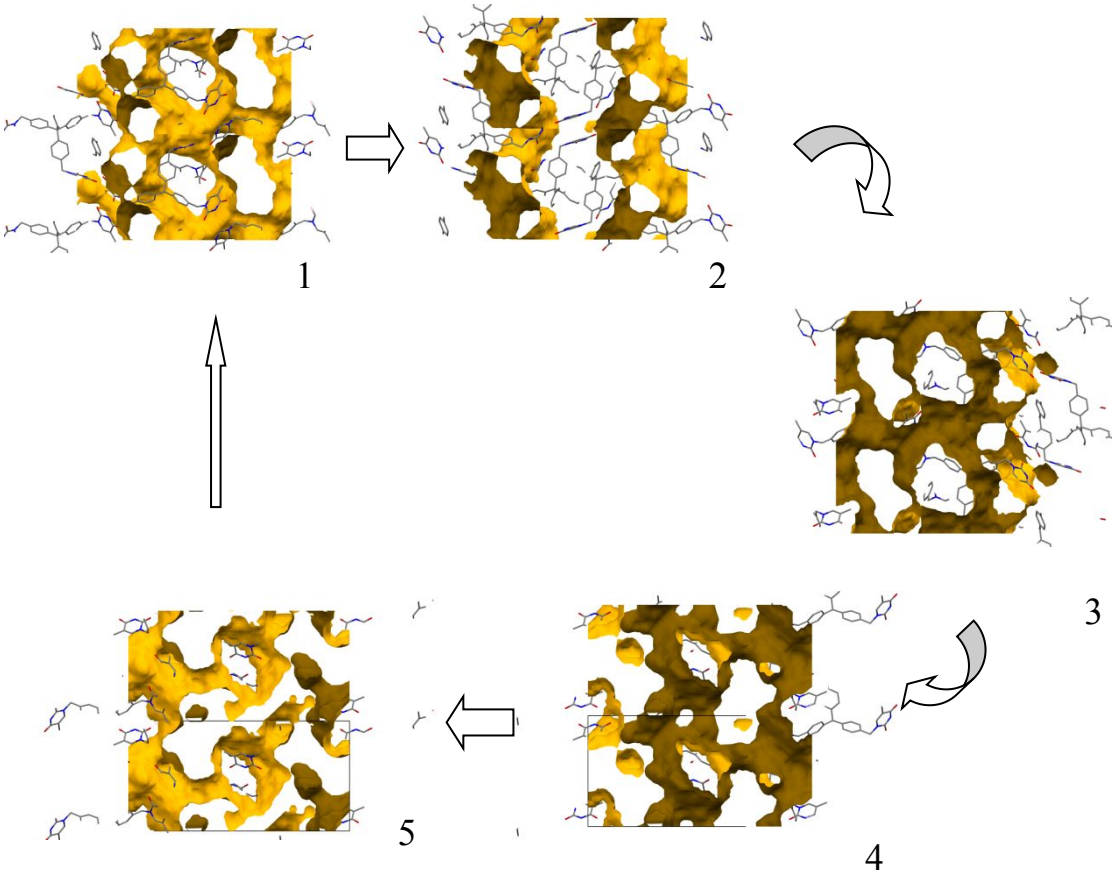

Figure 39: A series of five 5 Å thick slices of the crystal structure of Th4 viewed along the *c* axis. They illustrate the extended system of channels.

Table 9: XRD data of type B Th4 crystalline network

Crystal data		
Chemical formula	$C_{49}H_{44}N_8O_8$	
Mr	872.94	
Space group	Monoclinic *P* 21/c	
Cell	*a* = 14.9614(17) *b* = 15.2536(16) *c* = 30.990(4)	α = 90 β = 96.288(3) γ = 90
V (Å$^{3)}$	7029.9(14)	
Solvent Accessible Volume (Å$^{3)}$	3306.5	
Z	4	
Radiation	Mo *Kα*	
wavelength	0.71073	
μ (mm^{-1})	0.057	
Temperature (K)	100	
Data collection		
T_{min}, T_{max}	0.742, 0.998	
Measured reflections	88019	
Independent reflections	16010	
Reflections with $I > 2\sigma(I)$	10446	
R_{int}	0.0727	
Refinement		
$R[F^2 > 2\sigma(F^2)]$	0.0727	
$wR(F^2)$	0.1814	
No. of reflections	16010	
No. of parameters	1201	
$\Delta\rho_{max}$, $\Delta\rho_{min}$		

13. Conclusion

Comparison of two types of Th4 crystalline networks

It was noticeable that the same compound Th4 gave two crystal forms from different solvent systems by the same method. Viewing the modeling structures, the difference of phenyl ring and thymine ring orientations could be noticed (**Figure 40)**.

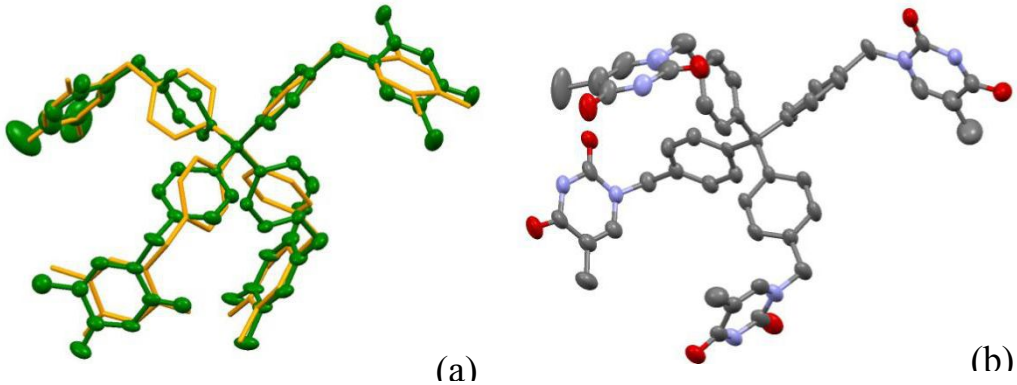

Figure 40: (a) The molecular overlay view of crystal from HFP-MeOH system. Orange: molecule A; Green: molecule B. (b) The molecular structure from HFP-IPA system.

This specificity might be a result of by the flexibility at -CH_2- positions which allowed the thymine arms to extend into several possible directions, especially in the presence of typical solvent effect via H-bonds.

The crystalline network with such a large void space filling with solvent molecules is highly unusual. Another feature of Th4 (**22**) is that these two types of crystalline networks exist respectively in 2D and 3D forms.

14. Future work

Considering two structures of Th4 (**22**) crystals, single hydrogen bond between thymine groups formed in both crystals. For a rigid network, a multiple hydrogen bond between nucleobases is more favorable to restrict the flexibility of the whole structure. In natrual DNA double helix, guanine and cytosine connect through three hydrogen bonds when adenine and thymine have two in between. Herein, the pair of guanine and cytosine may provide more opportunities to obtain a porous framework assembled via multiple hydrogen bonds. Although we mentioned that the syntheses of these two nucleobases derivatives may require more protecting and deprotecting reactions, it is worth attempts.

14.1. Design of node compounds

To avoid the flexibility in the molecular structure like in node compound Th4 (**22)**, and also considering about the difficulties towards synthesis, there are some candidates suggested in **Figure 41**.

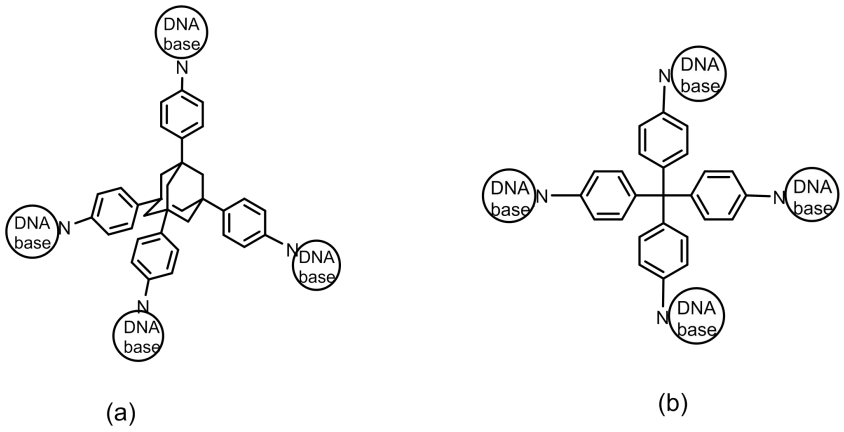

Figure 41: Two possible structures of novel node materials derived from tetra p-bromophenyl methane and adamantane.

Here, the 'Base' includes adenine, thymine, guanine and cytosine. These designed structures are all tetrahedral, which allow constructing 3D configurations.

Regarding (a) and (b), the nucleobase group directly connects to a phenyl derivative. This may be realized by *N*-arylation reaction with possible selectivity. A general approach to *N*-arylation of all four DNA nucleobases is undergoing the copper-mediated Chan-Lam-Evans-modified Ullmann condensation with a range of different

substituted phenyl boronic acids at room temperature.[119] Protected or masked nucleobases are required and would be subsequently converted back to the corresponding deprotected or unmasked adducts (**Scheme 25**).[120-122]

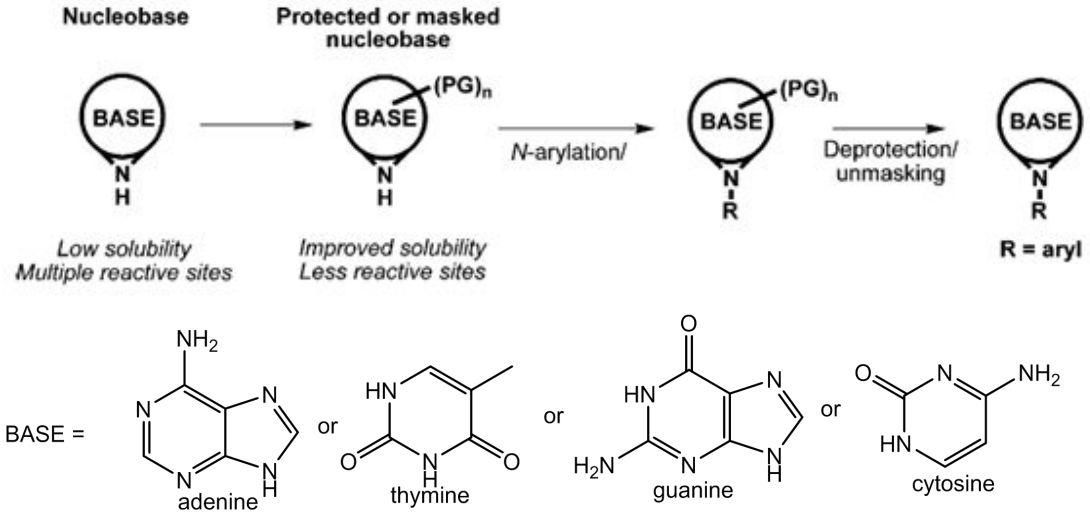

Scheme 25: General strategy for the N-Arylation of nucleobases.[119]

In the literature, they reported various aryl R groups. The lowest yield (40%) of a final product was observed for guanine *N*-arylation.

Substituted phenyl boronic acids corresponding to (a) and (b) should be tetra(4-dihydroxyborylphenyl) adamantane **24** and tetra(4-dihydroxyborylphenyl) methane **25** (**Figure 42**). Compound **25** is well known as a common building unit material for COFs.[32, 37] Adamantane derivatives were reported to follow the same synthetic routes in typical cross-coupling reactions.[123] Hence, all the essential materials for syntheses of (a) and (b) should be available. Similar to the prepared node compounds **22** and **23**, molecule (a) or (b) also contains four nucleobase groups, which may lead to a low solubility in common used solvents.

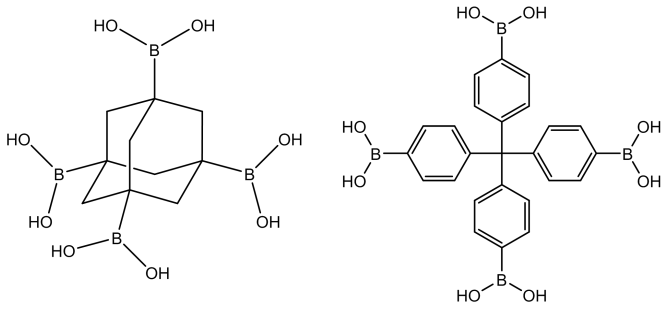

Figure 42: Strcutures of tetra(4-dihydroxyborylphenyl) adamantane and tetra(4-dihydroxyborylphenyl) methane

14.2. Options of linker materials

During the project, a key issue is about the solubility. The big gap between the solubilities of linker and node compounds is the main reason why these two materials precipitated separately from the solution so that the combination did not achieved. For this problem, the follwing alternatives can be regarded as linker options (**Figure 43**).

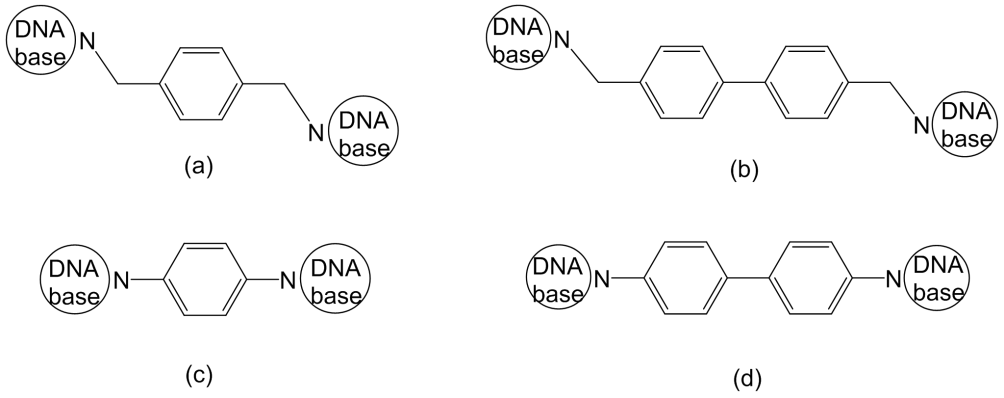

Figure 43: Four prospective structures of novel linker materials derived from benzene and biphenyl.

Here, the 'DNA base' extended to all four nucleobases. The compounds (a) and (b) have been prepared using 6-chloropurine as the starting material combined with amination at 6- position.[124] Syntheses of compounds (c) and (d) may undergo the same routes as that of designed node compounds (a) and (b). Regarding these structures, the *N*-arylation for linkers could be even faster with a higher yield than the reaction for synthesis of nodes. All the teactants are commertially or synthetically available.

All these candidates contain at least one benzene ring, and each of our node compounds Th4 **22** and Ad4 **23** have four benzene ring in their structure. In this way, the node and linker materials own some chemical similarities, especially for (a) and (b) with additional methylene groups. Similar molecular structures always have similar solubilities. In this case, the target molecules may contribute to reducing the solubility gap between linker and node, so there can be more significant possibility to form the complex of linker and node.

Part IV

Experimental

^{1}H NMR spectra were recorded at 600 MHz with a Bruker AV 600 instrument, at 400 MHz with a Bruker AVII 400 instrument, at 300 MHz with a Bruker DPX 300 or at 200 MHz with a Bruker DPX 200 instrument. The decoupled ^{13}C NMR spectra were recorded at 150, 100 or 75 MHz using instruments mentioned above. All *J* values are reported in Hertz. Mass spectra (EI) were recorded on a VG Prospec sector instrument at 70 eV ionizing voltage and presented as *m/z* (% rel. int.), while HRMS was performed with a double-focusing magnetic sector instrument. Electrospray mass (ESI) spectra were obtained on a Micromass QTOF II spectrometer. Melting points were determined with Büchi melting point B-545 apparatus and are uncorrected. Single-crystal X-ray crystallography was performed with a Bruker D8 venture diffractometer with MoKα irradiation at temperature of 100 K. Powder XRD spectra were recorded at Bruker D8 discover instrument at room temperature with scan scale from 2 to 90 or 60 degrees. Ultrasonic experiments were done with a VWR Ultrasonic cleaner instrument. Microwave experiments were conducted in sealed vessels in a synthesis reactor Monowave 300, Anton Paar GmbH, equipped with an internal IR probe.

Dry DMF, MeCN and CH_2Cl_2 were obtained from a MB SPS-800 solvent purification system. Benzenesulfonyl chloride was distilled under reduced pressure. Hexane was fresh distilled before using. TMSCl was distillated over CaH_2. Triethylamine was dried over KOH. Toluene was dried over sodium. Acetonitrile for microwave reaction was degassed by using the freeze-pump-thaw method with three cycles in liquid N_2. Other reagents were commercially available and used as received. Sodium iodide was dried at 120 ^{o}C under high vacuum overnight.

15. Syntheses

15.1. 9,9'-Dimethylene-bis(adenine) **2**.

Method A:

Adenine **1** (1.00 g, 7.40 mmol) and NaH (ca. 60 % in mineral oil, 501 mg, ca. 11.1 mmol) were added into dry DMF (30 mL) and stirred under N_2 at ambient temperature. After 1 h, 1,2-dibromoethane (1.01 g, 5.40 mmol) was added, then the reaction mixture was stirred under N_2 at ambient temperature for 48 h. After filtration, the solid was washed with water (10 mL), acetone (10 mL) and diethyl ether (10 mL). The crude product was crystallized from acetic acid-methanol (1:1). Yield 164 mg (15 %) of colorless amorphous powder.

Method B:

To a mixture of adenine (1.00 g, 7.40 mmol) and potassium carbonate (1.10 g, 7.80 mmol) in DMF (30 mL), 1,2-dibromoethane (733 mg, 3.90 mmol) was added. The mixture was stirred at ambient temperature for 60 h. The resulting mixture was filtrated and washed with water (10 mL), acetone (10 mL) and diethyl ether (10 mL) to give the crude product. Then the crude product was recrystallized from acetic acid-methanol (1:1). Yield 296 mg (27 %).

M.p. > 400 ^{o}C (Lit.[81] > 335 ^{o}C).

^{1}H NMR (TFA-d_1, 400 MHz): δ 8.82 (s, 2H, Ad H2), 8.40 (s, 2H, Ad H8), 5.05 (s, 4H, CH_2).

^{13}C NMR (TFA-d_1, 100 MHz): δ 151.62 (C6), 151.41 (C2), 149.03 (C4), 147.22 (C8), 116.40 (C5), 47.39(CH_2).

MS (EI): 296 (32, M^+), 162 (100), 148 (10), 135 (52), 108 (22), 67 (7).

HR-MS: 296.1251, calculated for $C_{12}H_{12}N_{10}$ 296.1246.

15.2. 9,9 '-Trimethylene-bis(adenine) **3**.

Adenine **1** (1.00 g, 7.40 mmol) and NaH (ca. 60 % in mineral oil, 376 mg, 9.40 mmol) were added into dry DMF (30 mL) and stirred under N_2 at ambient temperature. After

1 h, 1,3-dibromopropane (795 mg, 3.90 mmol) was added, then the reaction mixture was stirred under N_2 at ambient temperature for 6 days. After filtration, the solid was washed with water, acetone and diethyl ether. The crude product was crystallized from acetic acid-methanol (1:1). Yield 295 mg (26 %) of colorless amorphous powder.

M.p. 330 °C (Lit.[81] 330 °C).

^{1}H NMR (TFA-d_1, 400 MHz): δ 9.37(s, 2H, Ad H2), 8.78(s, 2H, Ad H8), 4.87(t, J=7.2 Hz, 4H, N-CH_2), 2.93(quintet, J=7.2, 2H, -CH_2-).

^{13}C NMR (TFA-d_1, 100 MHz): δ 151.22 (C6), 150.96 (C2), 149.50 (C4), 146.64 (C8), 115.05 (C5), 46.08 (N-CH_2), 31.78 (-CH_2-).

MS (EI): 310 (56, M^+), 175 (52), 162 (100), 148 (49), 136 (11), 108 (8).

HR-MS: 310.1408, calculated for $C_{13}H_{14}N_{10}$ 310.1403.

15.3. Pentaerythrityl bromide **6**.

Step 1:

Pentaerythritol **4** (2.73 g, 20.0 mmol) was stirred in pyridine (30 mL) at ambient temperature until dissolved. Benzenesulfonyl chloride (21.4 g, 121 mmol) was added dropwise during ca. 1.5 h while controling the reaction temperature below 35 °C. The reaction mixture was stirred at 40 °C for 4.5 h, then was poured slowly to a vigorously stirred solution of conc. hydrochloric acid (16 mL) in water (20 mL) and methanol (40 mL). The resulting mixture was filtered, and washed with water (100 mL), and cold methanol (2x10 mL). The crude product **5** was dried in high vacuum. Yield 12.1 g.

M.p. 102-103°C (lit.[112] 102-103 °C).

^{1}H NMR ($CDCl_3$, 200 MHz): δ 7.54-7.83 (m, 20H, Ph), 3.88 (s, 8H, CH_2).

Step 2:

NaBr (10.2 g, 99.0 mmol) was added into the solution of compound **5** (7.68 g, 11.0 mmol) in diethyleneglycol (20 mL). The reaction mixture was stirred at 130 °C for 19

h. The resulting mixture was cooled to ca. 60 °C, then rapidly added ice water (150 mL) to adjust the temperature to 10 °C. The mixture was filtered and washed with water (3x20 mL). The final product was crystallized from cold ethanol. Yield 3.56 g (84 %) of colorless crystalline solid corresponding to **4**.

M.p. 158-159 °C (lit.[113] 158 -160 °C).

^{1}H NMR ($CDCl_3$, 200 MHz): δ 3.59 (s, CH_2).

MS (EI): 388 (24, M^+), 311/309/307/305 (31/99/100/33), 229/227/225 (6/15/7), 215/213/211 (7/17/8), 147/145 (17/18), 133/131 (15/11).

HR-MS: 383.7358, calculated for $C_5H_8Br_4$ 383.7360.

15.4. Pentaerythrityl iodide **7**.

Step 1:

A mixture of pentaerythrityl bromide **6** (5.63 g, 14.5 mmol) and sodium iodide (17.4 g, 116 mmol) was stirred in ethyl methyl ketone (50 mL), and refluxed for 4 days under N_2 (g). The solvent was evaporated and the residue was washed into a Büchner funnel with hot water. The solid was washed with boiling water and 95 % ethanol to get the crude pentaerythrityl iodide. Yield 8.03 g of colorless crystalline crude product, and the purity was ca. 85 % from ^{1}H NMR integration.

Step 2:

The crude product (8.03 g) from step 1 and sodium iodide (4.35 g, 29.0 mmol) was stirred in ethyl methyl ketone (50 mL), and refluxed for 4 days under N_2 (g). The solvent was evaporated and the residue was washed into a Büchner funnel with hot water. The solid was washed with boiling water and 95 % ethanol to get the second crude pentaerythrityl iodide. Then sodium iodide (2.18 g, 14.6 mmol) was added into the second crude product while stirring in ethyl methyl ketone (50 mL), and the resulting mixture was refluxed for 2 days under N_2 (g). The solvent was evaporated and the residue was washed into a Büchner funnel with hot water. The solid was washed with boiling water and 95 % ethanol to get the final pure colorless crystalline compound **7.** The overall yield of **7** was 7.59 g (91 %).

M.p. 234 °C (lit.[113] 233 °C).

^{1}H NMR ($CDCl_3$, 400 MHz): δ 3.48 (s, CH_2).

MS (EI): 576 (37, M^+), 449 (100), 321 (5), 254 (2), 195 (16), 67 (52).

15.5. Attempted synthesis of tetrakis(9-adeninylmethyl)methane **8**.

Method A:

Adenine (305 mg, 2.20 mmol) and potassium carbonate (311 mg, 2.20 mmol) were mixed in DMF (15 mL). After 1 h, pentaerythrityl bromide (213 mg, 0.550 mmol) or pentaerythrityl iodide (316 mg, 0.550 mmol) was added. The mixture was stirred under N_2 and heated as corresponding temperature and time described in Table 2. The reaction was followed by TLC. There was no workup done after DMF decomposed. Mono substituted compound **8a** was observed in reaction mixture from NMR result:

^{1}H NMR (DMSO-d_6, 200 MHz): δ 8.17 (s, 1H, Ad H2), 8.09 (s, 1H, Ad H8), 7.27 (s, 2H, Ad NH_2), 4.45 (s, 2H, N-CH_2), 3.72 (s, 6H, Br-CH_2).

MS (EI): no molecular ion, 364/362/360 (1/3/1, M-Br^+), 149/148 (3/2), 135 (4), 108 (1), 44 (100).

Method B:

Adenine (106 mg, 0.740 mmol) and potassium carbonate (205 mg, 1.50 mmol) were mixed in degassed acetonitrile (15 mL) in a microwave vial filled with N_2. The mixture was stirred in microwave oven at 150 °C for 20 min. Pentaerythrity iodide (53.0 mg, 0.0920 mmol) was added. The mixture was stirred at 175 °C for corresponding time described in Table 3. The resulting mixture was filtered and washed with water, acetone and diethyl ether. Yield 53 mg of **8b** corresponding to starting adenine.

^{1}H NMR (DMSO-d_6, 400 MHz): δ 7.81 (s, 1H, Ad H2), 7.50 (s, 1H, Ad H8), 5.70 (s, 2H, Ad NH_2).

^{13}C NMR (DMSO-d_6, 100 MHz): δ 161.20 (C6), 153.73 (C2), 151.10 (C4), 147.50 (C8), 121.66 (C5).

Method C:

Adenine **1** (135 mg, 1.00 mmol) was dissolved in mixed solvent of DMSO (15 mL) and toluene (7.5 mL). Aq. NaOH (50 % (w/w), 80.0 mg) was added and water in reaction mixture was removed through a Dean-Stark condenser. Compound **7** (115 mg, 0.200 mmol) was added and the mixture was stirred at 120 ^{o}C for 4 h. The resulting mixture was filtered and the filtrate was concentrated under reduced pressure. The crude product was recrystallized from ethanol. 2 mg of unknown product was obtained.

15.6. 1,1'- Trimethylene-bis(thymine) **11**

Step 1:

Thymine **9** (1.30 g, 10.3 mmol) was stirred in dry toluene (30 mL) while chlorotrimethylsilane (2.55 g, 23.5 mmol) was added. Triethylamine (2.88 g, 28.5 mmol) dissolved in toluene (10 mL) was added to the reaction mixture and then stirred for 48 h. The resulting mixture was filtered and washed with dry toluene (3x10 mL). The filtrate was concentrated under reduced pressure to give O,O' bis(trimethylsilyl)thymine **10**.

Step 2:

To the intermediate product **10** (8.31 g, 30.7 mmol) dissolved in DMF (50 mL) 1,3-dibromopropane (3.16 g, 15.6 mmol) was added while stirring at ambient temperature. The solution was heated up to 170 ^{o}C and stirred for 24 h. The reaction mixture was cooled to 0 ^{o}C and MeOH (20 mL) was added while stirring. The resulting mixture was filtered and the solid was washed with 1:1 chloroform-methanol (100 mL). Yield 2.30 g (38 %) of **11** as colorless amorphous powder.

M.p. 330-332 ^{o}C (lit.[83] 330-334 ^{o}C).

^{1}H NMR (DMSO- d_6, 200 MHz): δ 11.22 (s, 2H, Th H3), 7.52 (s, 2H, Th H6), 3.65 (t, J=7.0 Hz, 4H, N-CH_2), 1.89 (quintet, J=7.0 Hz, 2H, -CH_2-), 1.73 (s, 6H, Th CH_3).

^{13}C NMR (DMSO- d_6, 100 MHz): δ 164.23 (C4), 150.89 (C2), 141.20 (C6), 108.52 (C5), 44.81 (N-CH_2), 27.86 (CH_2), 11.92 (CH_3).

MS (EI): 292 (28, M^+), 166 (100), 153 (38), 140 (33), 123 (9), 110 (42).

15.7. 1,1'- dimethylene-bis(thymine) **12**

Step 1:

The intermediate product *O,O*' bis(trimethylsilyl)thymine **10** was synthesized in the same way as described in 15.6 Step 1.

Step 2:

1,2-dibromoethane (1.15 g, 6.10 mmol) was added to intermediate product **10** (3.29 g, 12.2 mmol) in DMF (30 mL) while stirring at ambient temperature. The solution was heated to 170 ^oC and stirred for 36 h under N_2 (g). The reaction mixture was cooled to 0 ^oC and MeOH (10 mL) was added. The resulting mixture was filtered and the solid was washed with 1:1 chloroform-methanol. Yield 718 mg (50 %) of **12** as colorless amorphous powder.

M.p. >370 ^oC (lit.[125] > 310 ^oC).

^1H NMR (DMSO-d_6, 200 MHz): δ 11.20 (s, 2H, Th H3), 7.41 (s, 2H, Th H6), 3.87 (s, 4H, CH_2), 1.71 (s, 6H, Th CH_3).

^{13}C NMR (DMSO-d_6, 100 MHz): δ 164.21 (C4), 151.06 (C2), 141.20 (C6), 108.62 (C5), 46.08 (CH_2), 11.92 (CH_3).

MS (EI): 278 (24, M^+), 152 (100), 139 (10), 126 (11), 109 (37), 96 (78).

15.8. Attempted synthesis of tetrakis(1-thyminylmethyl)methane **13**

Step 1:

The intermediate product *O,O*' bis(trimethylsilyl)thymine **10** was synthesized in the same way as described in 15.6 Step 1.

Step 2:

Pentaerythrityl iodide (115 mg, 0.200 mmol) was added into solution of silylated thymine **10** (270 mg, 1.00 mmol) in DMF (5 mL). The mixture was stirred under N_2 (g) and heated to 170 ^oC for 8 days. The reaction was followed by TLC. The reaction mixture was cooled to 0 ^oC and methanol (10 mL) was added. The resulting mixture was filtered and washed with 1:1 MeOH-$CHCl_3$. Yield crude product 114 mg, and it was applied to column, using eluent system of MeOH in DCM as described in Table 4.

15.9. 1,3,5,7-Tetrabromoadamantane **15**

Method A:

A mixture of anhydrous $AlCl_3$ (12.0 g, 90.0 mmol) and bromine (6.00 mL, 120 mol) was cooled to 0^oC. Adamantane **14** (3.00 g, 22.0 mmol) was added in portions slowly. Evolved HBr gas was passed through a flask containing concentrated aqueous sodium bisulfite. The mixture was refluxed for 40 h. The reaction mixture was treated first with saturated sodium bisulfite solution (10 mL), and then with 6N HCl (10 mL). The resulting mixture was taken into chloroform, and washed with water (2×20 mL) and brine (20 mL). The organic phase was dried with magnesium sulfate, filtered and concentrated under reduced pressure. The crude product was recrystallized from 1:2 acetone-water to give 8.06 g product mixture of **15** and **15a** (ratio 95:5).

Method B:

A mixture of anhydrous $AlBr_3$ (11.7 g, 44.0 mmol) and bromine (3.00 mL, 60.0 mmol) was cooled to 0^oC. Adamantane **14** (1.50 g, 11.0 mmol) was added in portions slowly. Evolved HBr gas was passed through a flask containing concentrated aqueous sodium bisulfite. The mixture was refluxed for 28 h. The reaction mixture was treated first with saturated sodium bisulfite solution (10 mL), and then with 6N HCl (10 mL). The resulting mixture was taken into chloroform, and washed with water (2×20 mL) and brine (20 mL). The organic phase was dried with magnesium sulfate, filtered and concentrated under reduced pressure. The crude product was recrystallized from 1:2 acetone-water. Yield 4.54 g (91 %) of colorless crystal product **15**.

Mp 246-248 ^oC (lit: 246-248 ^oC).

^{1}H NMR ($CDCl_3$, 300 MHz): δ 2.70 (s. CH_2).

^{13}C NMR (DMSO-d_6, 100 MHz): δ 57.34 (CH_2), 52.93 (C-Br).

MS (EI): no molecular ion, 375/373/371/369 (28/98/100/30), 329/327/325 (13/18/8), 293/291/289 (6/12/6), 213/211/209 (10/16/6), 130 (15), 115 (10).

15.10. Attempted synthesis of 1,3,5,7-Tetraiodoadamantane **16**

$AlBr_3$ (58.0 mg, 0.440 mmol) in iodomethane (3.00 mL, 48.0 mmol) was stirred at room temp for 30 min. Tetrabromoadamantane **15** (100 mg, 0.220 mmol) was added and the reaction mixture was stirred for 20 h. The mixture was treated with concentrated $NaHSO_3$ aq. (50 mL) and 6N HCl (25 mL). The resulting mixture was extraced with chloroform, washed with water and brine, and dried with magnesium sulfate. From ^{1}H NMR spectra of reaction mixture and organic phase after extraction, only starting material **15** was observed.

15.11. Attempted synthesis of 1, 3, 5, 7-tetrathymineadamantane **17**

K_2CO_3 (30.5 mg, 0.220 mmol) were added to a solution of thymine **9** (126 mg, 1.00 mmol) in DMF and stirred for 1 h. 1,3,5,7-tetrabromoadamantane **15** (100 mg, 0.220 mmol) was added into the mixture and stirred at 60 °C for 48 h or at 160 °C for 24 h. The reaction mixture was filtered and some insoluble solid was remained on filter paper, while washing with water, the solid dissolved. From ^{1}H NMR spectrum of filtrate, no target compound **17** was observed.

15.12. Attempted synthesis of 1, 3, 5, 7-tetrauraciladamantane **19**.

K_2CO_3 (30.5 mg, 0.220 mmol) were added to a solution of uracil **18** (112 mg, 1.00 mmol) in DMF and stirred for 1 h. 1,3,5,7-tetrabromoadamantane **15** (100 mg, 0.220 mmol) was added into the mixture and stirred at 60 °C for 24 h, or at 160^{o}C for 24 h. After getting rid of solvent, the residue was applied into column with eluent system of

8 % MeOH in dichloromethane. 19 mg unknown solid was obtained. From ^{1}H NMR spectrum of this solid product, there was no signal indicating the target compound **19**.

15.13. Tetrakis(4-(bromomethyl)phenyl)methane **21**

Tetraphenylmethane **20** (1.28 g, 4.00 mmol) and titanium tetrabromide (4.40 g, 12.0 mmol) were stirred in dry dichloromethane (20 mL). To the reaction mixture, cooled in an ice-bath, add bromomethoxymethane (2.70 g, 20.0 mmol) dropwise. The mixture was stirred at room temperature under N_2 atmosphere for 28 h, and then water (20 mL) was added dropwise. The resulting mixture was extracted with dichloromethane (3×50 mL). The combined organic phase was washed with water (2×20 mL) and brine (20 mL), dried over $MgSO_4$ and concentrated under reduced pressure, the product **21** was obtained by recrystallization from CH_2Cl_2 as a colorless solid. Yield: 1.61 g (58 %).

M.p. 284-286 ^{o}C (lit. [126] 285-286 ^{o}C).

^{1}H NMR ($CDCl_3$, 300 MHz): δ 7.29-7.18 (m, 16 H, Ph), 4.47 (s, 8 H, CH_2).

^{13}C NMR ($CDCl_3$, 75 MHz): δ 146.46, 135.81, 131.37, 128.61, 64.50, 33.24.

MS (EI): 692 (2, M^+), 613/611 (24/24), 600/598 (13/13), 519 (100), 431/429/427 (13/29/18), 361 (11).

15.14. Tetrakis(4-thyminylmethylphenyl)methane **22**

Step 1:

The intermediate product O,O' bis(trimethylsilyl)thymine **10** was synthesized in the same way as described in 15.6 Step 1.

Step 2:

The silylated thymine **10** from first step was dissolved in DMF (15 ml). Tetra bromide compound **21** (415 mg, 0.600 mmol) was added. The reaction mixture was stirred under N_2 (g) and heated to 160 ^{o}C for 24 hours. The resulting mixture was cooled to

room temperature, and concentrated under reduced pressure to give solid mixture as crude product. The crude product was purified by flash chromatography for twice, using the same eluent system of 5 % MeOH saterated with NH_3 in DCM. The pure product was obtained as colorless powder with the yield of 255 mg (49 %).

M.p. >380 ^oC.

^1H NMR (DMSO-d_6, 600 MHz): δ 11.28 (s, 4H, Th H2), 7.61 (s, 4H, Th H6), 7.16 (m, 16 H, Ph), 4.78 (s, 8 H, CH_2), 1.73 (d, 12H, Th CH_3).

^{13}C NMR (DMSO-d_6, 150 MHz): δ 164.26, 150.98, 145.65, 141.44, 134.57, 130.40, 126.64, 109.00, 63.73, 49.60, 11.95.

MS (ESI): 895.3 (100, M+Na).

15.15. Tetrakis(4-adeninylmethylphenyl)methane **23**

Adenine (616 mg, 4.56 mmol) and potassium carbonate (1.05 g, 7.60 mmol) were mixed in DMF (20 ml). After 1 h, tetra bromide compound **21** (529 mg, 0.760 mmol) was added. The mixture was stirred under N_2 at ambient temperature for 38 hours. After filtration of resulting mixture with Buchner funnel, the filtrate was concentrated under reduced pressure and dried under high vacuum to remove DMF. The crude product was applied to column for three times, using the eluent system of 5 % MeOH saterated with NH_3 in DCM. The best purity of product **23** reached ca. 90 %.

^1H NMR (DMSO-d_6, 300 MHz): δ 8.20 (s, 4 H, Ad H2), 8.11 (s, 4 H, Ad H8), 7.22 (s, 8 H, Ad NH_2), 7.06- 7.15 (m, 16 H, Ph), 5.27 (s, 8 H, CH_2).

^{13}C NMR (DMSO-d_6, 75 MHz): δ 155.96, 152.61, 149.43, 145.71, 140.81, 134.64, 130.38, 126.88, 118.58, 63.71, 45.51.

MS (ESI): 931.4 (86, M+Na). 158.1 (100)

16. Crystal growing

16.1. General setup

16.1.1. Vapor diffusion:

A small straight-wall vial containing the starting materials dissolved in a specific solvent was covered with parafilm which was stabbed a tiny hole on it to allow for vapour diffusion. This vial was placed in a bigger vial with lid and precipitating reagent (ca. 2 mL) inside. The big vial was subsequently capped and stored at ambient temperature without disturbing (**Picture 3**).

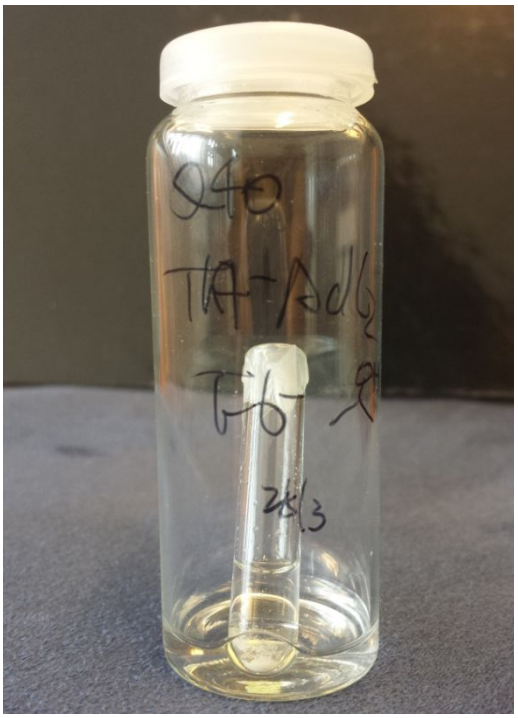

Picture 3: The general setup of crystal growth by the method of vapor diffusion.

16.1.2. Slow evaporation

A small straight wall and round bottom vial containing the starting materials dissolved in a specific solvent was covered with parafilm which was stabbed a tiny hole on it to allow the evaporation of solvent. This setup was placed in a hood at ambient temperature without disturbing.

16.2. Crystal growth of AdC2Ad (**2**)

Using the vapor diffusion method, in the small vial 2.9 mg of 9,9'-dimethylene-bis(adenine) **2** (AdC2Ad) was dissolved in HFP (0.3 mL). MeOH, MeCN and DCM were chosen separately as precipitating reagent in the big vial. This whole setup was left at ambient temperature for approximately 1 week, and only amorphous powder was precipitated.

16.3. Crystal growth of ThC2Th (**11**)

For vapor diffusion, in the small vial 2.7 mg of 1,1'- bimethylene-bis(thymine) **11** (ThC2Th) was dissolved in HFP (0.3 mL). MeOH, MeCN and DCM were tried separately as precipitating reagent in the big vial. This whole setup was stored at ambient temperature for approximately 5 days, and only amorphous powder was observed.

16.4. Crystal growth of ThC2Th (**11**)-AdC2Ad (**2**) complex

Using vapor diffusion method, in the small vial a mixture of 2.7 mg ThC2Th **11** and 2.9 mg AdC2Ad **2** (ratio 1:1) was dissolved in HFP (0.3 mL). MeOH, MeCN EtOAc and DCM were tried separately as precipitating reagent in the big vial. All the setups were stored at ambient temperature for approximately 1 week, but for all of them only amorphous powder was observed.

16.5. Crystal growth of Th4 (**22)**

With vapor diffusion method, in the small vial 4.4 mg ThC4 **22** was dissolved in mixed solvent of MeOH and DCM (0.3 mL). MeCN was applied as precipitating reagent in the big vial. The setup was stored at ambient temperature for approximately 1 week, but only amorphous powder was observed.

For slow evaporation, HFP, DMSO and mixed solvent of MeOH-DCM were chosen as the specific solvent.

16.6. Crystal growth of Th4 (**22**)-AdC2Ad(**2**) complex

According to slow evaporation, 2.9 mg AdC2Ad **2** and 4.4 mg Th4 **22** (ratio 2:1) were dissolved in HFP or DMSO (0.3 mL) in a suitable vial. The setup was left in the hood for 2 days or 10 days.

Using vapor diffusion method and setup, in the small vial 2.9 mg AdC2Ad and 4.4 mg Th4 (ratio 2:1) were dissolved in HFP (0.3 mL). MeOH, MeCN EtOAc, IPA, H_2O and DCM were used separately as precipitating reagent in the big vial. Each setup was left at ambient temperature for 1-2 weeks, and various phenomena were observed as in Table 5.

16.7. Crystal growth of Th4 (**22**)-AdC3Ad (**3**) complex

Similar to that for Th4-AdC2Ad complex, vapor diffusion method was used in a scale of 3.1 mg AdC3Ad **3** and 4.4 mg Th4 **22** (ratio 2:1). MeOH, MeCN EtOAc, IPA, H_2O and DCM were used separately as precipitating reagent. Each setup was left at ambient temperature for 1-2 weeks, and the phenomena were observed as in Table 5.

17. X-ray diffractions

17.1. Crystal handling

For the unstable and sensitive crystals, flash frozen technique in liquid nitrogen was used to minimize the solvent evaporation time. As soon as the suitable crystal was picked up under a microscope, it was put into liquid nitrogen.

17.2. Single crystal XRD data collection

The crystal data was collected on a single-crystal X-ray diffractometer using Mo as radiation source and liquid nitrogen to maintain the constant temperature of sample environment. Firstly, to examine the crystal quality, a quick scan of twenty-four frames of diffractions was collected at 100K, so that the unit cell of crystal lattice can

be determined. Then the program calculated and set up the data collection strategy according to which the whole process took several hours.

Appendix

1. NMR spectra

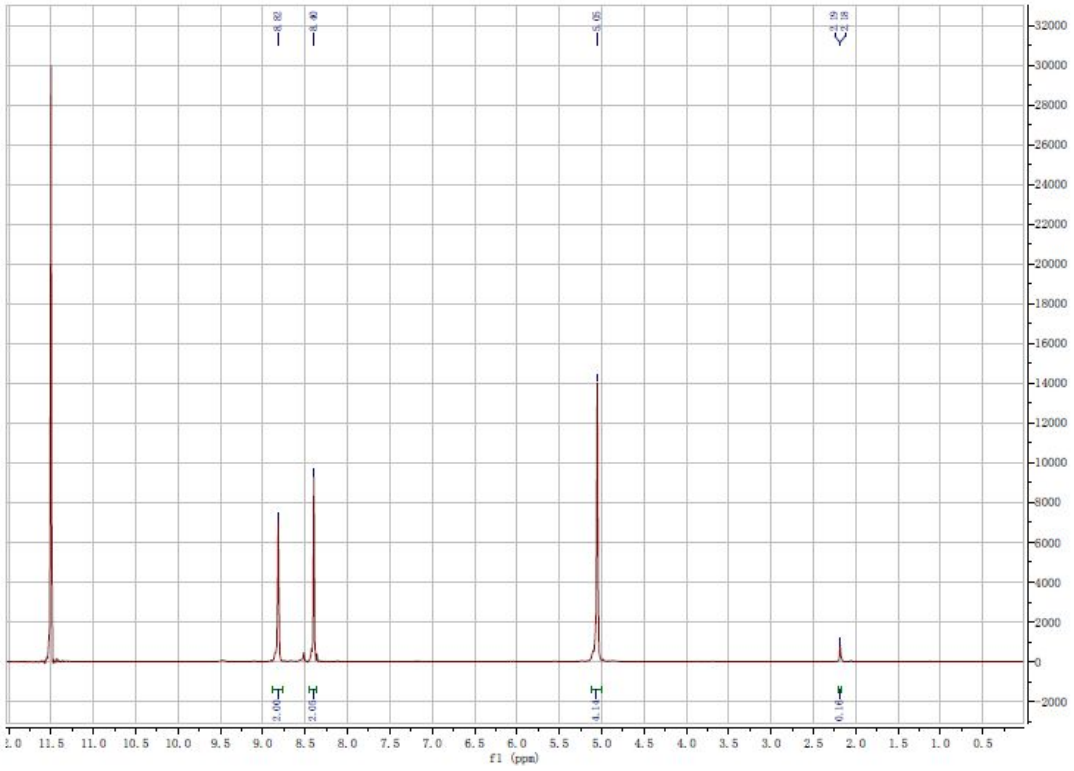

Spectrum 1: ^{1}H NMR spectrum of 9,9'-dimethylene-bis(adenine) (2)

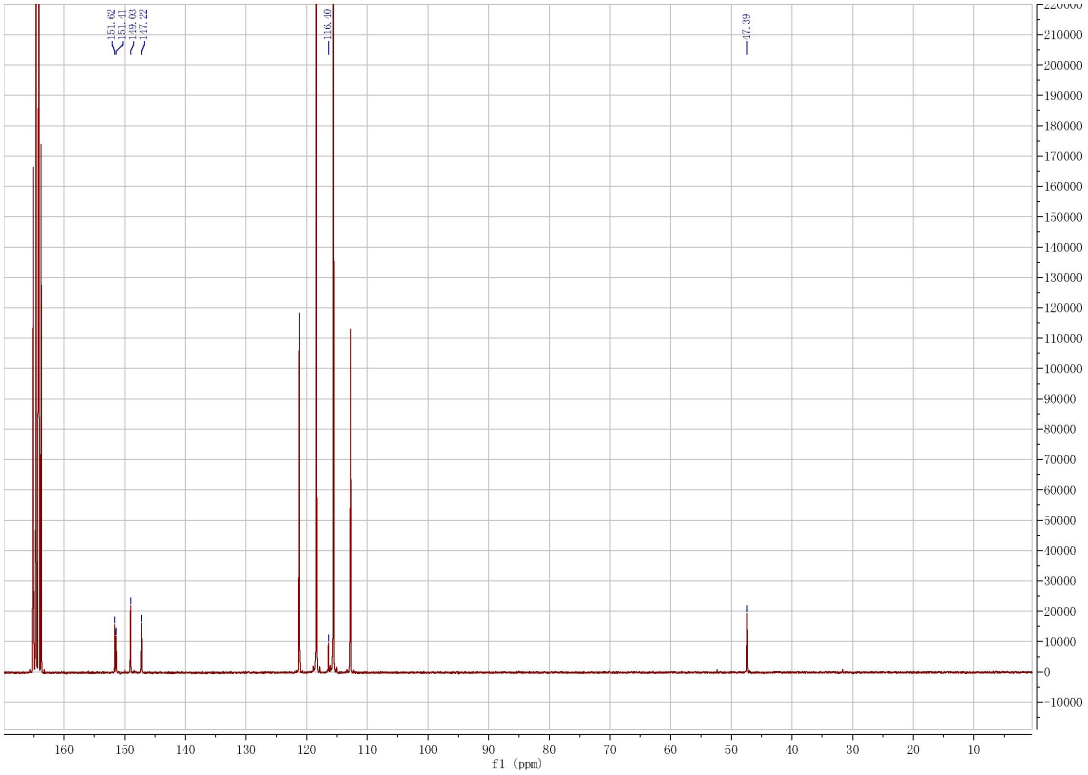

Spectrum 2: ^{13}C NMR spectrum of 9,9'-dimethylene-bis(adenine) (2)

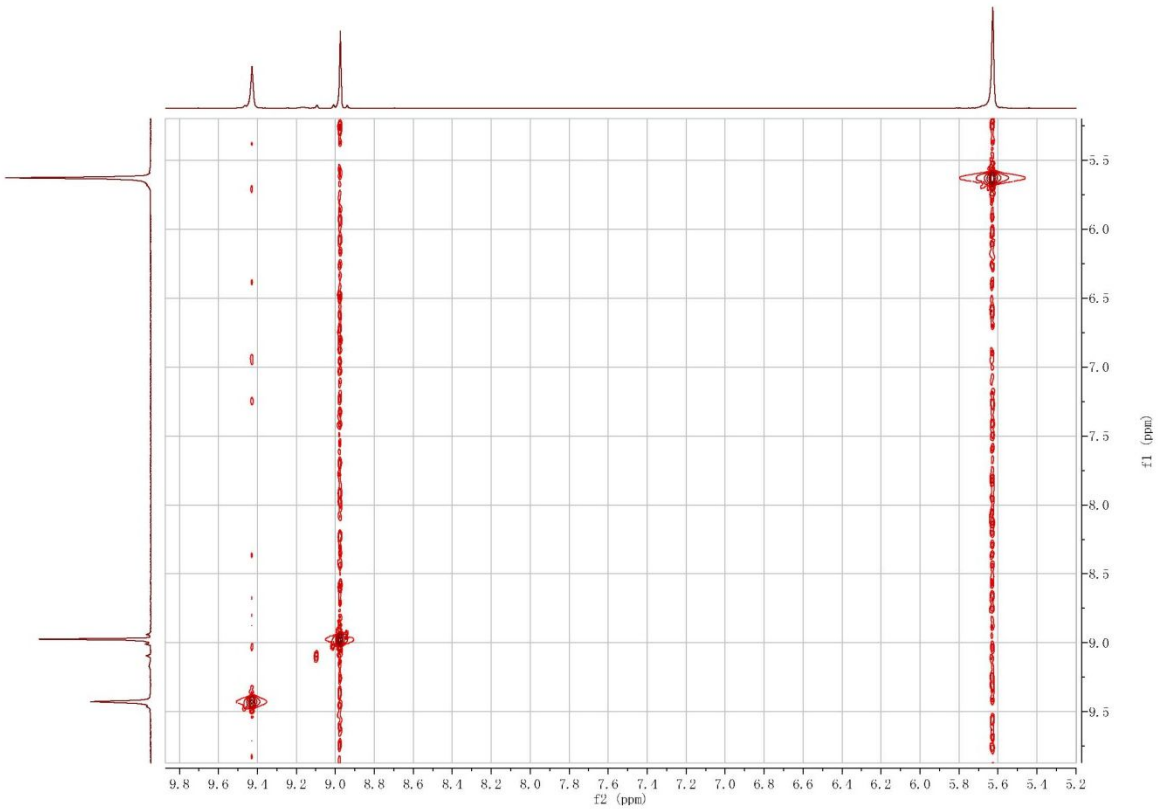

Spectrum 3: COSY spectrum of 9,9'-dimethylene-bis(adenine) (2)

Spectrum 4: HSQC spectrum of 9,9'-dimethylene-bis(adenine) (2)

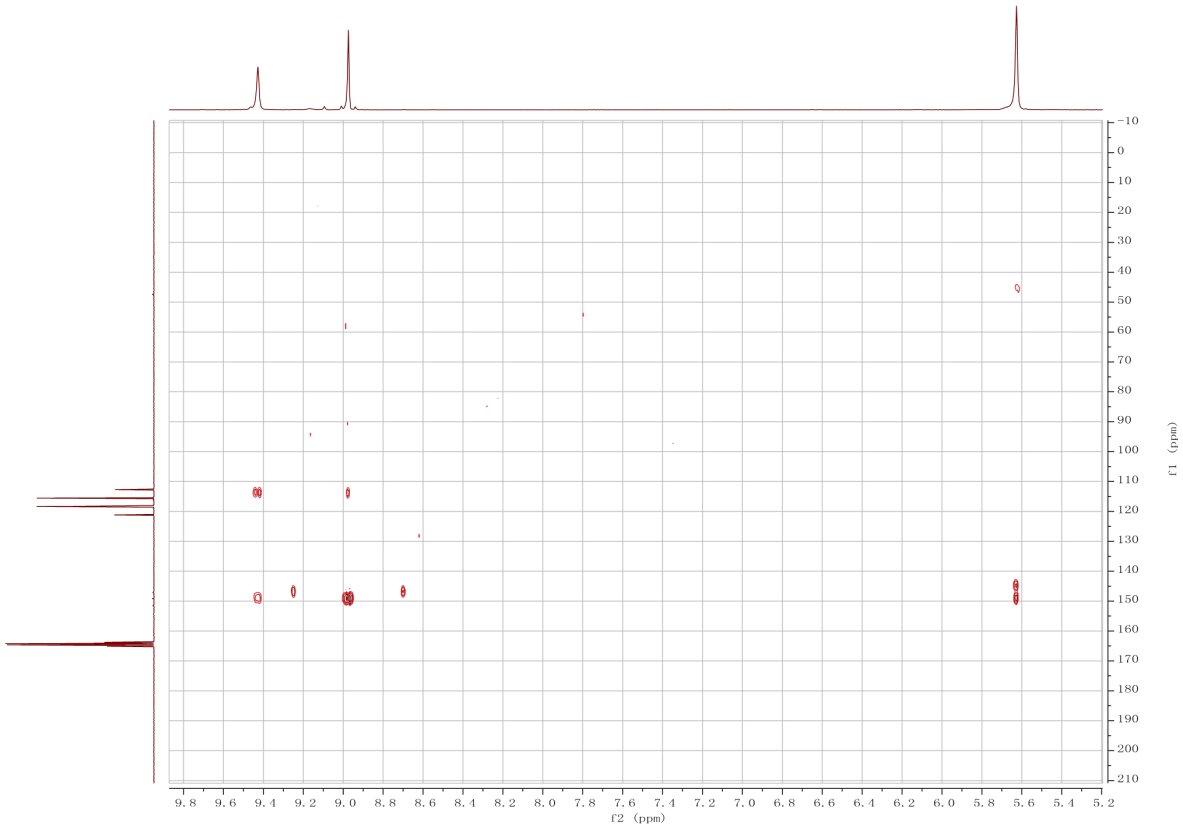

Spectrum 5: HMBC spectrum of 9,9'-dimethylene-bis(adenine) (2)

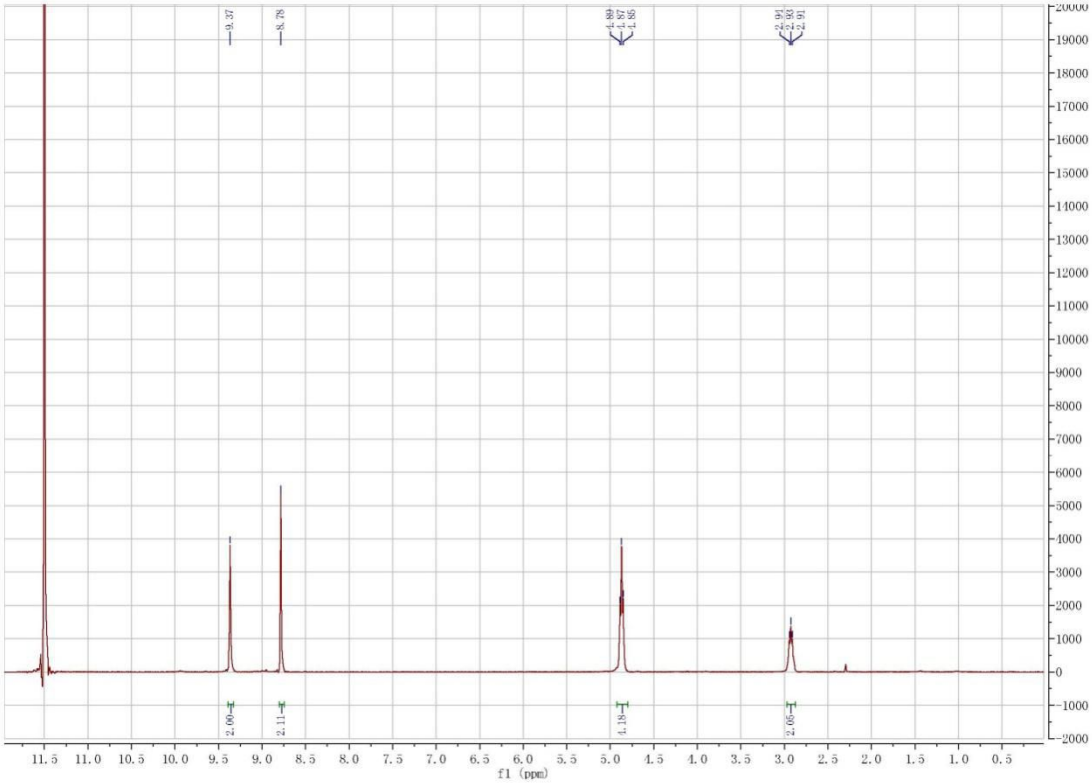

Spectrum 6: ^{1}H NMR spectrum of 9,9'-trimethylene-bis(adenine) (3)

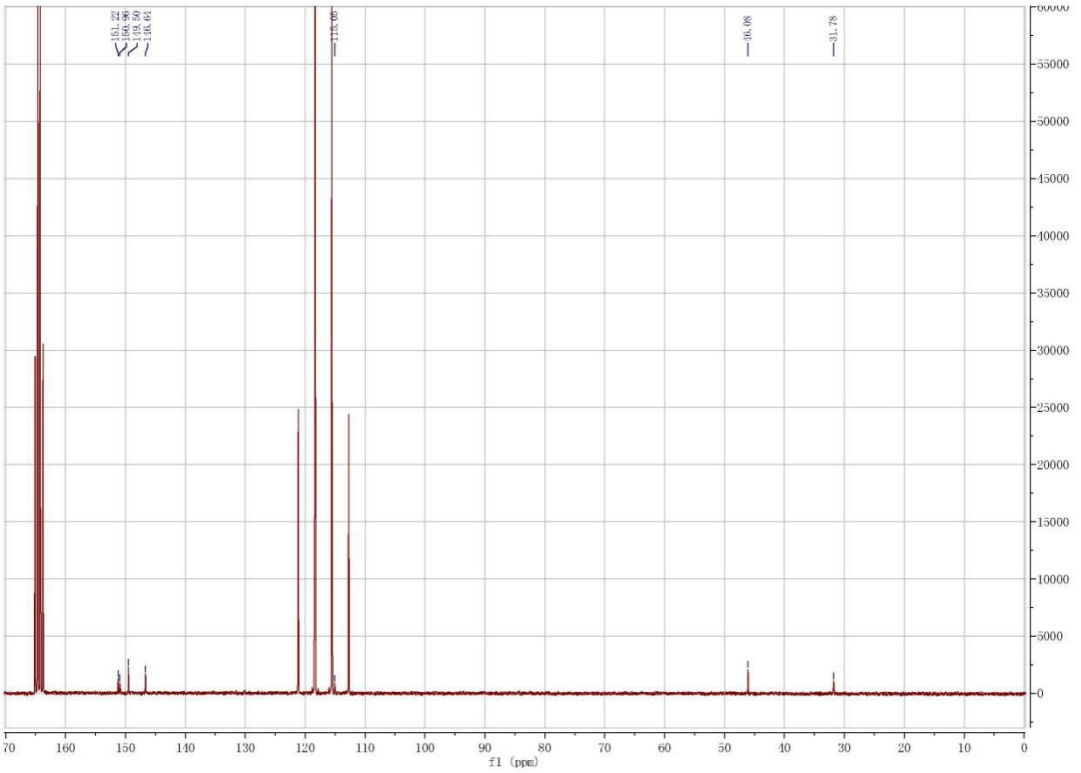

Spectrum 7: ^{13}C NMR spectrum of 9,9'-trimethylene-bis(adenine) (3)

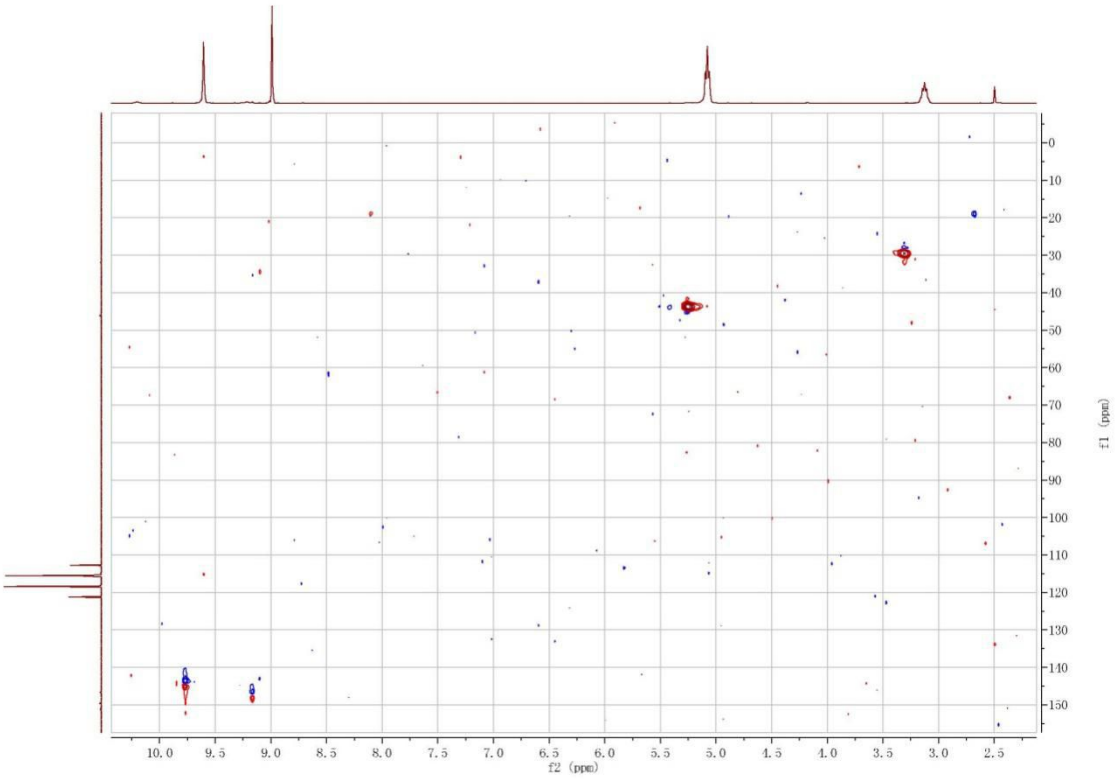

Spectrum 8: HSQC spectrum of 9,9'-trimethylene-bis(adenine) (3)

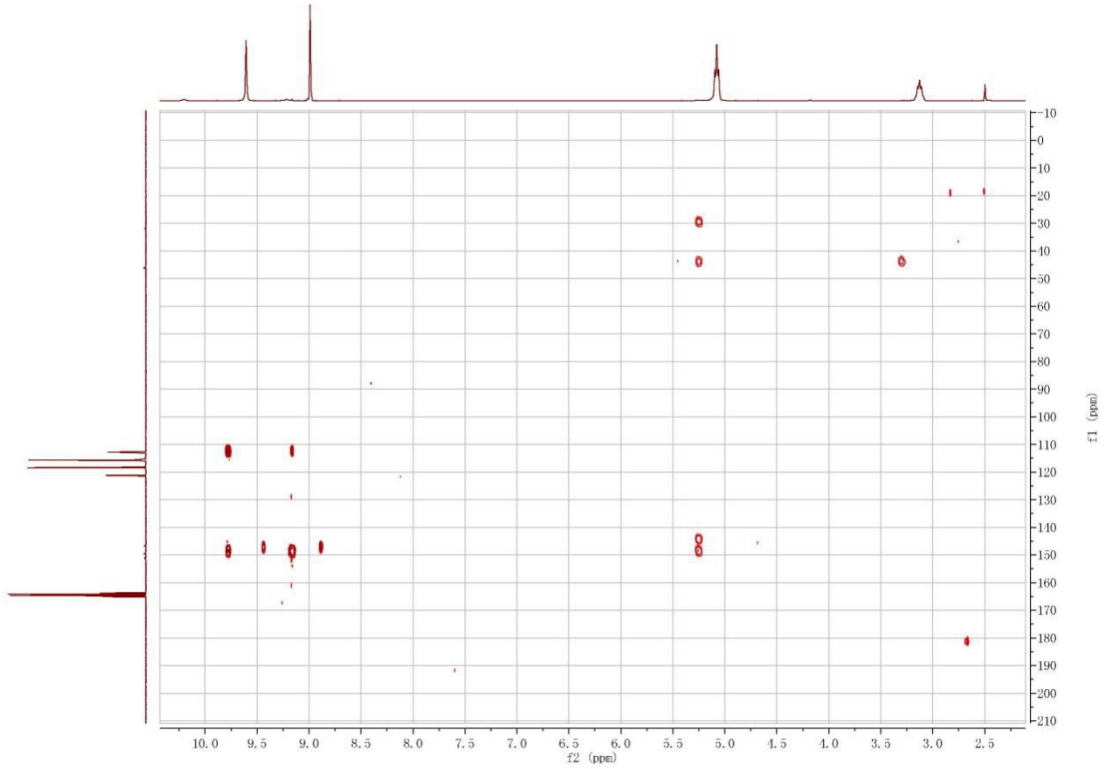

Spectrum 9: HMBC spectrum of 9,9'-trimethylene-bis(adenine) (3)

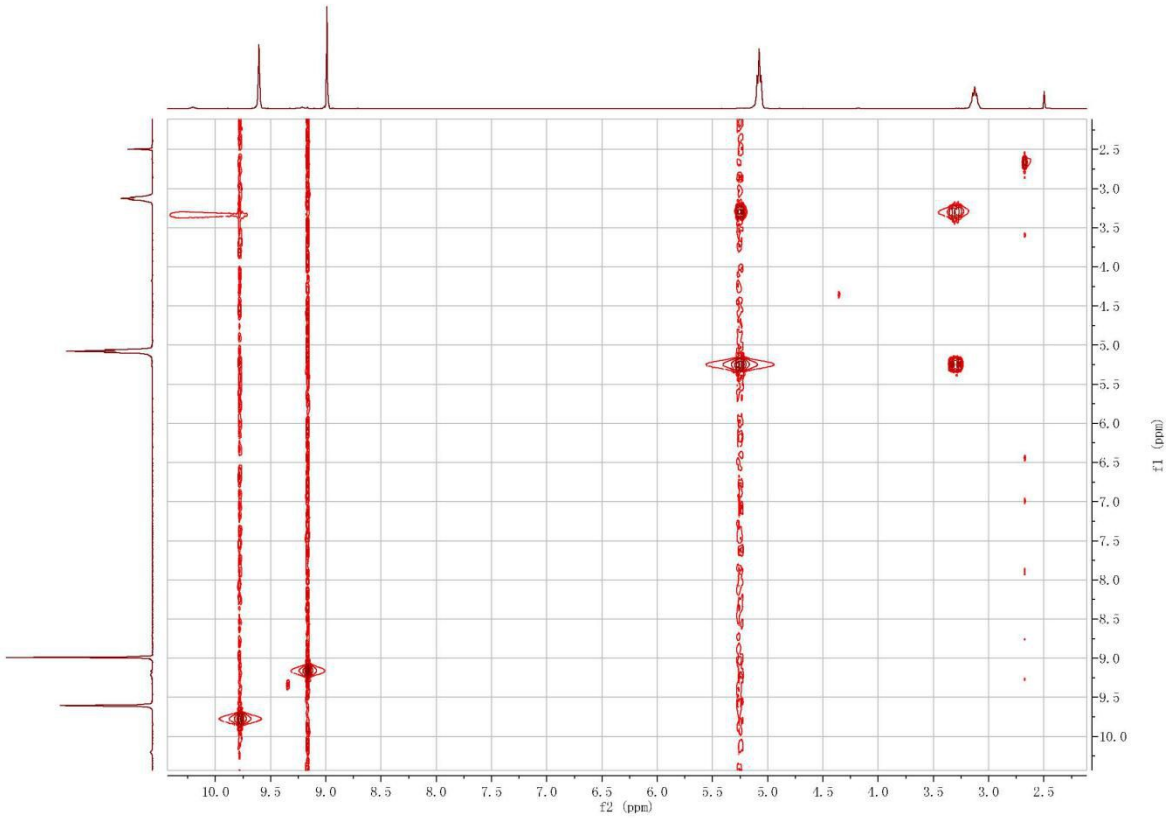

Spectrum 10: COSY spectrum of 9,9'-trimethylene-bis(adenine) (3)

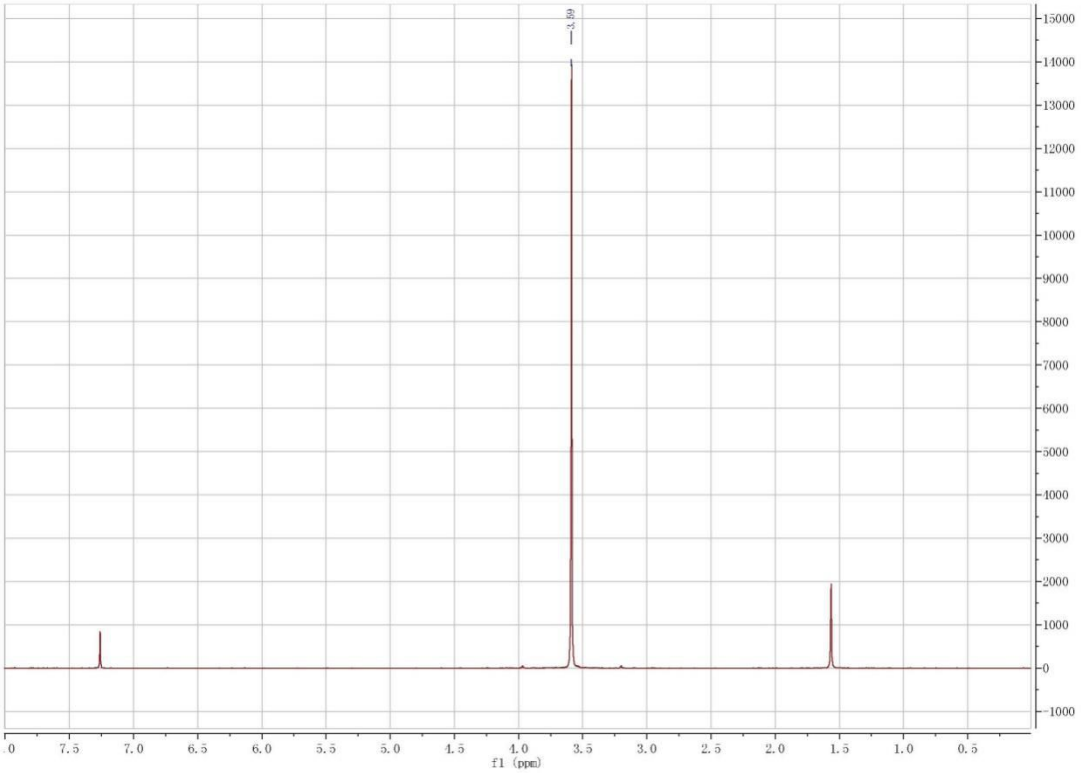

Spectrum 11: ^{1}H NMR spectrum of pentaerythrityl bromide (6)

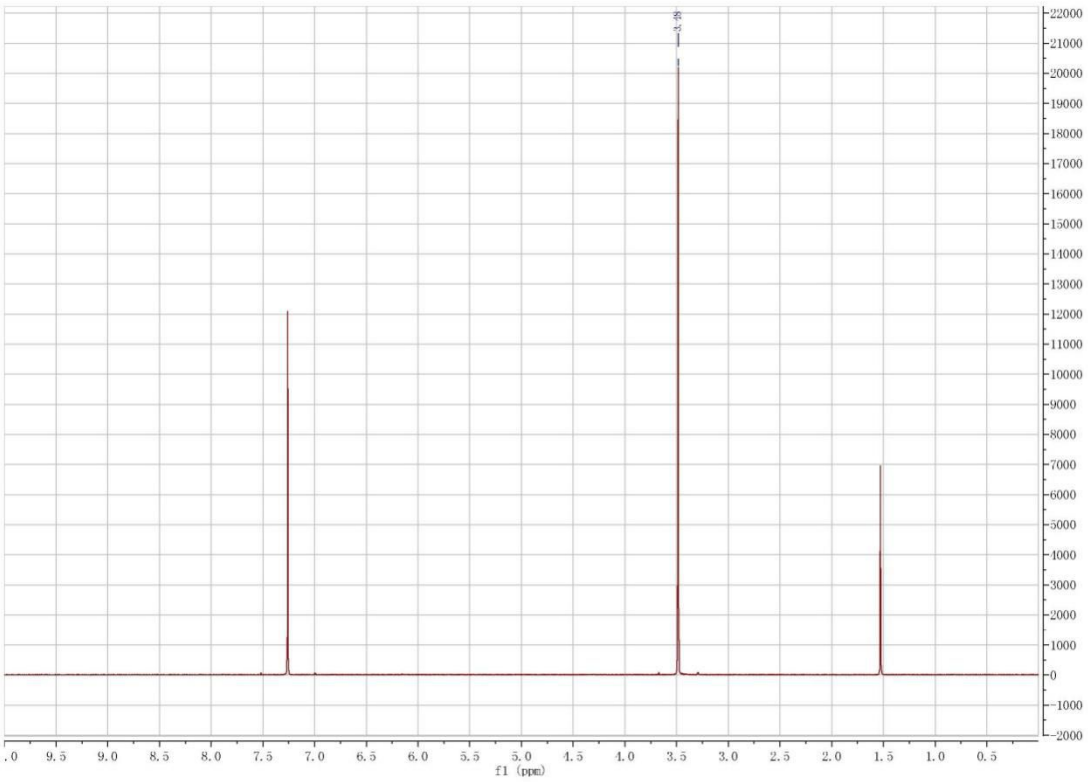

Spectrum 11: ^{1}H NMR spectrum of pentaerythrityl iodide 7

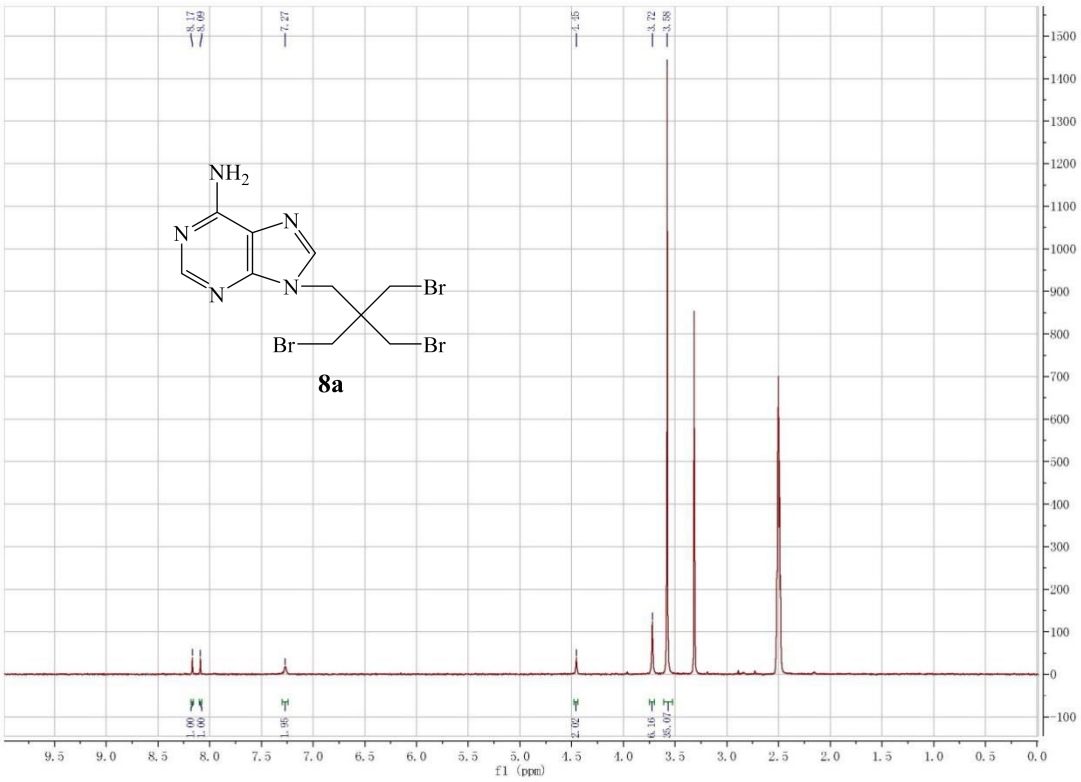

Spectrum 12: ^{1}H NMR spectrum of 8a

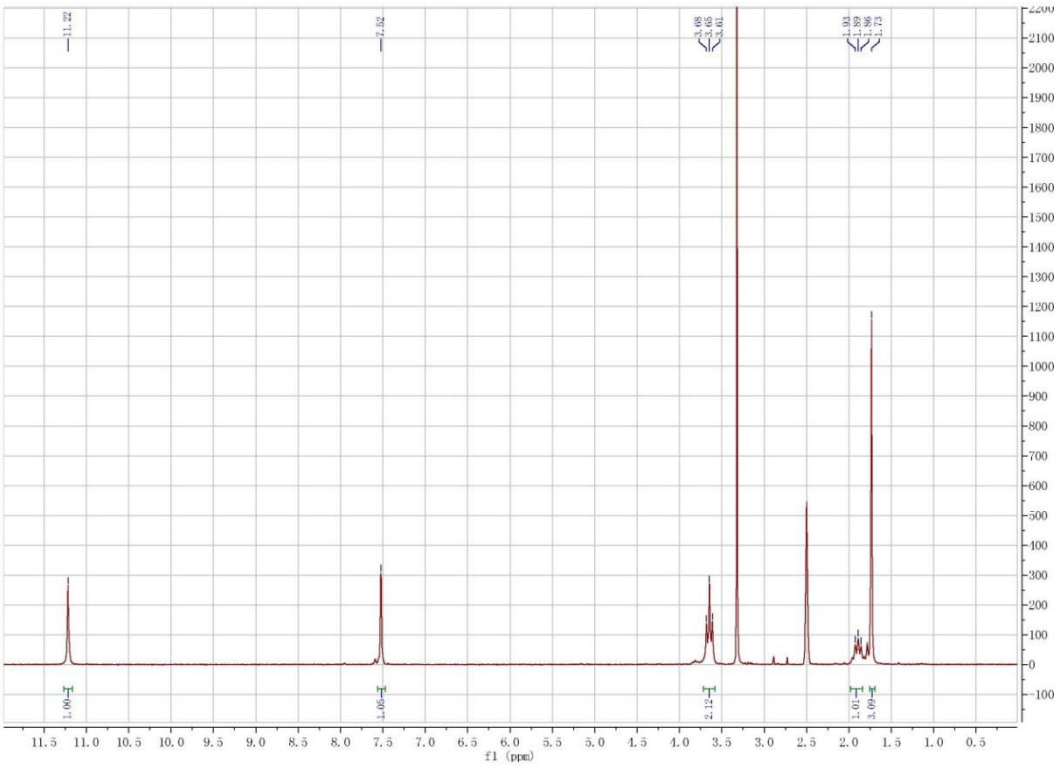

Spectrum 13: ^{1}H NMR spectrum of 1,1'- trimethylene-bis(thymine) (11)

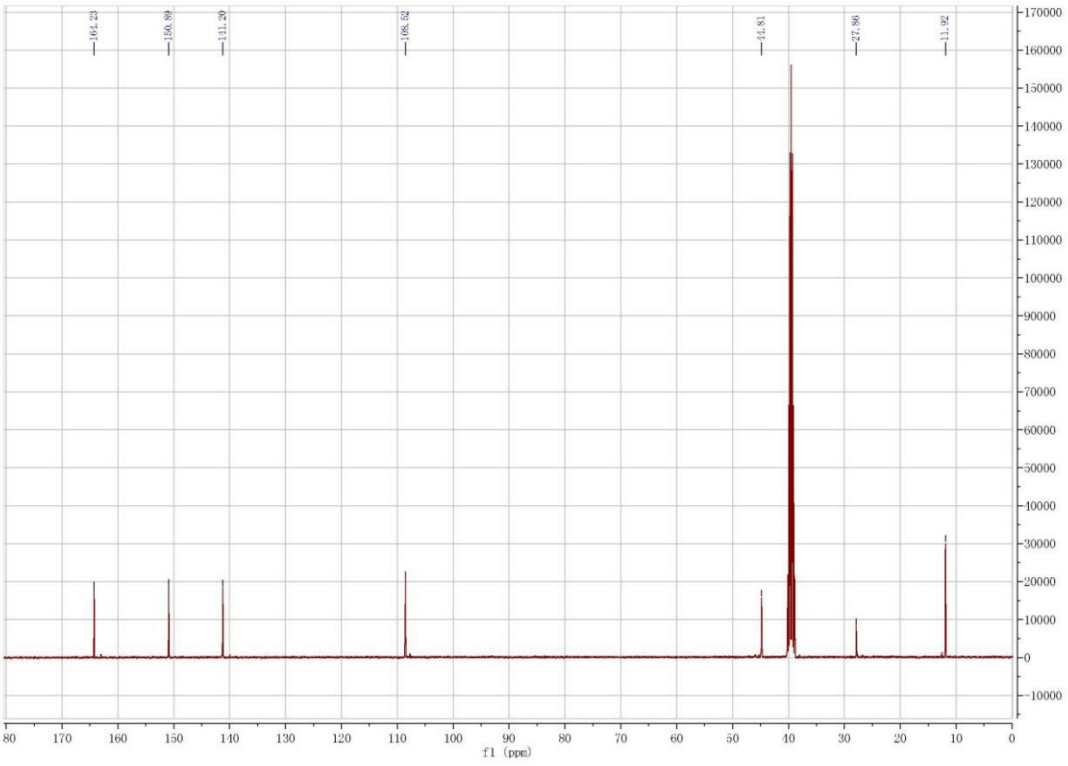

Spectrum 14: ^{13}C NMR spectrum of 1,1'- trimethylene-bis(thymine) (11)

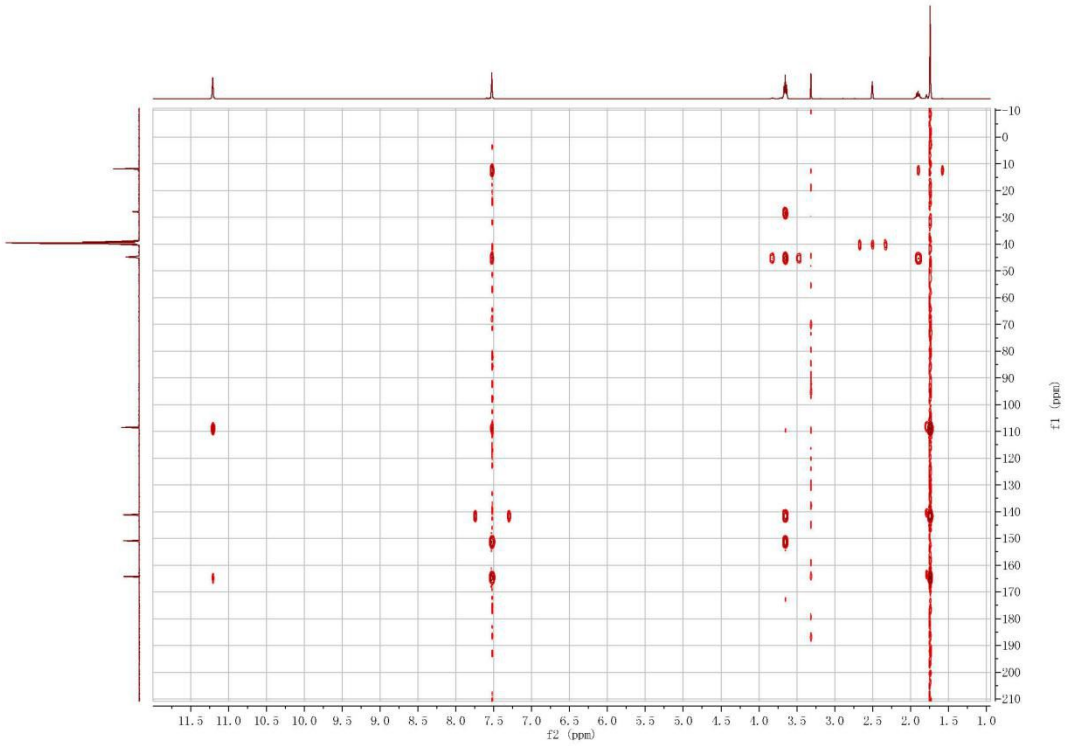

Spectrum 15: HMBC spectrum of 1,1'- trimethylene-bis(thymine) (11)

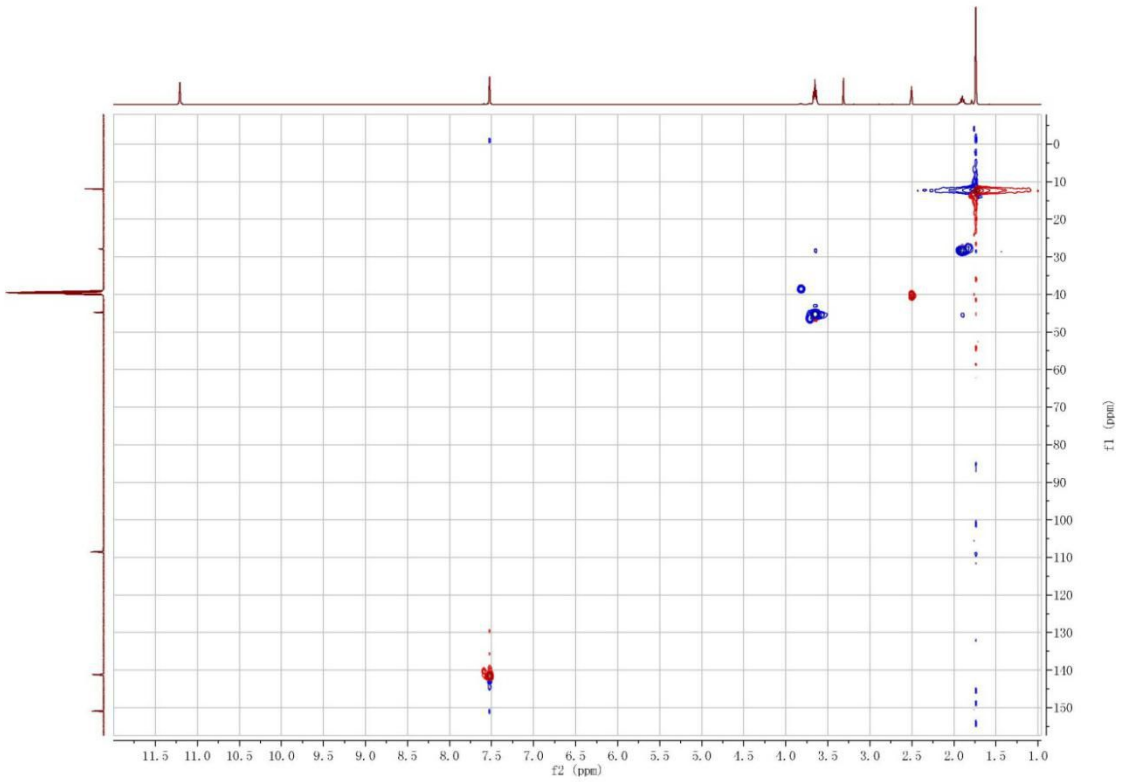

Spectrum 16:HSQC spectrum of 1,1'- trimethylene-bis(thymine) (11)

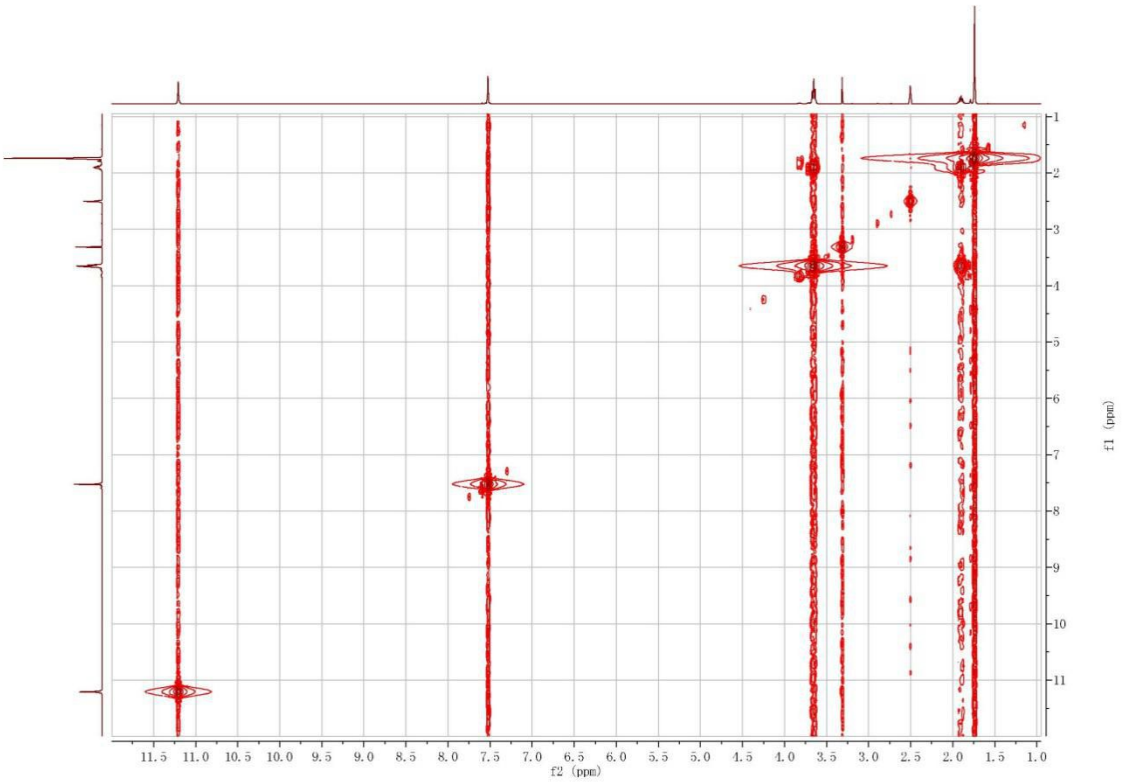

Spectrum 17: COSY spectrum of 1,1'- trimethylene-bis(thymine) (11)

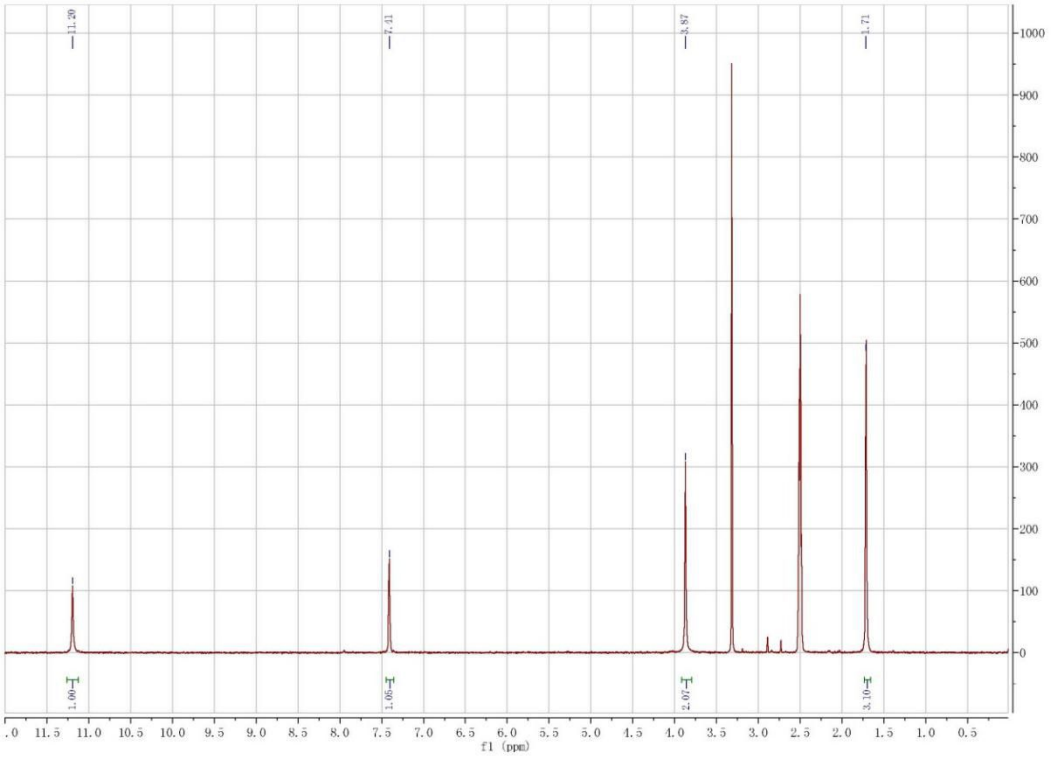

Spectrum 18: ^{1}H NMR spectrum of 1,1'- bimethylene-bis(thymine) (12)

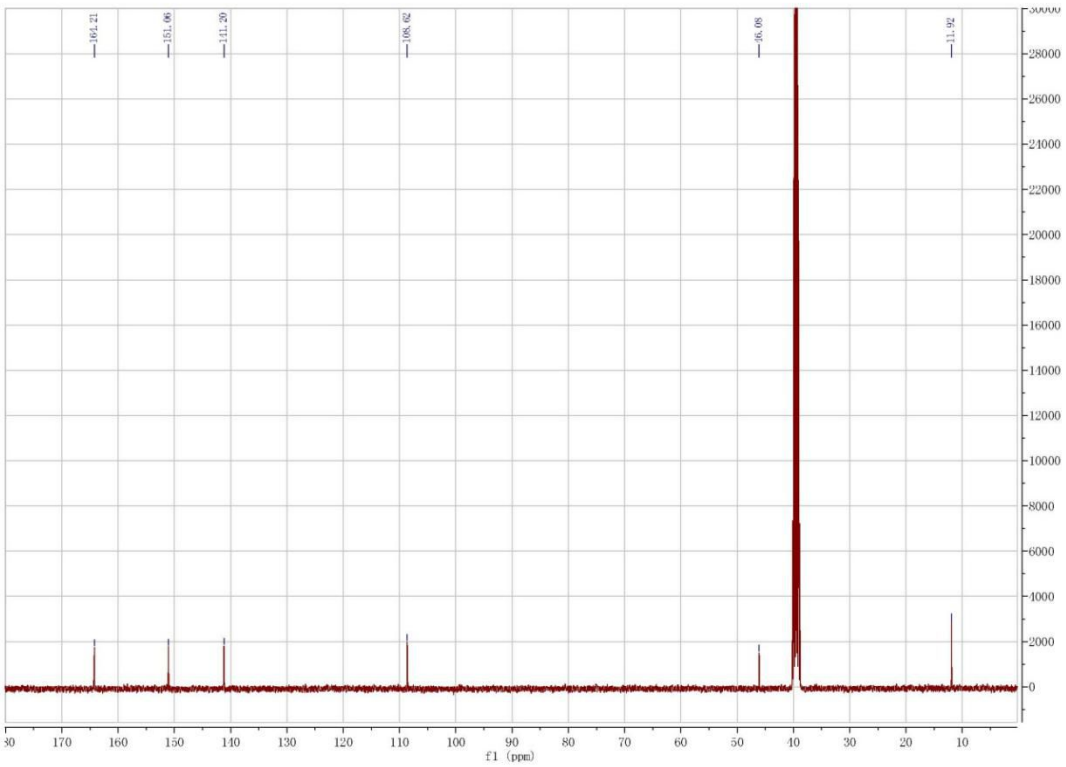

Spectrum 19: ^{13}C NMR spectrum of 1,1'- bimethylene-bis(thymine) (12)

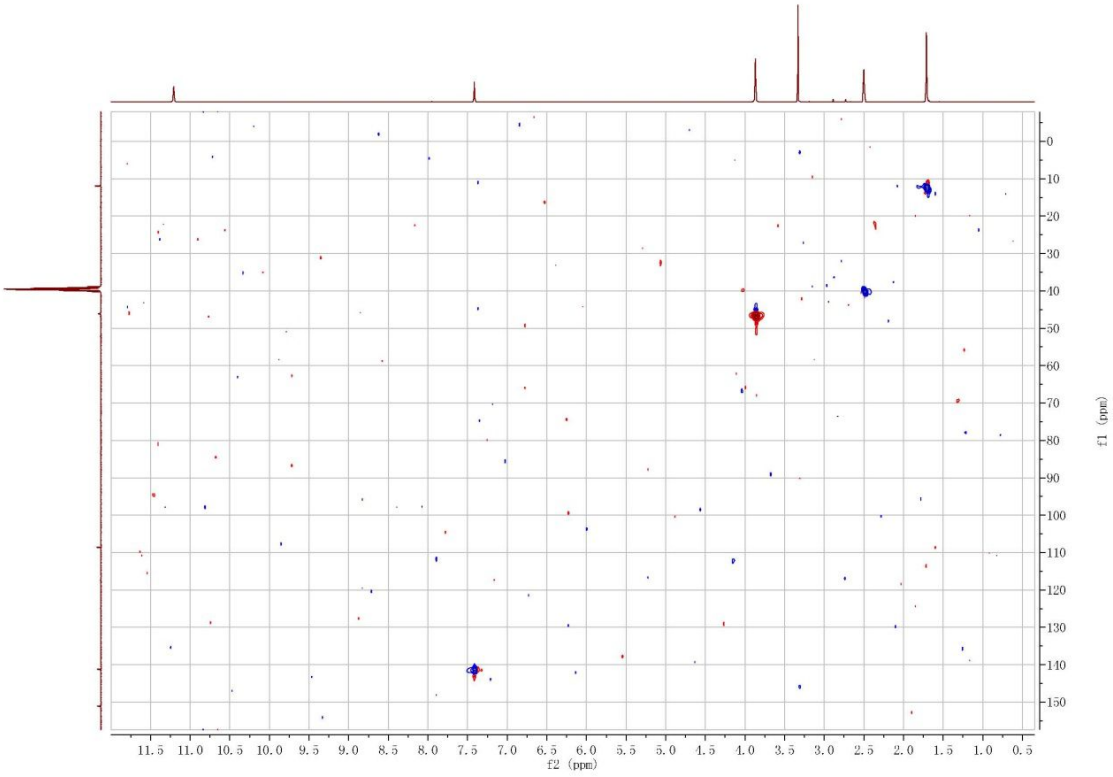

Spectrum 20: HMQC spectrum of 1,1'- bimethylene-bis(thymine) (12)

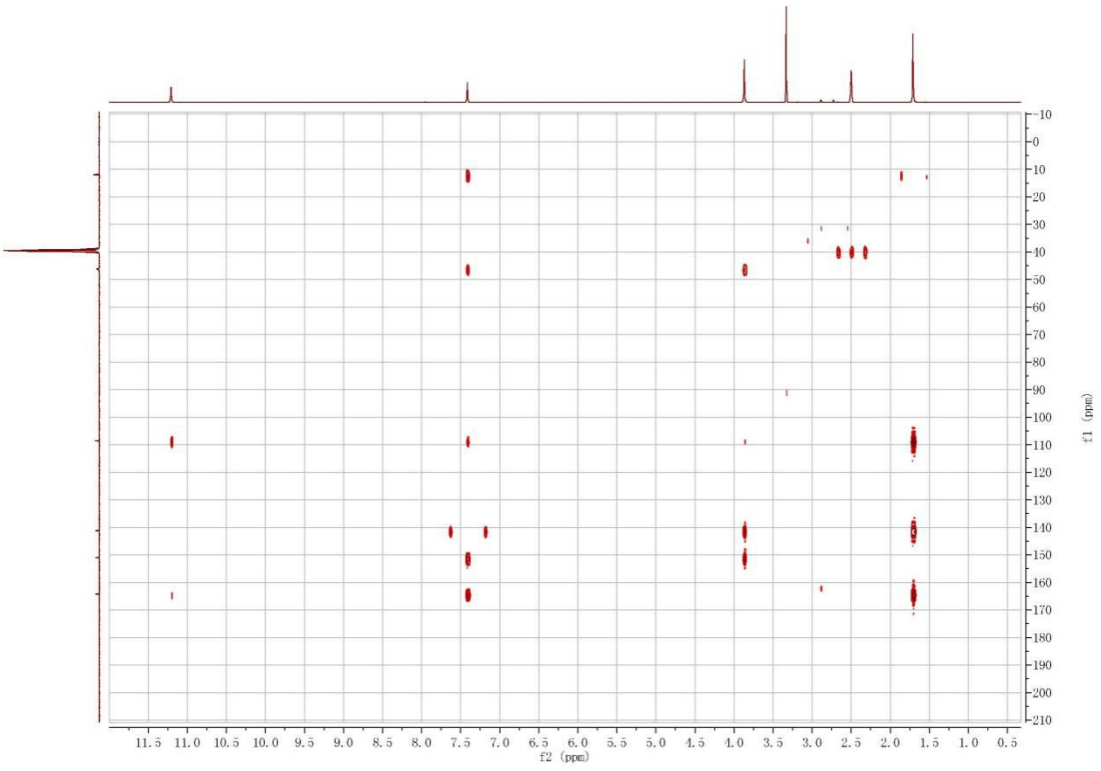

Spectrum 21: HMBC spectrum of 1,1'- bimethylene-bis(thymine) (12)

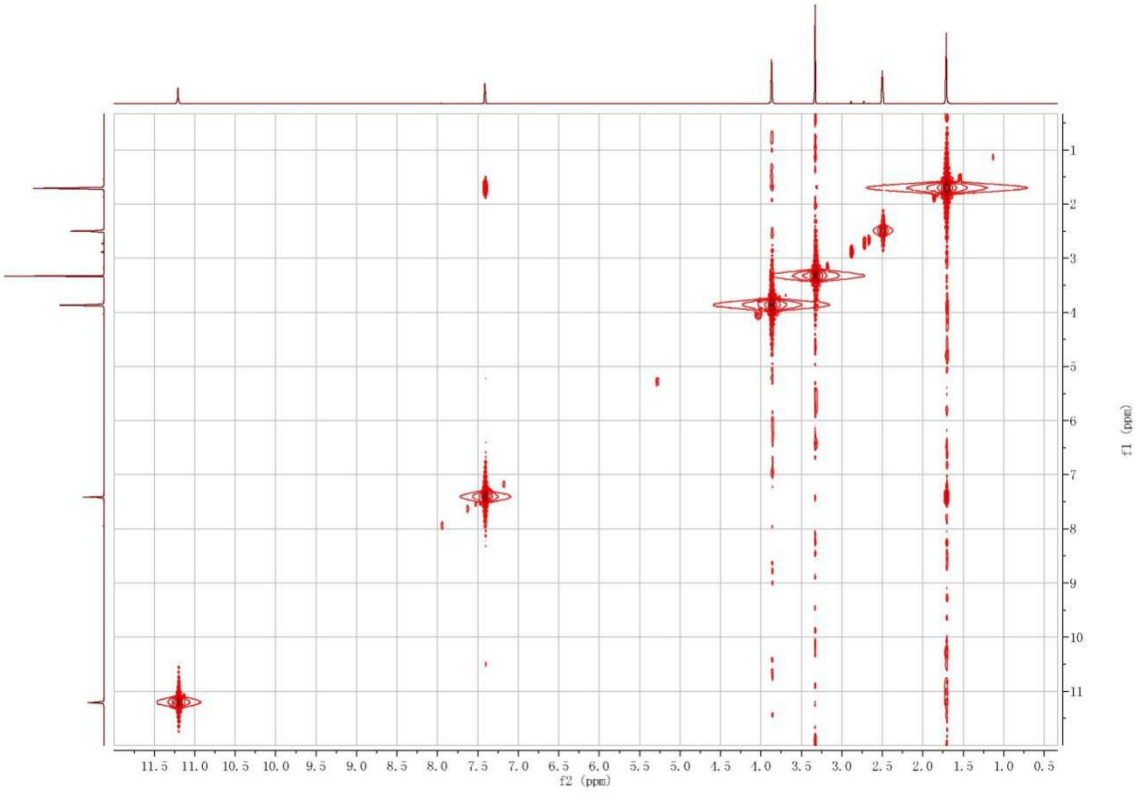

Spectrum 22: COSYspectrum of 1,1'- bimethylene-bis(thymine) (12)

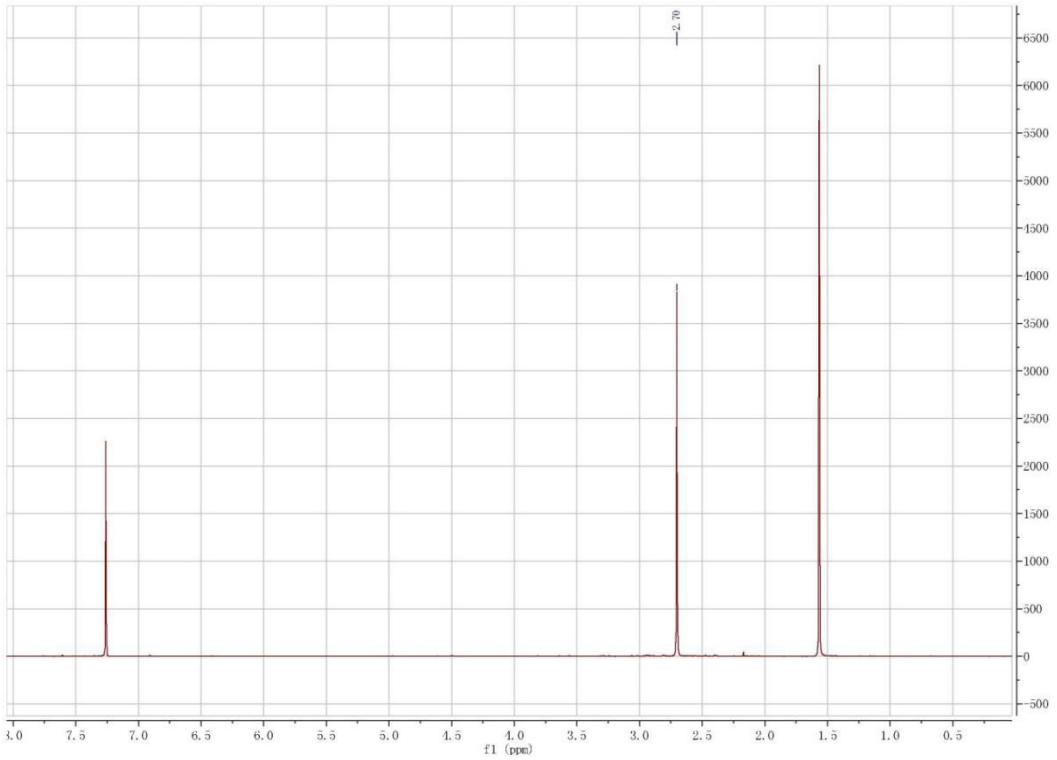

Spectrum 23: ^{1}H NMR spectrum of 1,3,5,7-tetrabromoadamantane (15)

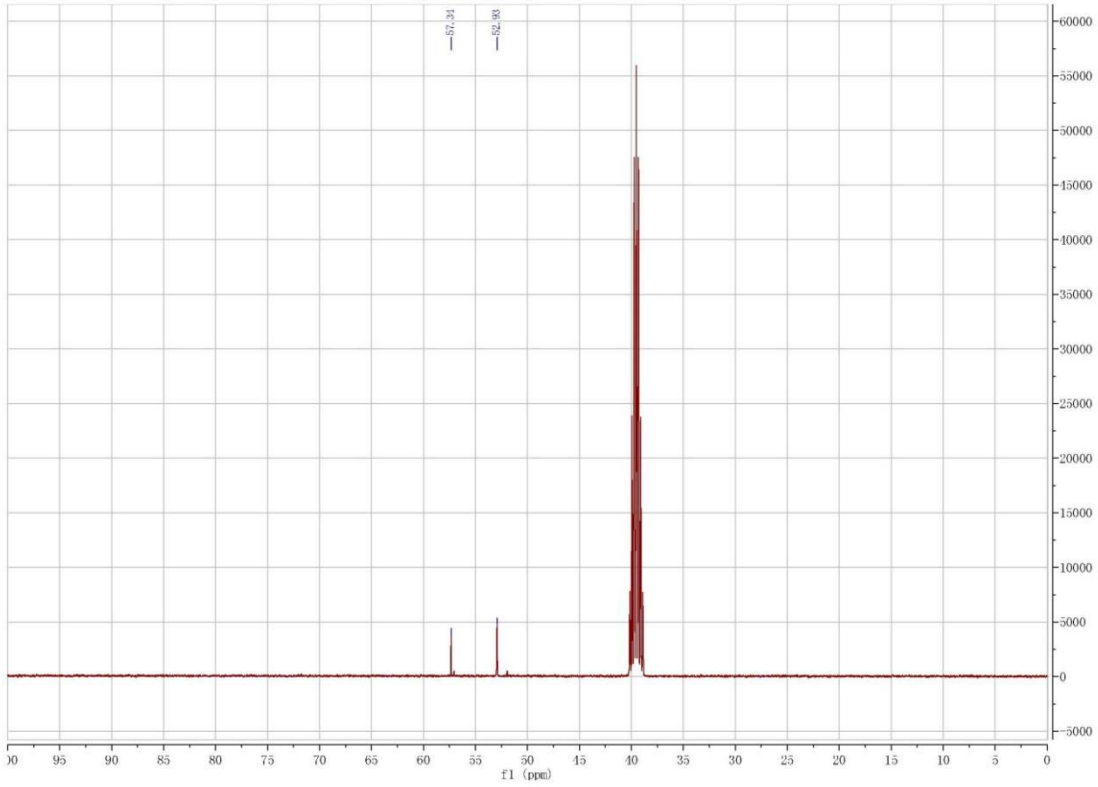

Spectrum 24: ^{13}C NMR spectrum of 1,3,5,7-tetrabromoadamantane (15)

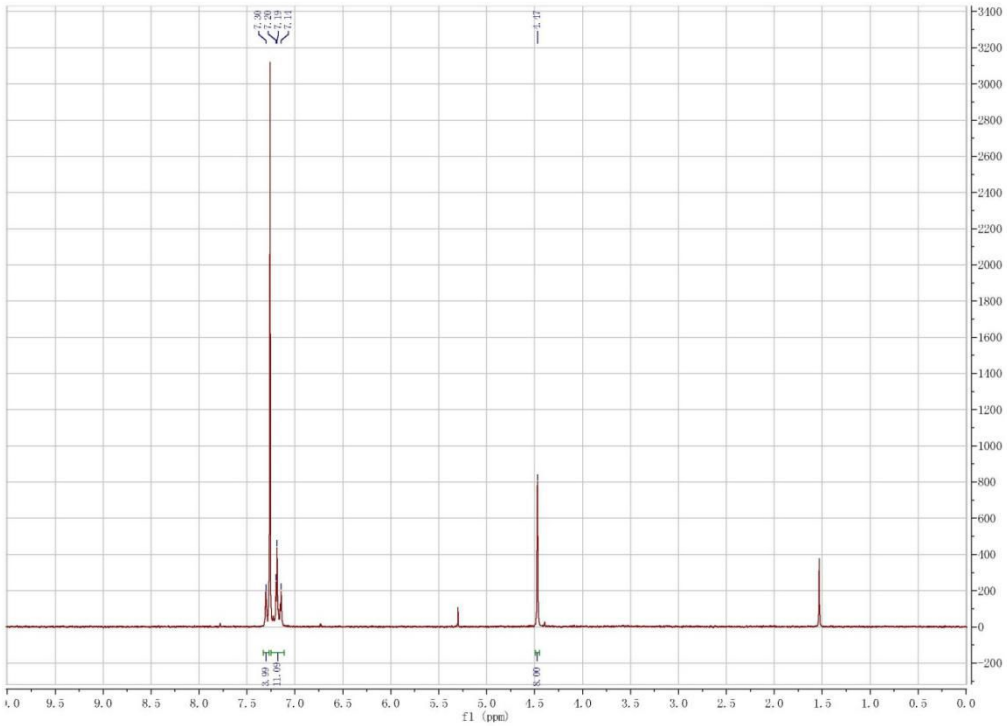

Spectrum 25: ^{1}H NMR spectrum of tetrakis(4-(bromomethyl)phenyl)methane (21)

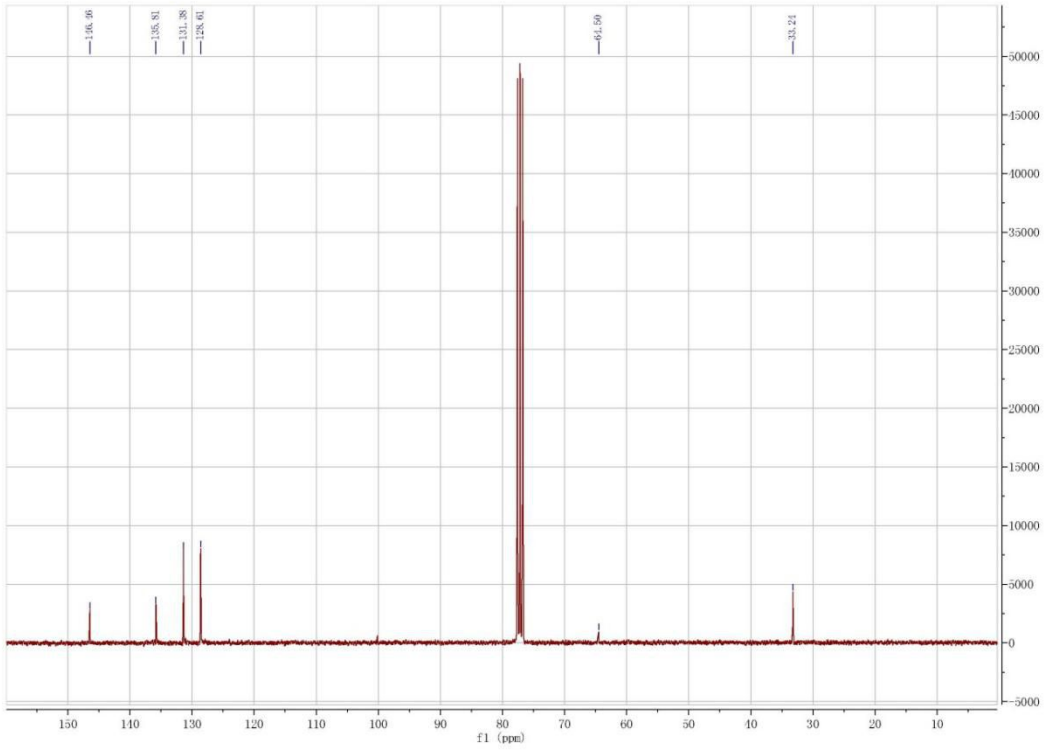

Spectrum 26: ^{13}C NMR spectrum of tetrakis(4-(bromomethyl)phenyl)methane (21)

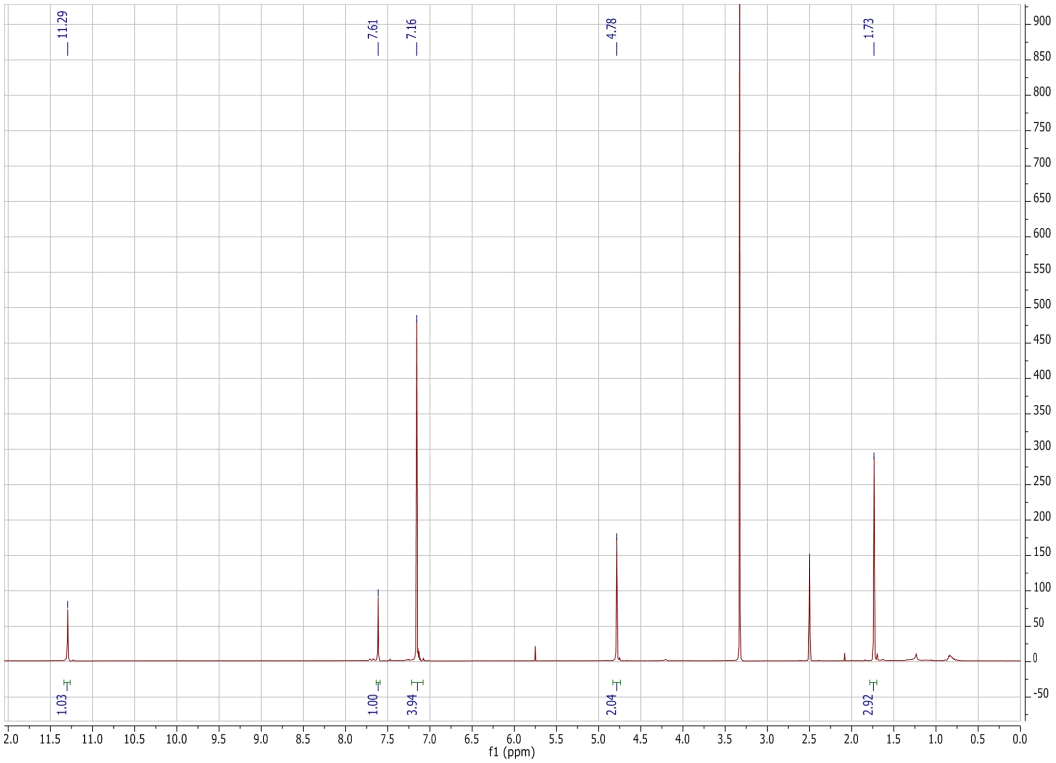

Spectrum 27: ^{1}H NMR spectrum of tetrakis(4-thyminylmethylphenyl)methane (22)

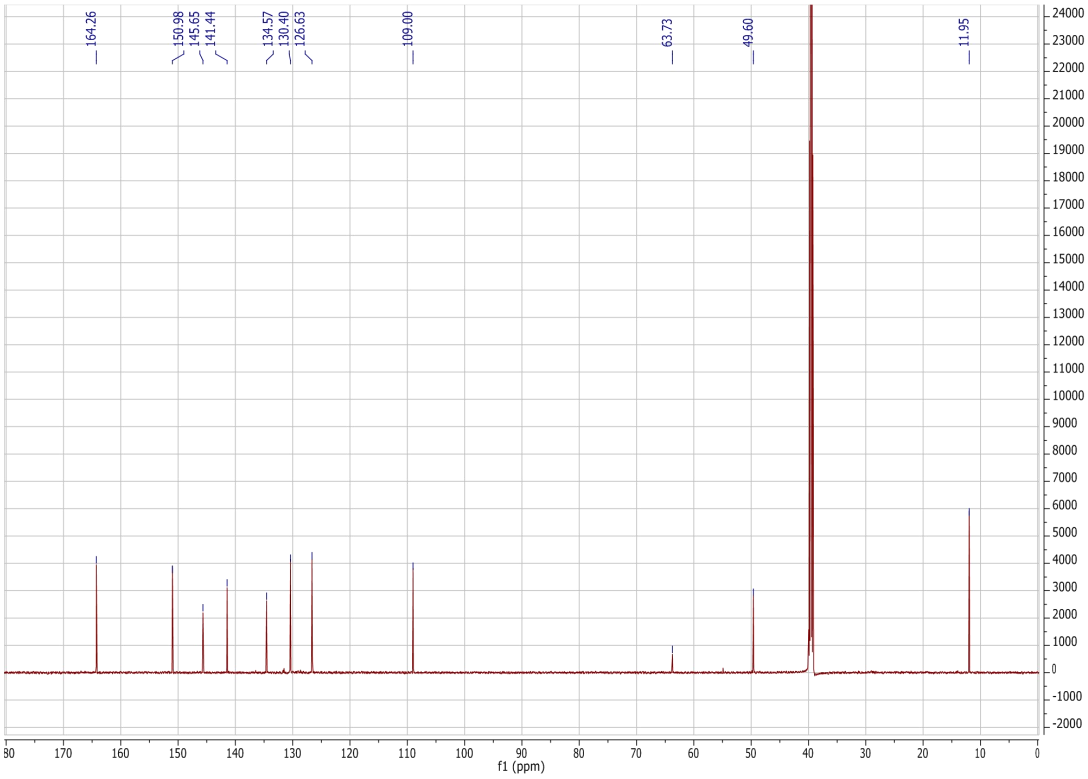

Spectrum 28: ^{13}C NMR spectrum of tetrakis(4-thyminylmethylphenyl)methane (22)

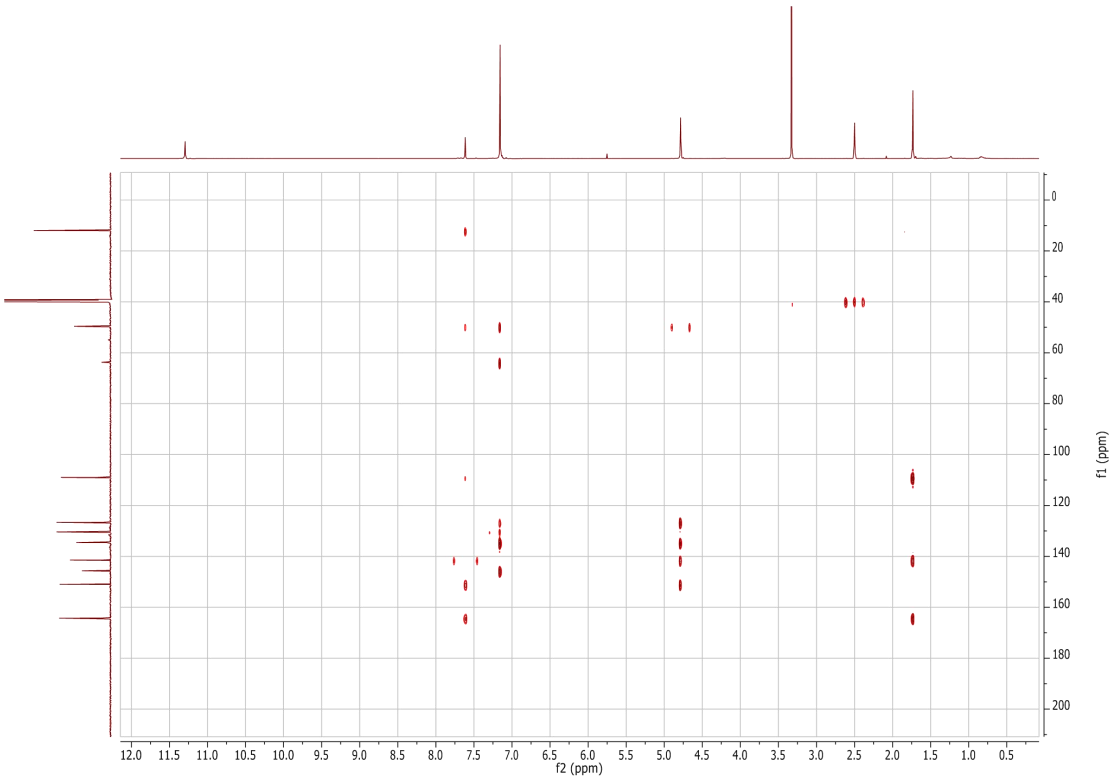

Spectrum 29: HMBC spectrum of tetrakis(4-thyminylmethylphenyl)methane (22)

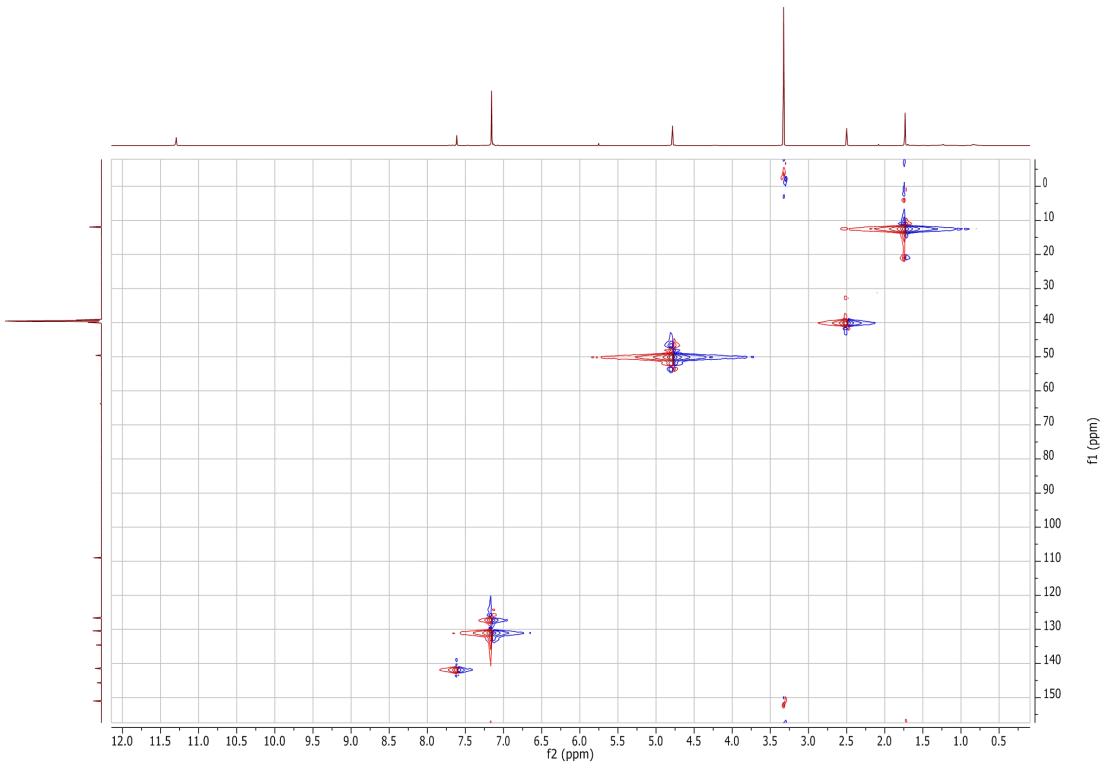

Spectrum 30: HSQC spectrum of tetrakis(4-thyminylmethylphenyl)methane (22)

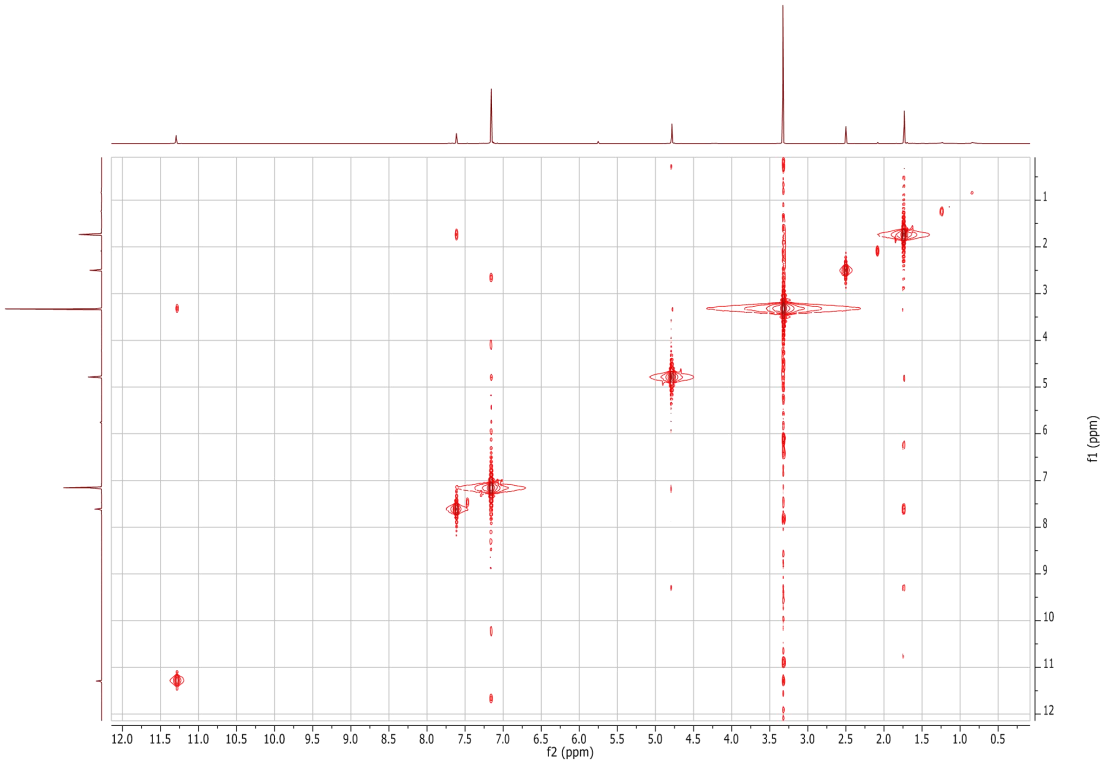

Spectrum 31: COSY spectrum of tetrakis(4-thyminylmethylphenyl)methane (22)

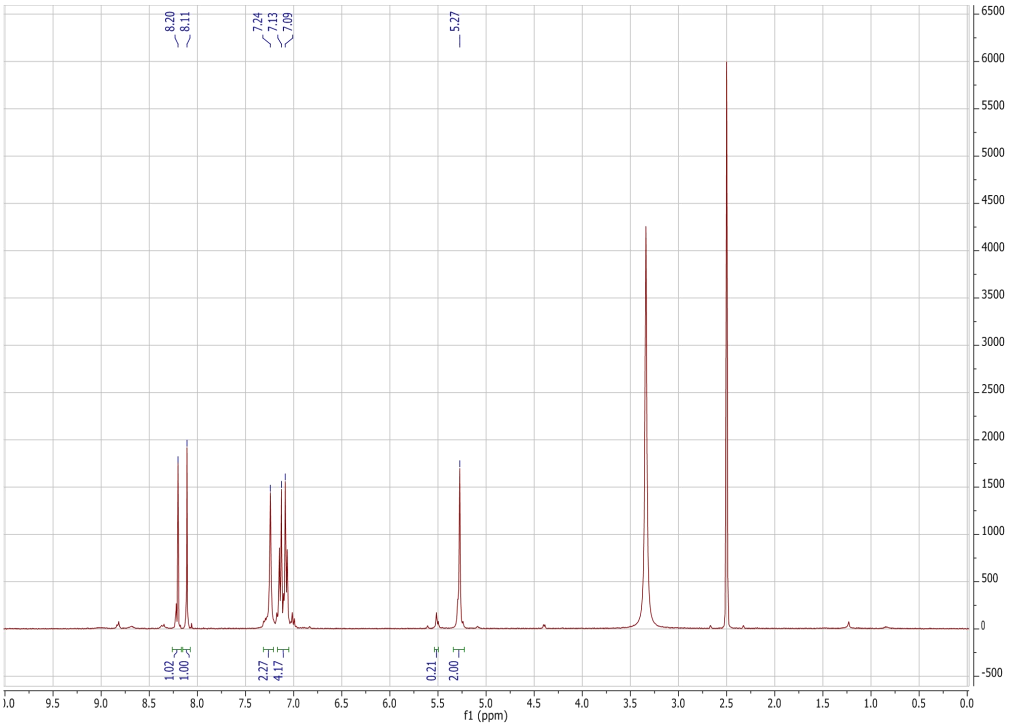

Spectrum 32: ^{1}H NMR spectrum of tetrakis(4-adeninylmethylphenyl)methane (23)

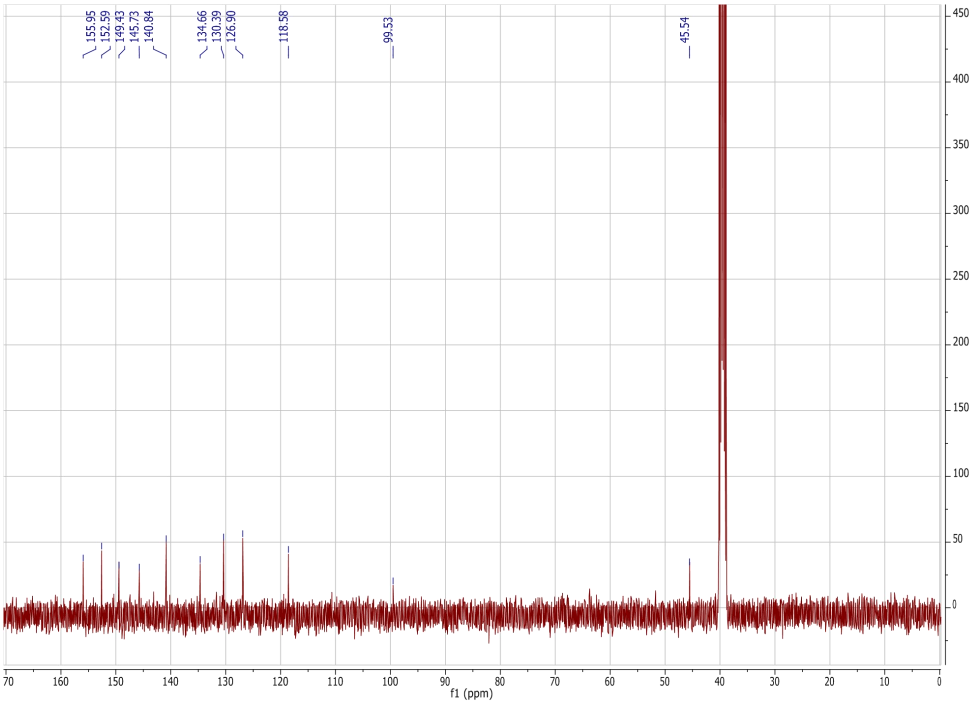

Spectrum 33: ^{13}C NMR spectrum of tetrakis(4-adeninylmethylphenyl)methane (23)

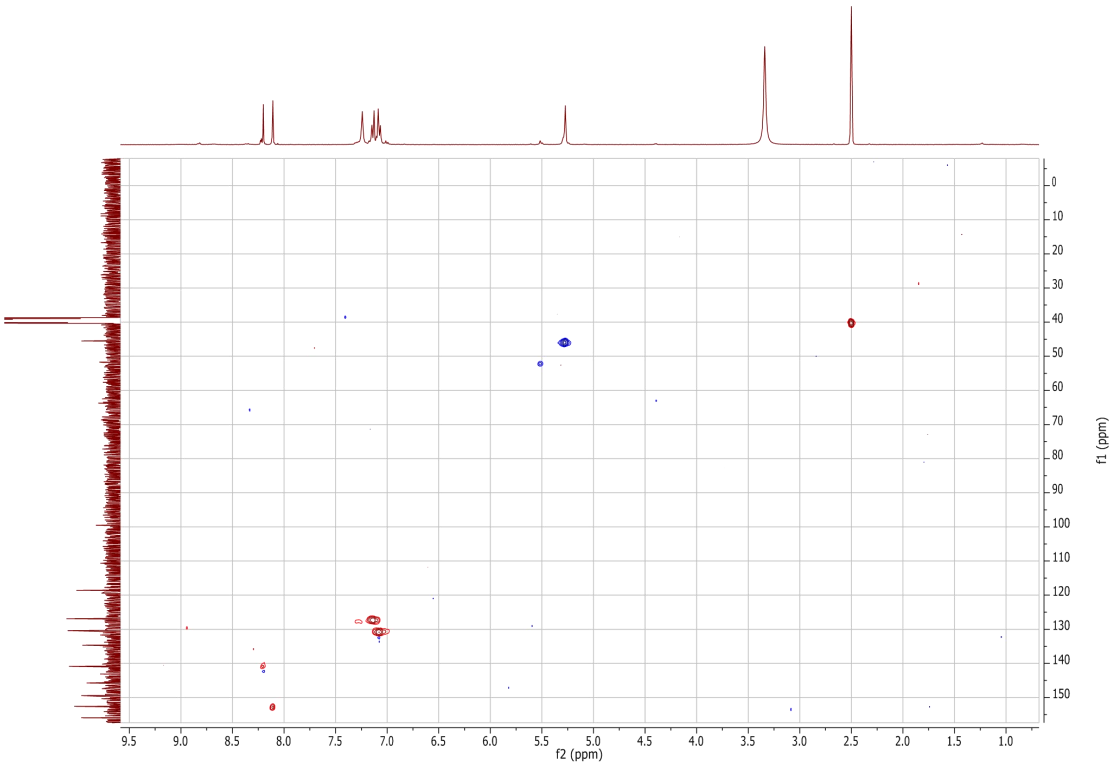

Spectrum 34: HSQC spectrum of tetrakis(4-adeninylmethylphenyl)methane (23)

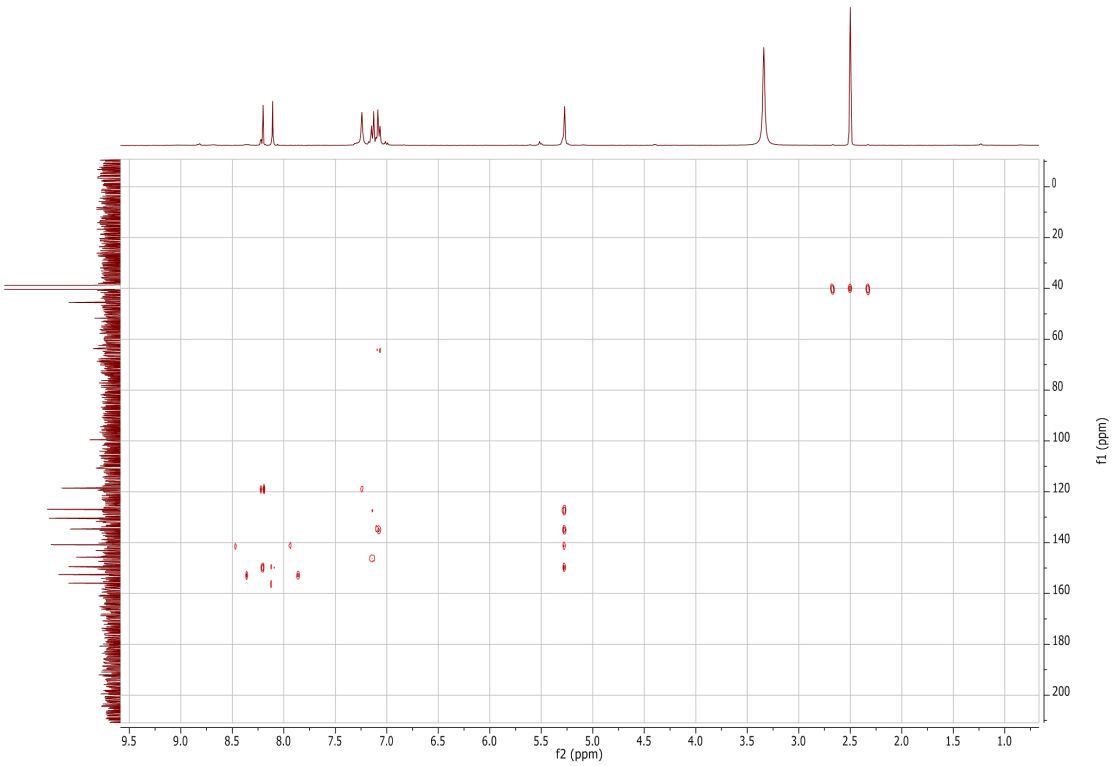

Spectrum 35: HMBC spectrum of tetrakis(4-adeninylmethylphenyl)methane (23)

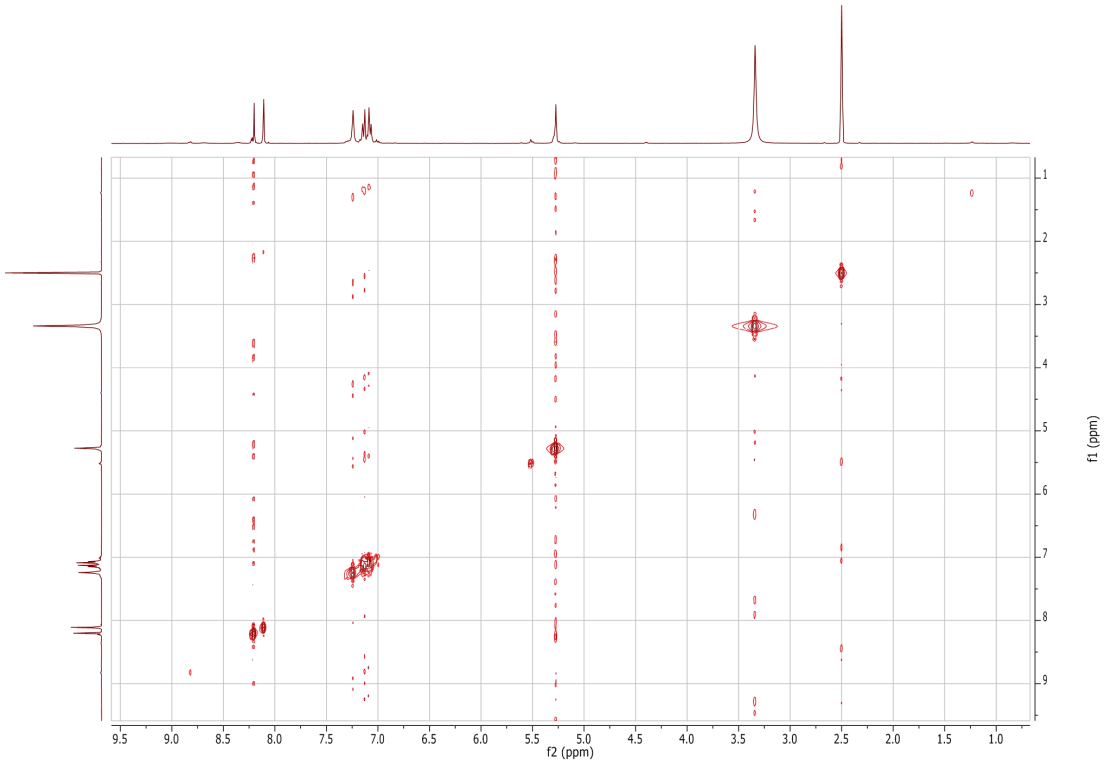

Spectrum 36: COSY spectrum of tetrakis(4-adeninylmethylphenyl)methane (23)

2. PXRD patterns

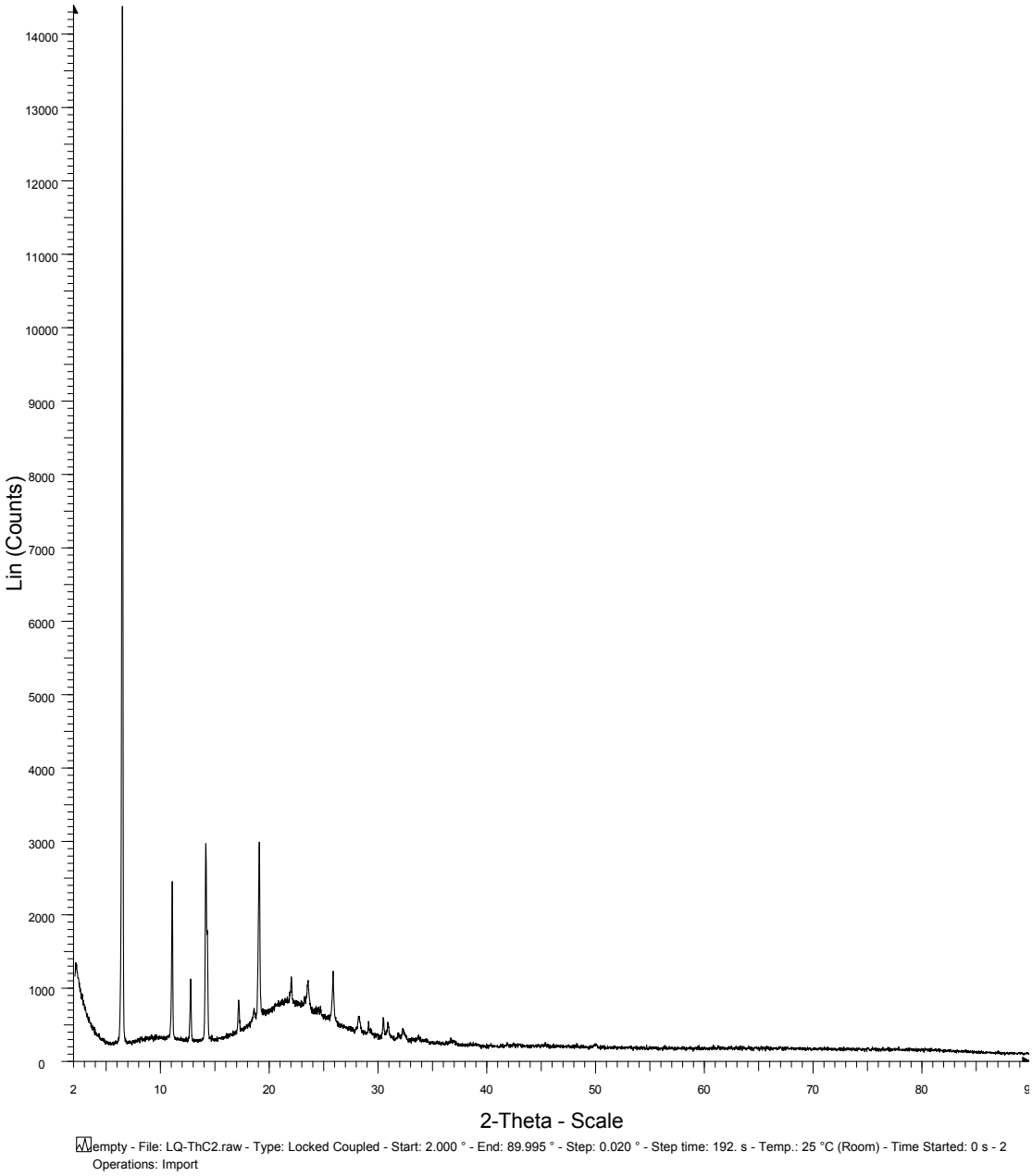

Figure A1: PXRD pattern of 1,1'- dimethylene-bis(thymine) (12) ThC2Th

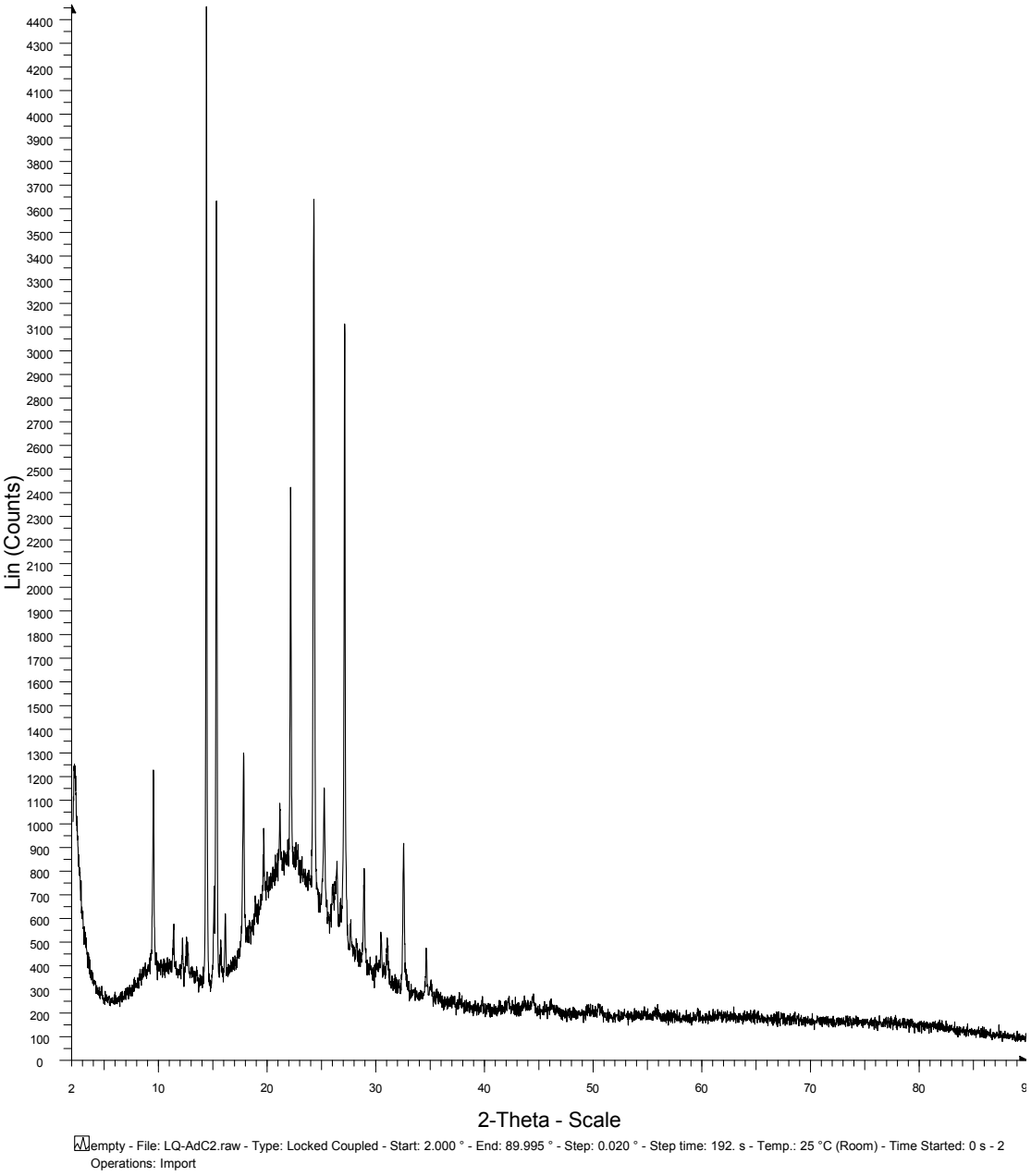

Figure A2: PXRD pattern of 1,1'- dimethylene-bis(adenine) (2) AdC2Ad

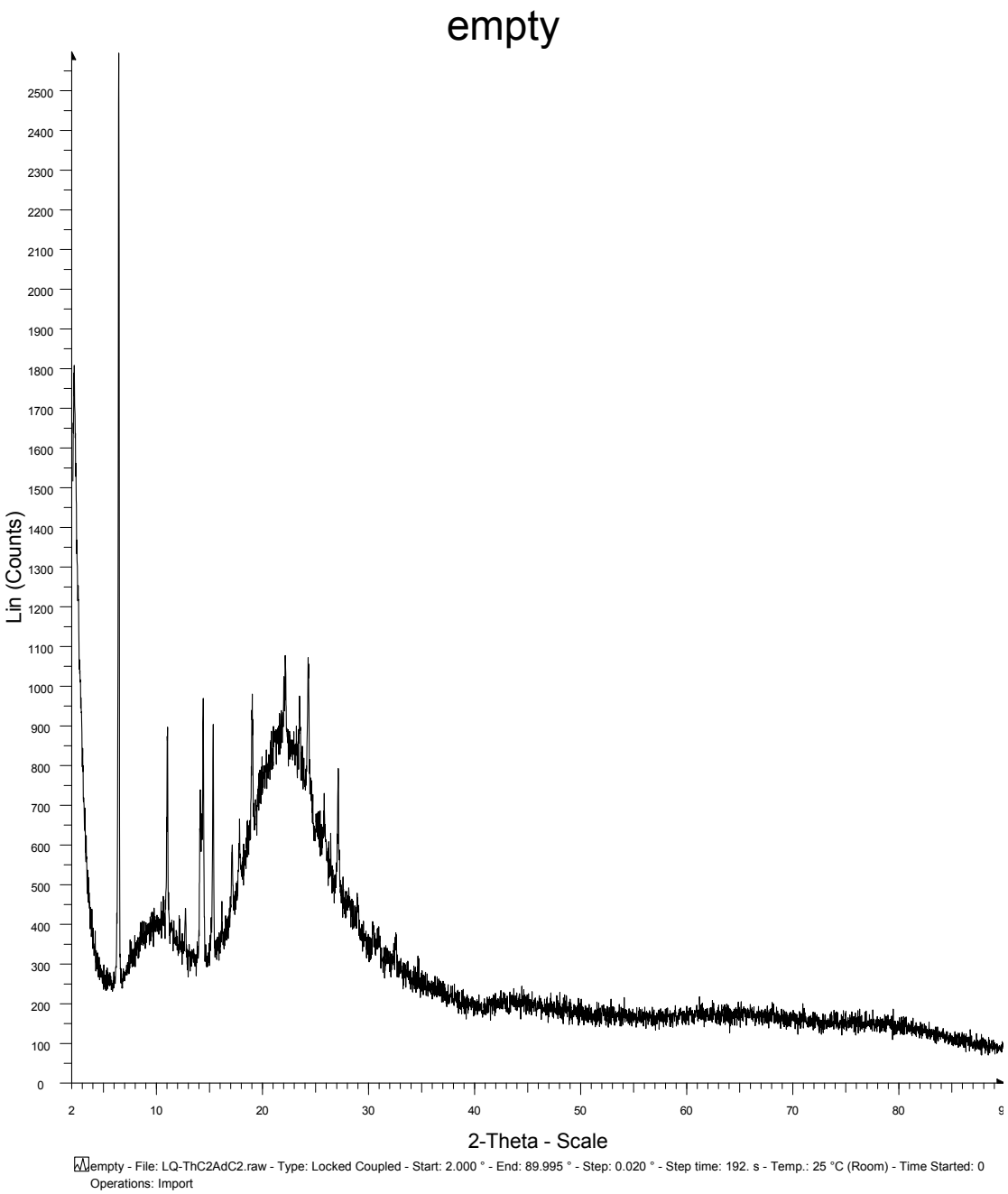

Figure A3: PXRD pattern of mixture of AdC2Ad-ThC2Th from vapor diffusion of HFP-MeOH

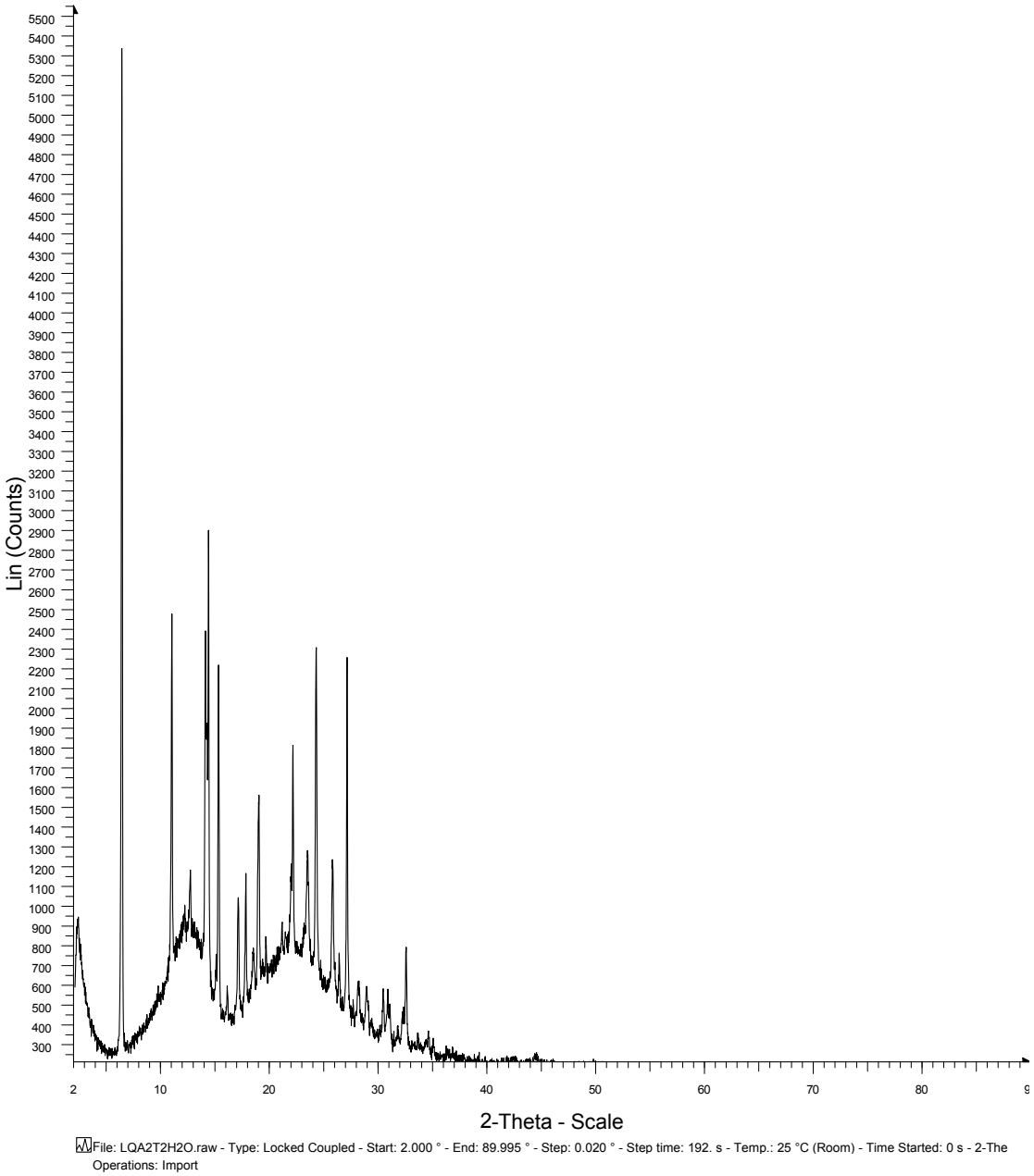

Figure A4: PXRD pattern of mixture of AdC2Ad-ThC2Th grinded in H_2O

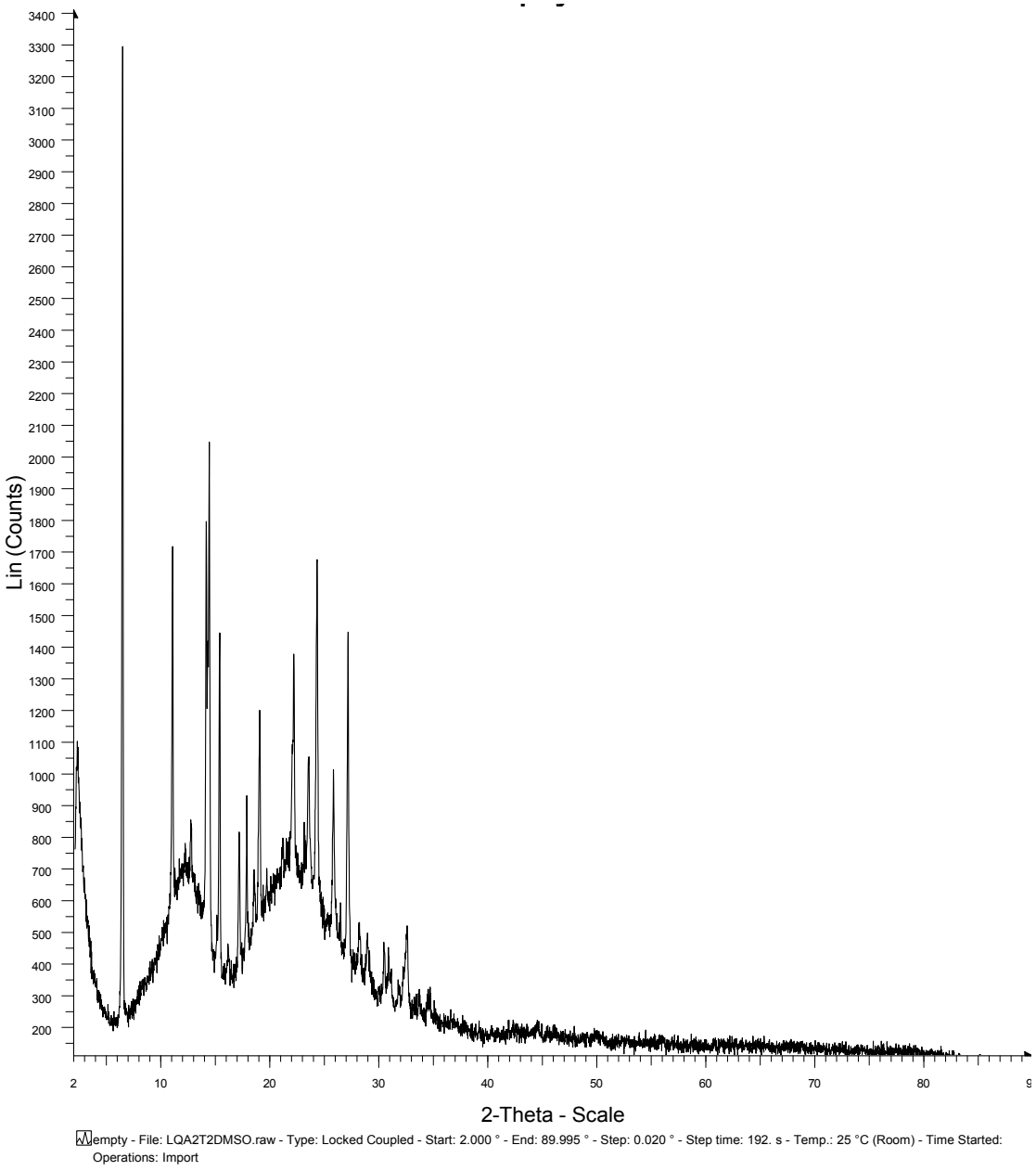

Figure A5: PXRD pattern of mixture of AdC2Ad-ThC2Th grinded in DMSO

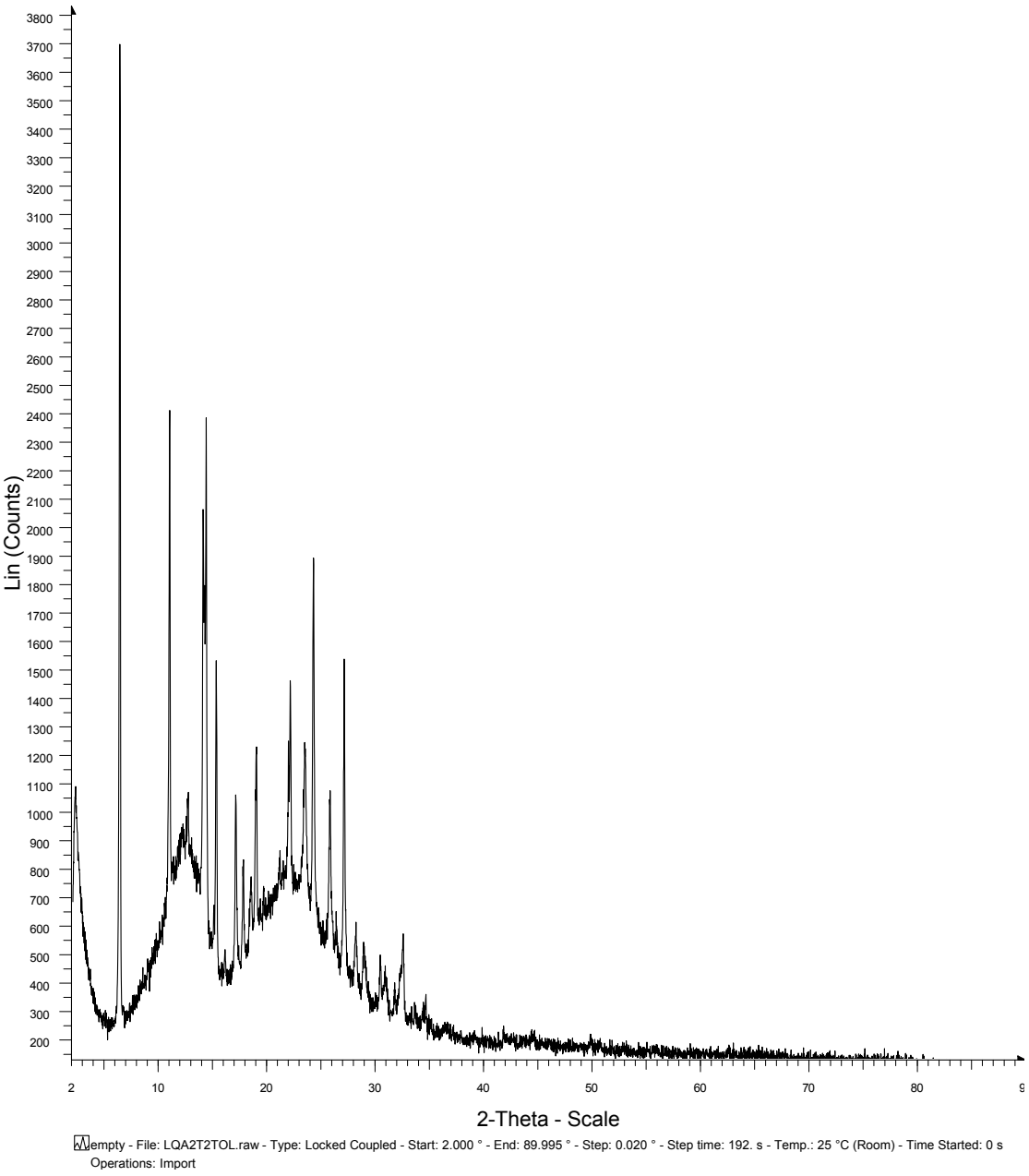

Figure A6: PXRD pattern of mixture of AdC2Ad-ThC2Th grinded in toluene

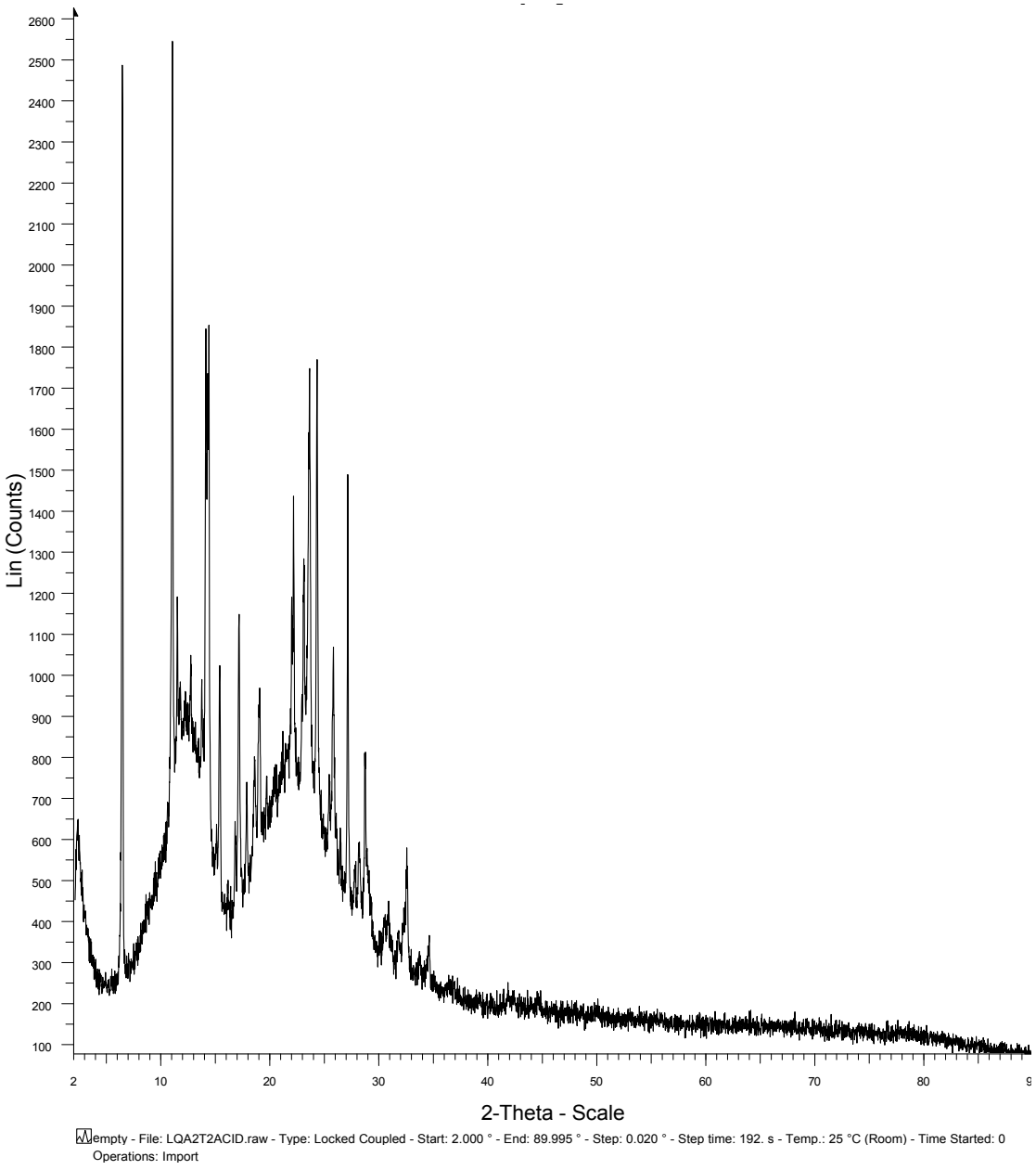

Figure A7: PXRD pattern of mixture of AdC2Ad-ThC2Th grinded in acetic acid

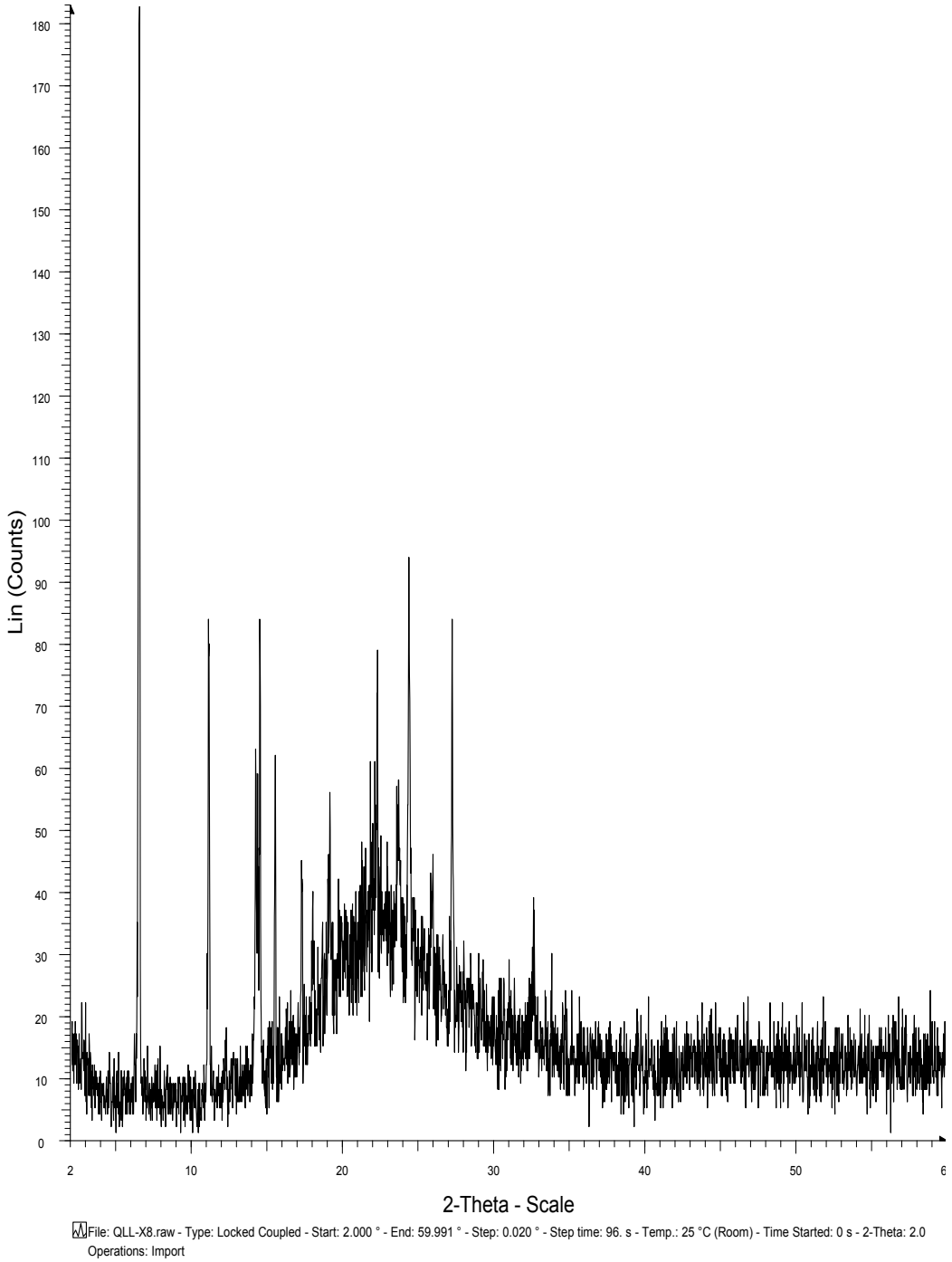

Figure A8: PXRD pattern of mixture of AdC2Ad-ThC2Th from DMSO in ultrasonic bath for 5 h

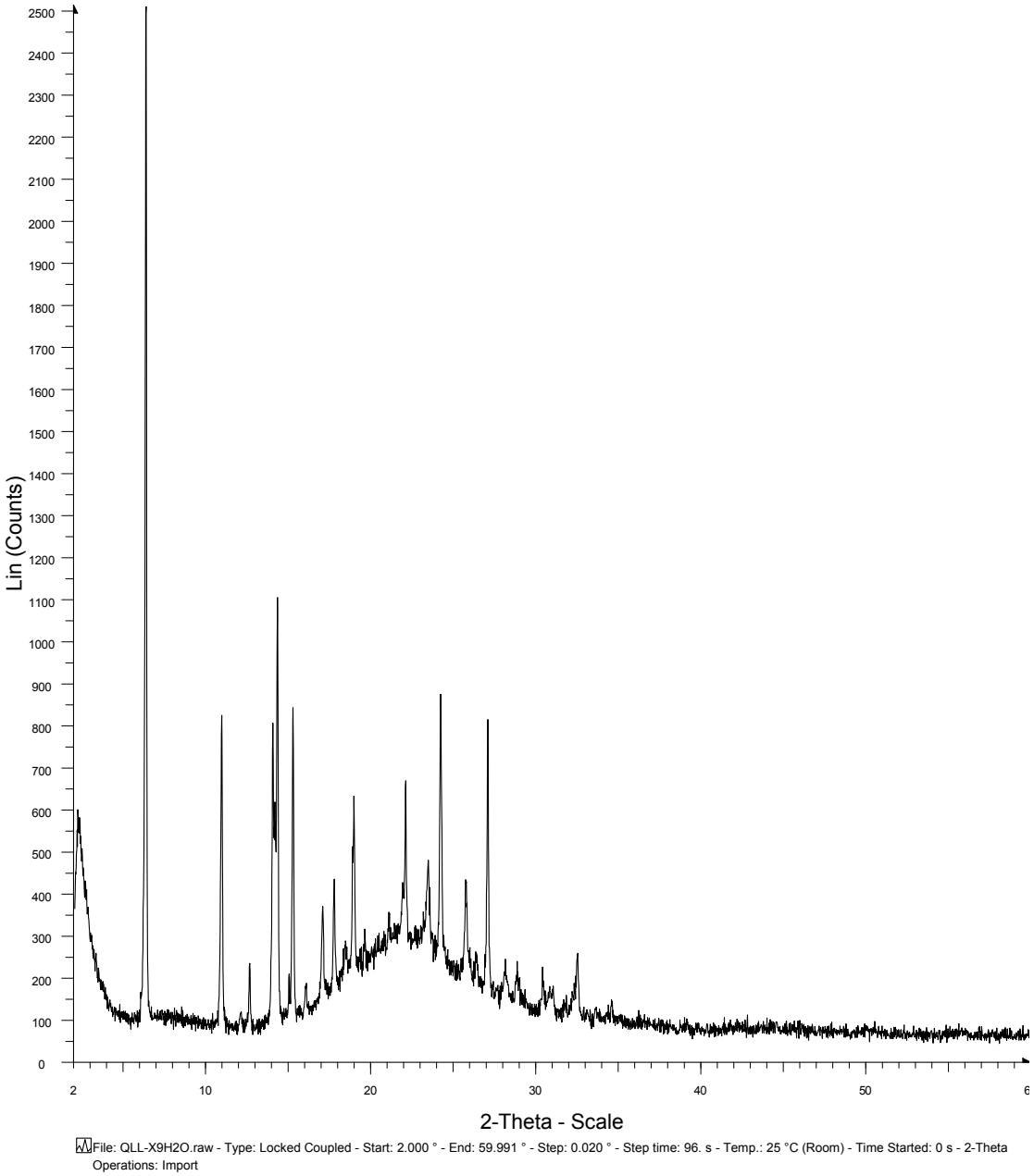

Figure A9: PXRD pattern of mixture of AdC2Ad-ThC2Th from H_2O in ultrasonic bath for 5 h

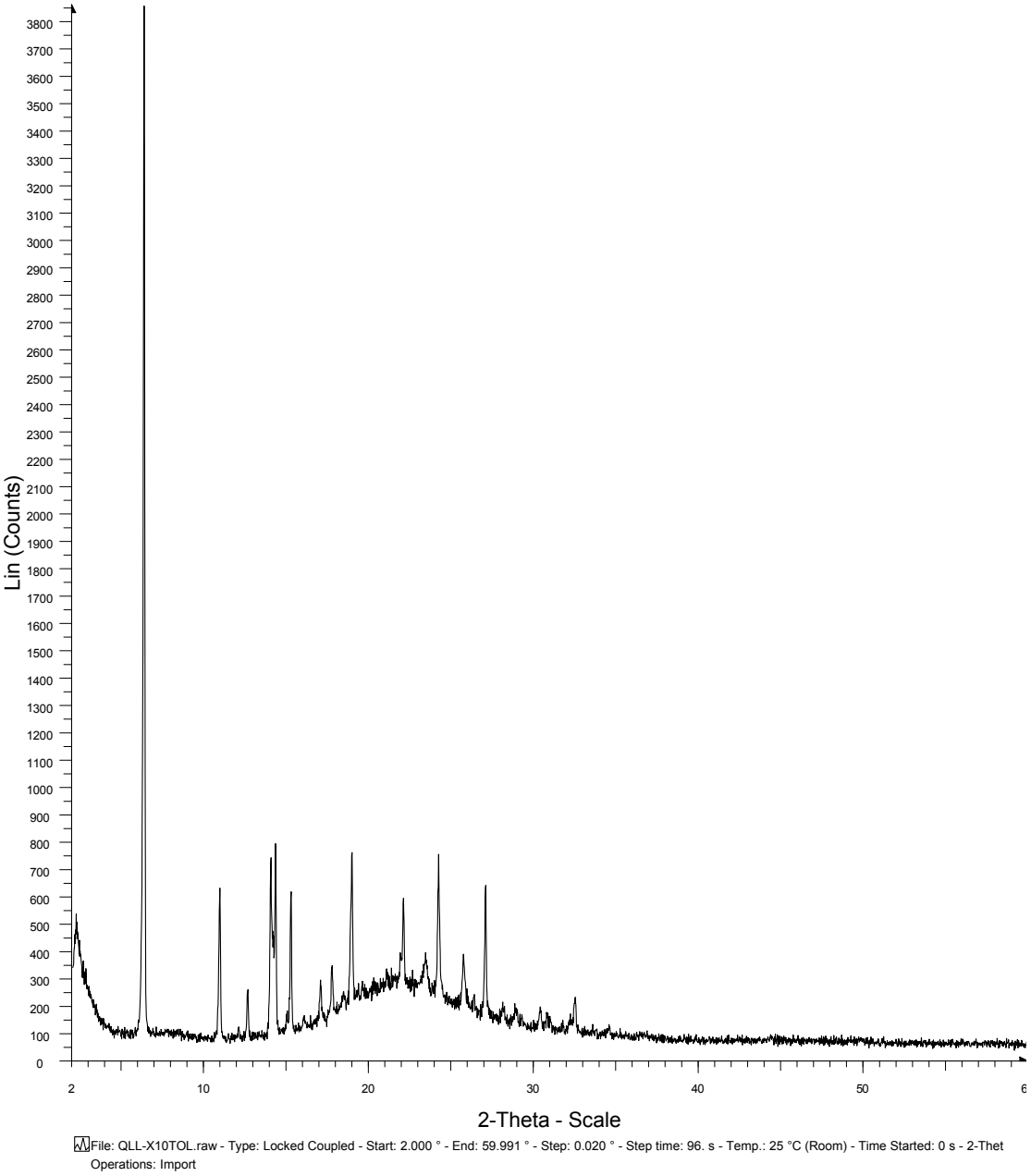

Figure A10: PXRD pattern of mixture of AdC2Ad-ThC2Th from toluene in ultrasonic bath for 5 h

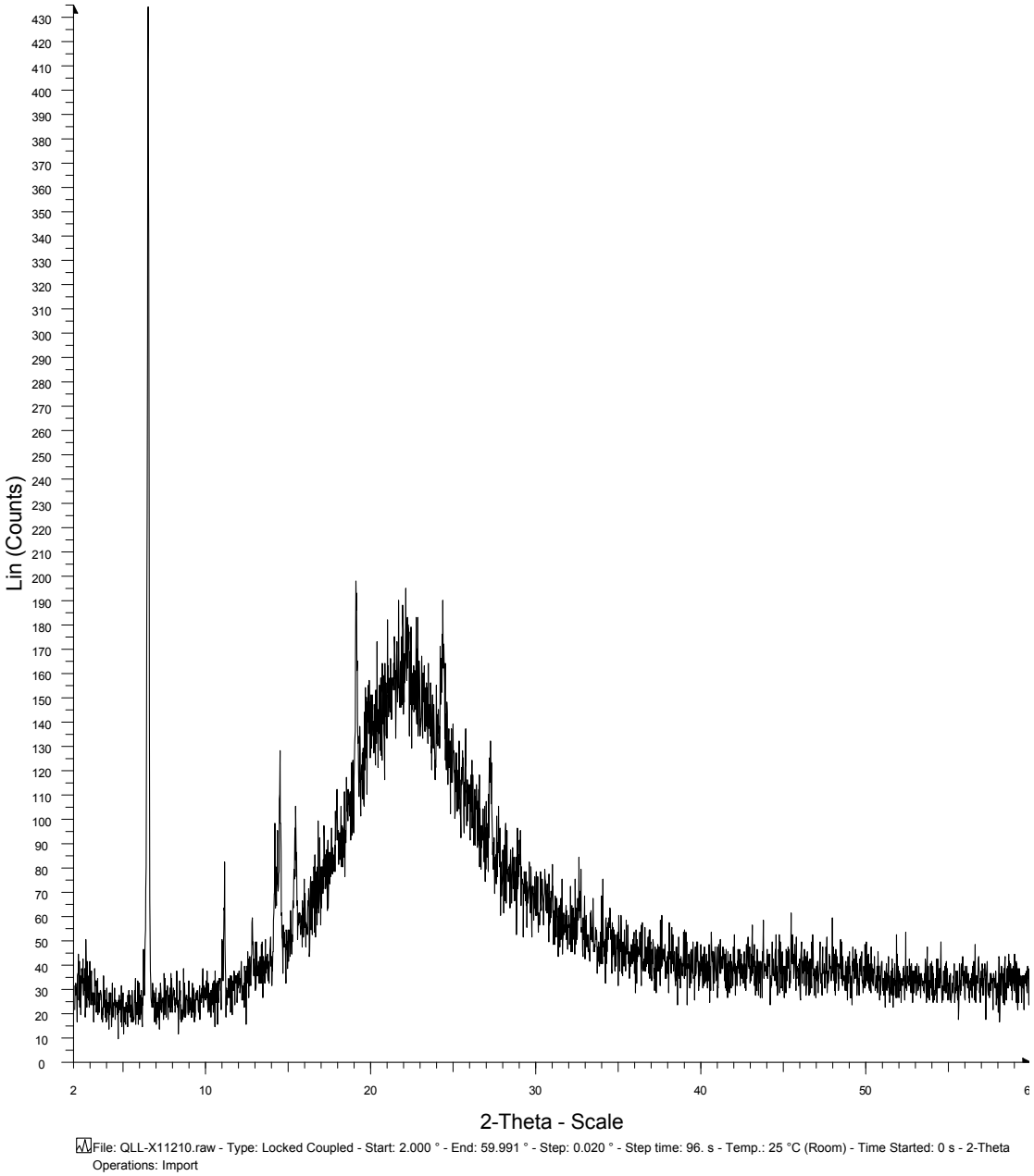

Figure A11: PXRD pattern of mixture of AdC2Ad-ThC2Th heated to 210 ºC for 5 min

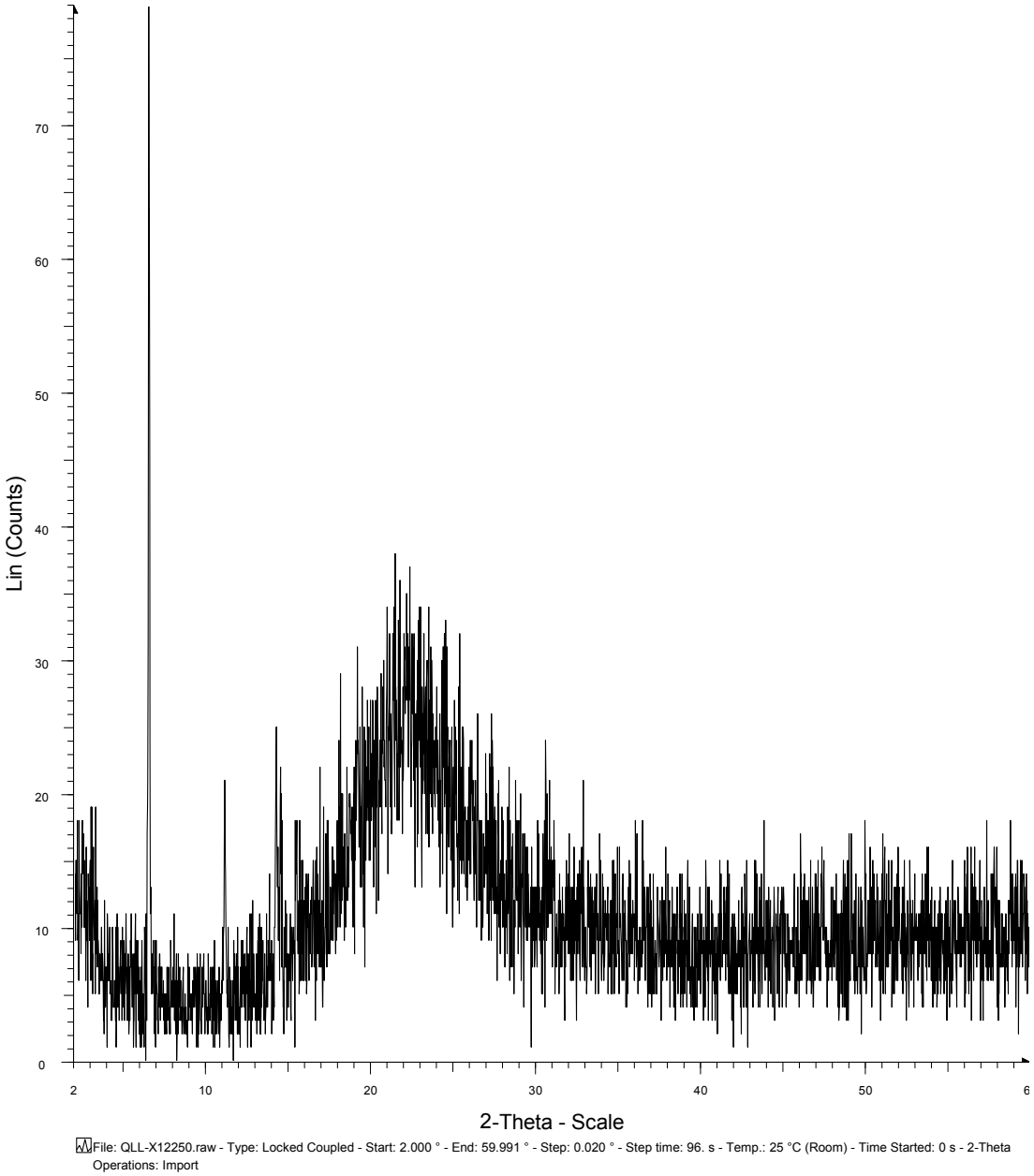

Figure A12: PXRD pattern of mixture of AdC2Ad-ThC2Th heated to 250 ºC for 5 min

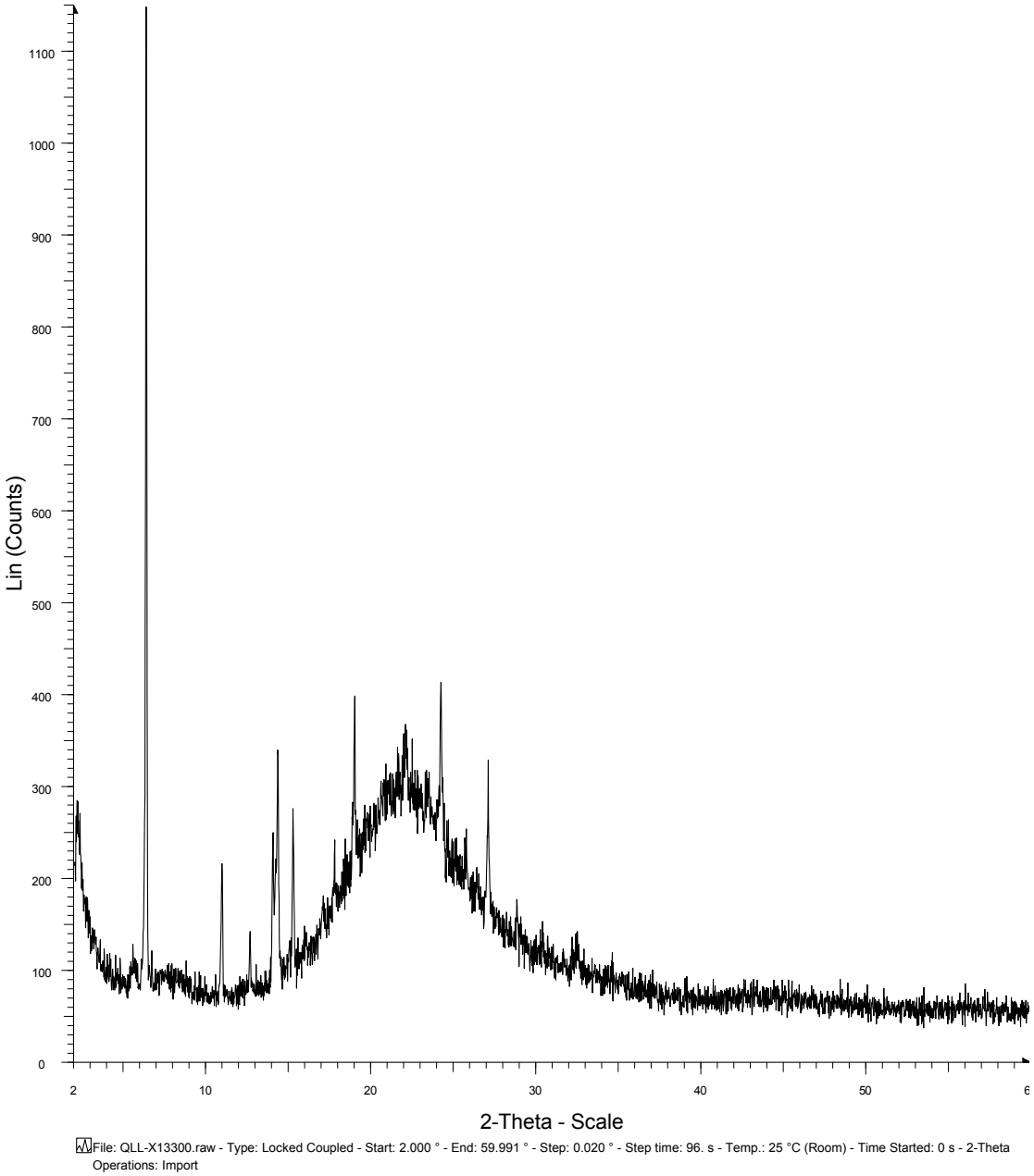

Figure A13: PXRD pattern of mixture of AdC2Ad-ThC2Th heated to 300 ºC for 5 min

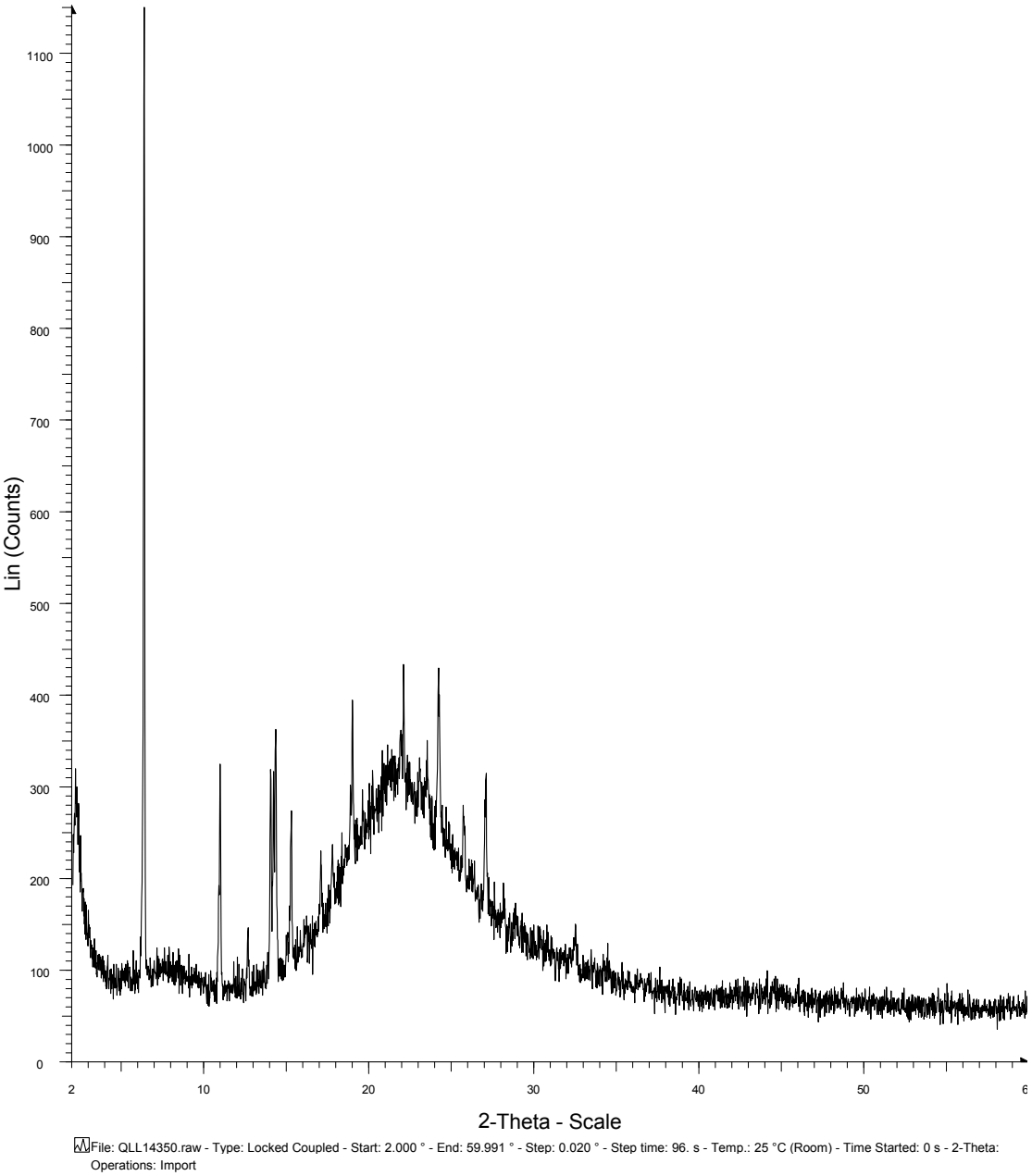

Figure A14: PXRD pattern of mixture of AdC2Ad-ThC2Th heated to 350 ºC for 5 min

3. Single crystal data

3.1. Th4 crystal from HFP-MeOH

Cif for Th4 from HFP-MeOH (lists of coordinates and molecular geometry parameters have been left out).

```
data_Th4 from HFP-MeOH


_audit_creation_method                  SHELXL-2013

_chemical_name_systematic               C49H44N8O8

_chemical_name_common                   ?

_chemical_melting_point                 ?

_chemical_formula_moiety                ?

_chemical_formula_sum                   'C24.75 H23 N4 O4.25'

_chemical_formula_weight                444.47


loop_

 _atom_type_symbol

 _atom_type_description

 _atom_type_scat_dispersion_real

 _atom_type_scat_dispersion_imag

 _atom_type_scat_source

'C'  'C'   0.0033   0.0016

'International Tables Vol C Tables 4.2.6.8 and 6.1.1.4'
```

'H' 'H' 0.0000 0.0000

'International Tables Vol C Tables 4.2.6.8 and 6.1.1.4'

'N' 'N' 0.0061 0.0033

'International Tables Vol C Tables 4.2.6.8 and 6.1.1.4'

'O' 'O' 0.0106 0.0060

'International Tables Vol C Tables 4.2.6.8 and 6.1.1.4'

_space_group_crystal_system triclinic

_space_group_IT_number 2

_space_group_name_H-M_alt 'P -1'

_space_group_name_Hall '-P 1'

_shelx_space_group_comment

;

The symmetry employed for this shelxl refinement is uniquely defined

by the following loop, which should always be used as a source of

symmetry information in preference to the above space-group names.

They are only intended as comments.

loop_

_space_group_symop_operation_xyz

'x, y, z'

'-x, -y, -z'

_cell_length_a	14.4613(17)
_cell_length_b	20.326(2)
_cell_length_c	23.303(3)
_cell_angle_alpha	65.194(3)
_cell_angle_beta	85.341(3)
_cell_angle_gamma	73.765(3)
_cell_volume	5964.7(12)
_cell_formula_units_Z	8
_cell_measurement_temperature	100(2)
_cell_measurement_reflns_used	?
_cell_measurement_theta_min	?
_cell_measurement_theta_max	?

_exptl_crystal_description	?
_exptl_crystal_colour	?
_exptl_crystal_density_meas	?
_exptl_crystal_density_method	?
_exptl_crystal_density_diffrn	0.990

_exptl_crystal_F_000	1868
_exptl_transmission_factor_min	?
_exptl_transmission_factor_max	?
_exptl_crystal_size_max	?
_exptl_crystal_size_mid	?
_exptl_crystal_size_min	?
_exptl_absorpt_coefficient_mu	0.069
_shelx_estimated_absorpt_T_min	?
_shelx_estimated_absorpt_T_max	?
_exptl_absorpt_correction_type	?
_exptl_absorpt_correction_T_min	?
_exptl_absorpt_correction_T_max	?
_exptl_absorpt_process_details	?

_exptl_special_details

_diffrn_ambient_temperature	100(2)
_diffrn_radiation_wavelength	0.71073
_diffrn_radiation_type	MoK\a
_diffrn_source	?
_diffrn_measurement_device_type	?
_diffrn_measurement_method	?

```
_diffrn_detector_area_resol_mean  ?
_diffrn_reflns_number             88019
_diffrn_reflns_av_unetI/netI      0.0699
_diffrn_reflns_av_R_equivalents   0.0834
_diffrn_reflns_limit_h_min        -15
_diffrn_reflns_limit_h_max        15
_diffrn_reflns_limit_k_min        -22
_diffrn_reflns_limit_k_max        22
_diffrn_reflns_limit_l_min        -25
_diffrn_reflns_limit_l_max        25
_diffrn_reflns_theta_min          2.087
_diffrn_reflns_theta_max          22.722
_diffrn_reflns_theta_full         25.242
_diffrn_measured_fraction_theta_max   0.998
_diffrn_measured_fraction_theta_full  0.742
_diffrn_reflns_Laue_measured_fraction_max    0.998
_diffrn_reflns_Laue_measured_fraction_full   0.742
_diffrn_reflns_point_group_measured_fraction_max   0.998
_diffrn_reflns_point_group_measured_fraction_full  0.742
_reflns_number_total              16010
_reflns_number_gt                 10446
_reflns_threshold_expression      'I > 2\s(I)'
```

_reflns_Friedel_coverage 0.000

_reflns_Friedel_fraction_max .

_reflns_Friedel_fraction_full .

_reflns_special_details

;

Reflections were merged by SHELXL according to the crystal class for the calculation of statistics and refinement.

Structure factors included contributions from the .fab file.

_reflns_Friedel_fraction is defined as the number of unique

Friedel pairs measured divided by the number that would be possible theoretically, ignoring centric projections and systematic absences.

_computing_data_collection ?

_computing_cell_refinement ?

_computing_data_reduction ?

_computing_structure_solution ?

```
_computing_structure_refinement   'SHELXL-2013 (Sheldrick,
2013)'
_computing_molecular_graphics     ?
_computing_publication_material   ?


_refine_special_details


_refine_ls_structure_factor_coef  Fsqd
_refine_ls_matrix_type            full
_refine_ls_weighting_scheme       calc
_refine_ls_weighting_details
;
 w=1/[\s^2^(Fo^2^)+(0.0907P)^2^+6.8839P]
 where P=(Fo^2^+2Fc^2^)/3
;
_atom_sites_solution_primary      ?
_atom_sites_solution_secondary    ?
_atom_sites_solution_hydrogens    mixed
_refine_ls_hydrogen_treatment     mixed
_refine_ls_extinction_method      none
_refine_ls_extinction_coef        .
_refine_ls_number_reflns          16010
```

_refine_ls_number_parameters	1201
_refine_ls_number_restraints	794
_refine_ls_R_factor_all	0.1112
_refine_ls_R_factor_gt	0.0727
_refine_ls_wR_factor_ref	0.2045
_refine_ls_wR_factor_gt	0.1814
_refine_ls_goodness_of_fit_ref	1.032
_refine_ls_restrained_S_all	1.009
_refine_ls_shift/su_max	0.000
_refine_ls_shift/su_mean	0.000

Hydrogen-bond geometry (Å, º)

D	—H	···*A*	*D*—H	H···*A*	*D*···*A*	*D*—H···*A*
N4A	H4A	O2B	0.88	1.98	2.843(5)	165.2
N6A	H6A	O1C	0.88	1.99	2.868(5)	175.6
N8A	H8A	O7A	0.88	1.95	2.817(4)	167.9
N2B	H2B	O1B	0.88	1.97	2.843(4)	174.2
N4B	H4B	O8A	0.88	1.99	2.864(4)	170.2
N6B	H6B	O2A	0.88	1.92	2.783(6)	166.8
N8B	H8B	O8B	0.88	1.95	2.828(4)	171.4
O1C	H1C	O8B	0.884(15)	2.002(16)	2.874(4)	169(5)

3.2. AdC2Ad crystal from HFP-DCM

Cif for AdC2Ad from HFP-DCM (lists of molecular geometry parameters have been left out).

data_ AdC2Ad from HFP-DCM

_audit_creation_method	'SHELXL-2014/7'
_shelx_SHELXL_version_number	'2014/7'
_chemical_name_systematic	$C_{12}H_{12}N_{10}$
_chemical_name_common	?
_chemical_melting_point	?
_chemical_formula_moiety	?
_chemical_formula_sum	
'C24 H20 F24 N10 O4'	
_chemical_formula_weight	968.50

```
loop_
 _atom_type_symbol
 _atom_type_description
 _atom_type_scat_dispersion_real
 _atom_type_scat_dispersion_imag
 _atom_type_scat_source
'C'  'C'   0.0033   0.0016
'International Tables Vol C Tables 4.2.6.8 and 6.1.1.4'
'H'  'H'   0.0000   0.0000
'International Tables Vol C Tables 4.2.6.8 and 6.1.1.4'
'N'  'N'   0.0061   0.0033
'International Tables Vol C Tables 4.2.6.8 and 6.1.1.4'
'O'  'O'   0.0106   0.0060
'International Tables Vol C Tables 4.2.6.8 and 6.1.1.4'
'F'  'F'   0.0171   0.0103
```

'International Tables Vol C Tables 4.2.6.8 and 6.1.1.4'

_space_group_crystal_system triclinic
_space_group_IT_number 2
_space_group_name_H-M_alt 'P -1'
_space_group_name_Hall '-P 1'
_shelx_space_group_comment
;
The symmetry employed for this shelxl refinement is uniquely defined
by the following loop, which should always be used as a source of
symmetry information in preference to the above space-group names.
They are only intended as comments.

loop_
 _space_group_symop_operation_xyz
 'x, y, z'
 '-x, -y, -z'

_cell_length_a 7.1752(7)
_cell_length_b 10.3078(10)
_cell_length_c 12.3995(12)
_cell_angle_alpha 86.613(2)
_cell_angle_beta 87.488(2)
_cell_angle_gamma 71.906(2)
_cell_volume 869.89(15)
_cell_formula_units_Z 1
_cell_measurement_temperature 100(2)
_cell_measurement_reflns_used ?

_cell_measurement_theta_min	?
_cell_measurement_theta_max	?
_exptl_crystal_description	?
_exptl_crystal_colour	?
_exptl_crystal_density_meas	?
_exptl_crystal_density_method	?
_exptl_crystal_density_diffrn	1.849
_exptl_crystal_F_000	482
_exptl_transmission_factor_min	?
_exptl_transmission_factor_max	?
_exptl_crystal_size_max	?
_exptl_crystal_size_mid	?
_exptl_crystal_size_min	?
_exptl_absorpt_coefficient_mu	0.213
_shelx_estimated_absorpt_T_min	?
_shelx_estimated_absorpt_T_max	?
_exptl_absorpt_correction_type	?
_exptl_absorpt_correction_T_min	?
_exptl_absorpt_correction_T_max	?
_exptl_absorpt_process_details	?
_exptl_absorpt_special_details	?
_diffrn_ambient_temperature	100(2)
_diffrn_radiation_wavelength	0.71073
_diffrn_radiation_type	MoK\a
_diffrn_source	?
_diffrn_measurement_device_type	?
_diffrn_measurement_method	?
_diffrn_detector_area_resol_mean	?
_diffrn_reflns_number	21096
_diffrn_reflns_av_unetI/netI	0.0242

```
_diffrn_reflns_av_R_equivalents   0.0281
_diffrn_reflns_limit_h_min        -9
_diffrn_reflns_limit_h_max        9
_diffrn_reflns_limit_k_min        -14
_diffrn_reflns_limit_k_max        14
_diffrn_reflns_limit_l_min        -17
_diffrn_reflns_limit_l_max        17
_diffrn_reflns_theta_min          2.081
_diffrn_reflns_theta_max          29.652
_diffrn_reflns_theta_full         25.242
_diffrn_measured_fraction_theta_max   0.994
_diffrn_measured_fraction_theta_full  0.997
_diffrn_reflns_Laue_measured_fraction_max    0.994
_diffrn_reflns_Laue_measured_fraction_full   0.997
_diffrn_reflns_point_group_measured_fraction_max   0.994
_diffrn_reflns_point_group_measured_fraction_full  0.997
_reflns_number_total              4878
_reflns_number_gt                 3936
_reflns_threshold_expression      'I > 2\s(I)'
_reflns_Friedel_coverage          0.000
_reflns_Friedel_fraction_max      .
_reflns_Friedel_fraction_full     .

_reflns_special_details
;
 Reflections were merged by SHELXL according to the crystal
 class for the calculation of statistics and refinement.

 _reflns_Friedel_fraction is defined as the number of
unique
 Friedel pairs measured divided by the number that would be
```

possible theoretically, ignoring centric projections and systematic absences.

_computing_data_collection ?
_computing_cell_refinement ?
_computing_data_reduction ?
_computing_structure_solution ?
_computing_structure_refinement 'SHELXL-2014/7 (Sheldrick, 2014)'
_computing_molecular_graphics ?
_computing_publication_material ?
_refine_special_details ?
_refine_ls_structure_factor_coef Fsqd
_refine_ls_matrix_type full
_refine_ls_weighting_scheme calc
_refine_ls_weighting_details
'w=1/[\s^2^(Fo^2^)+(0.0347P)^2^+0.4485P] where P=(Fo^2^+2Fc^2^)/3'
_atom_sites_solution_primary ?
_atom_sites_solution_secondary ?
_atom_sites_solution_hydrogens difmap
_refine_ls_hydrogen_treatment refxyz
_refine_ls_extinction_method none
_refine_ls_extinction_coef .
_refine_ls_number_reflns 4878
_refine_ls_number_parameters 319
_refine_ls_number_restraints 0
_refine_ls_R_factor_all 0.0506
_refine_ls_R_factor_gt 0.0365
_refine_ls_wR_factor_ref 0.0884
_refine_ls_wR_factor_gt 0.0818

_refine_ls_goodness_of_fit_ref	1.025
_refine_ls_restrained_S_all	1.025
_refine_ls_shift/su_max	0.000
_refine_ls_shift/su_mean	0.000

Fractional atomic coordinates and isotropic or equivalent isotropic displacement parameters (Å²)

	x	*y*	*z*	*U*iso*/*U*eq
N1A	0.92967(15)	0.34004(10)	0.53002(8)	0.0151(2)
N2A	0.79782(15)	0.15486(10)	0.57514(8)	0.0151(2)
N3A	0.80337(17)	0.50932(11)	0.39766(9)	0.0179(2)
H31A	0.719(3)	0.5462(18)	0.3501(14)	0.027(4)
H32A	0.888(2)	0.5457(16)	0.4122(13)	0.018(4)
N4A	0.47846(15)	0.37354(10)	0.38085(8)	0.0149(2)
N5A	0.49609(15)	0.18179(10)	0.47996(8)	0.0144(2)
C1A	0.92398(18)	0.22507(13)	0.58379(10)	0.0158(2)
H11A	1.022(2)	0.1885(16)	0.6341(13)	0.019
C2A	0.65722(17)	0.21849(12)	0.50458(9)	0.0133(2)
C3A	0.64437(17)	0.33707(12)	0.44320(9)	0.0138(2)
C4A	0.79239(17)	0.39835(12)	0.45501(9)	0.0142(2)
C5A	0.39489(18)	0.27878(12)	0.40537(10)	0.0155(2)
H51A	0.277(2)	0.2735(15)	0.3773(12)	0.017(4)
C6A	0.44133(18)	0.06534(12)	0.52697(10)	0.0155(2)
H61A	0.304(2)	0.0816(15)	0.5151(12)	0.015(4)
H62A	0.462(2)	0.0566(15)	0.6020(12)	0.015(4)
O1B	0.88411(15)	-0.09848(10)	0.67281(7)	0.0218(2)
H1B	0.856(3)	-0.019(2)	0.6381(16)	0.043(5)
C1B	1.11855(19)	-0.11919(14)	0.80887(11)	0.0216(3)
C2B	0.90224(18)	-0.07704(12)	0.78151(10)	0.0166(2)
H21B	0.851(2)	0.0156(15)	0.7978(12)	0.012(3)
C3B	0.7874(2)	-0.15492(14)	0.84977(11)	0.0216(3)
F1B	1.20967(13)	-0.05116(11)	0.74004(8)	0.0361(2)
F2B	1.14607(12)	-0.08916(10)	0.90840(7)	0.0306(2)
F3B	1.21006(13)	-0.25185(9)	0.79837(7)	0.0328(2)
F4B	0.80150(14)	-0.14299(10)	0.95494(7)	0.0333(2)
F5B	0.59772(12)	-0.10607(10)	0.82561(8)	0.0345(2)
F6B	0.84499(14)	-0.28752(8)	0.83102(7)	0.0333(2)
O1C	0.42937(14)	0.60850(9)	0.26997(7)	0.01872(19)
H1C	0.429(3)	0.533(2)	0.3053(18)	0.053(6)
C1C	0.52762(19)	0.68188(13)	0.10009(11)	0.0209(3)
C2C	0.41571(18)	0.59465(12)	0.15970(10)	0.0165(2)
H2C	0.474(2)	0.5026(16)	0.1374(12)	0.016(4)
C3C	0.20044(19)	0.63477(13)	0.12935(10)	0.0195(3)
F1C	0.46448(13)	0.81166(8)	0.12750(7)	0.0292(2)
F2C	0.71692(12)	0.63329(9)	0.12393(8)	0.0323(2)
F3C	0.51487(13)	0.68097(9)	-0.00677(7)	0.0308(2)
F4C	0.10425(12)	0.76684(8)	0.14274(7)	0.02459(18)
F5C	0.11022(13)	0.56288(9)	0.19347(7)	0.0309(2)

Atomic displacement parameters (Å²)

	U_{11}	U_{22}	U_{33}	U_{12}	U_{13}	U_{23}
N1A	0.0147(5)	0.0171(5)	0.0160(5)	-0.0004(4)	-0.0009(4)	-0.0085(4)
N2A	0.0145(5)	0.0142(5)	0.0171(5)	-0.0002(4)	-0.0006(4)	-0.0054(4)
N3A	0.0212(5)	0.0189(5)	0.0184(5)	0.0041(4)	-0.0049(4)	-0.0137(5)
N4A	0.0156(5)	0.0145(5)	0.0160(5)	-0.0007(4)	-0.0021(4)	-0.0065(4)
N5A	0.0147(5)	0.0116(4)	0.0184(5)	-0.0003(4)	-0.0011(4)	-0.0065(4)
C1A	0.0140(5)	0.0169(6)	0.0165(5)	-0.0001(4)	-0.0003(4)	-0.0050(5)
C2A	0.0141(5)	0.0124(5)	0.0148(5)	-0.0024(4)	0.0015(4)	-0.0058(4)
C3A	0.0148(5)	0.0135(5)	0.0138(5)	-0.0009(4)	-0.0007(4)	-0.0055(4)
C4A	0.0160(5)	0.0151(5)	0.0132(5)	-0.0020(4)	0.0018(4)	-0.0075(4)
C5A	0.0149(5)	0.0147(5)	0.0180(6)	-0.0014(4)	-0.0012(4)	-0.0056(5)
C6A	0.0155(6)	0.0129(5)	0.0203(6)	-0.0010(4)	0.0021(4)	-0.0077(5)
O1B	0.0318(5)	0.0175(4)	0.0181(4)	0.0028(3)	-0.0074(4)	-0.0105(4)
C1B	0.0181(6)	0.0257(7)	0.0195(6)	0.0018(5)	-0.0014(5)	-0.0048(5)
C2B	0.0176(6)	0.0136(5)	0.0186(6)	-0.0005(4)	-0.0027(4)	-0.0047(5)
C3B	0.0230(6)	0.0205(6)	0.0233(6)	0.0007(5)	-0.0027(5)	-0.0096(5)
F1B	0.0224(4)	0.0526(6)	0.0356(5)	0.0143(4)	-0.0017(4)	-0.0175(4)
F2B	0.0260(4)	0.0426(5)	0.0246(4)	-0.0041(4)	-0.0081(3)	-0.0115(4)
F3B	0.0266(4)	0.0301(5)	0.0301(5)	-0.0010(4)	-0.0006(4)	0.0078(4)
F4B	0.0395(5)	0.0471(5)	0.0207(4)	-0.0011(4)	0.0034(4)	-0.0246(4)
F5B	0.0205(4)	0.0382(5)	0.0482(6)	0.0052(4)	-0.0043(4)	-0.0150(4)
F6B	0.0481(6)	0.0176(4)	0.0366(5)	0.0032(3)	0.0005(4)	-0.0148(4)
O1C	0.0247(5)	0.0171(4)	0.0161(4)	0.0020(3)	-0.0043(3)	-0.0090(4)
C1C	0.0207(6)	0.0193(6)	0.0218(6)	0.0001(5)	0.0007(5)	-0.0053(5)
C2C	0.0190(6)	0.0128(5)	0.0175(6)	-0.0003(4)	-0.0027(4)	-0.0044(5)
C3C	0.0223(6)	0.0151(6)	0.0219(6)	0.0006(5)	-0.0054(5)	-0.0065(5)
F1C	0.0326(5)	0.0176(4)	0.0399(5)	-0.0025(3)	0.0090(4)	-0.0127(3)
F2C	0.0177(4)	0.0375(5)	0.0405(5)	0.0048(4)	-0.0008(3)	-0.0078(4)
F3C	0.0370(5)	0.0354(5)	0.0193(4)	0.0035(3)	0.0032(3)	-0.0117(4)
F4C	0.0212(4)	0.0168(4)	0.0336(4)	-0.0009(3)	-0.0055(3)	-0.0022(3)
F5C	0.0273(4)	0.0291(4)	0.0417(5)	0.0086(4)	-0.0066(4)	-0.0177(4)
F6C	0.0341(5)	0.0323(5)	0.0265(4)	-0.0060(3)	-0.0137(4)	-0.0067(4)

Hydrogen-bond geometry (Å, º)

D	—	H	···	*A*	*D*— H	H···*A*	*D*···*A*	*D*— H···*A*
N3A	—	H31A	···	O1C	0.850(18)	2.233(18)	3.0382(15)	158.1(16)
N3A	—	H32A	···	N1A	0.840(17)	2.177(17)	3.0078(15)	170.0(15)
O1B	—	H1B	···	N2A	0.87(2)	1.84(2)	2.7124(14)	175.5(19)
O1C	—	H1C	···	N4A	0.87(2)	1.79(2)	2.6456(14)	169(2)

3.3. Th4 crystal from HFP- IPA

Cif for Th4 from HFP-IPA (lists of coordinates and molecular geometry parameters have been left out).

```
data_Th4 from HFP-IPA

_audit_creation_method                  SHELXL-2013
_chemical_name_systematic               C49H44N8O8
_chemical_name_common                   ?
_chemical_melting_point                 ?
_chemical_formula_moiety                ?
_chemical_formula_sum
 'C49 H44 N8 O8'
_chemical_formula_weight                872.92

loop_
 _atom_type_symbol
 _atom_type_description
 _atom_type_scat_dispersion_real
 _atom_type_scat_dispersion_imag
 _atom_type_scat_source
 'C'  'C'   0.0033   0.0016
 'International Tables Vol C Tables 4.2.6.8 and 6.1.1.4'
 'H'  'H'   0.0000   0.0000
 'International Tables Vol C Tables 4.2.6.8 and 6.1.1.4'
 'N'  'N'   0.0061   0.0033
 'International Tables Vol C Tables 4.2.6.8 and 6.1.1.4'
 'O'  'O'   0.0106   0.0060
 'International Tables Vol C Tables 4.2.6.8 and 6.1.1.4'

_space_group_crystal_system             monoclinic
_space_group_IT_number                  14
```

```
_space_group_name_H-M_alt          'P 21/c'
_space_group_name_Hall             '-P 2ybc'

_shelx_space_group_comment
;
The symmetry employed for this shelxl refinement is
uniquely defined
by the following loop, which should always be used as a
source of
symmetry information in preference to the above space-group
names.
They are only intended as comments.

loop_
 _space_group_symop_operation_xyz
 'x, y, z'
 '-x, y+1/2, -z+1/2'
 '-x, -y, -z'
 'x, -y-1/2, z-1/2'

_cell_length_a                     14.9614(17)
_cell_length_b                     15.2536(16)
_cell_length_c                     30.990(4)
_cell_angle_alpha                  90
_cell_angle_beta                   96.288(3)
_cell_angle_gamma                  90
_cell_volume                       7029.9(14)
_cell_formula_units_Z              4
_cell_measurement_temperature      100(2)
_cell_measurement_reflns_used      ?
_cell_measurement_theta_min        ?
```

_cell_measurement_theta_max	?
_exptl_crystal_description	?
_exptl_crystal_colour	?
_exptl_crystal_density_meas	?
_exptl_crystal_density_method	?
_exptl_crystal_density_diffrn	0.825
_exptl_crystal_F_000	1832
_exptl_transmission_factor_min	?
_exptl_transmission_factor_max	?
_exptl_crystal_size_max	?
_exptl_crystal_size_mid	?
_exptl_crystal_size_min	?
_exptl_absorpt_coefficient_mu	0.057
_shelx_estimated_absorpt_T_min	?
_shelx_estimated_absorpt_T_max	?
_exptl_absorpt_correction_type	?
_exptl_absorpt_correction_T_min	?
_exptl_absorpt_correction_T_max	?
_exptl_absorpt_process_details	?
_exptl_special_details	
_diffrn_ambient_temperature	100(2)
_diffrn_radiation_wavelength	0.71073
_diffrn_radiation_type	MoK\a
_diffrn_source	?
_diffrn_measurement_device_type	?
_diffrn_measurement_method	?
_diffrn_detector_area_resol_mean	?
_diffrn_reflns_number	54204

```
_diffrn_reflns_av_unetI/netI      0.0689
_diffrn_reflns_av_R_equivalents   0.0697
_diffrn_reflns_limit_h_min        -16
_diffrn_reflns_limit_h_max        15
_diffrn_reflns_limit_k_min        -16
_diffrn_reflns_limit_k_max        16
_diffrn_reflns_limit_l_min        -34
_diffrn_reflns_limit_l_max        34
_diffrn_reflns_theta_min          2.072
_diffrn_reflns_theta_max          23.278
_diffrn_reflns_theta_full         25.242
_diffrn_measured_fraction_theta_max   0.991
_diffrn_measured_fraction_theta_full  0.790
_diffrn_reflns_Laue_measured_fraction_max    0.991
_diffrn_reflns_Laue_measured_fraction_full   0.790
_diffrn_reflns_point_group_measured_fraction_max   0.991
_diffrn_reflns_point_group_measured_fraction_full  0.790
_reflns_number_total              10044
_reflns_number_gt                 6141
_reflns_threshold_expression      'I > 2\s(I)'
_reflns_Friedel_coverage          0.000
_reflns_Friedel_fraction_max      .
_reflns_Friedel_fraction_full     .
_reflns_special_details
;
 Reflections were merged by SHELXL according to the crystal
 class for the calculation of statistics and refinement.

 Structure factors included contributions from the .fab
file.
```

_reflns_Friedel_fraction is defined as the number of unique
Friedel pairs measured divided by the number that would be possible theoretically, ignoring centric projections and systematic absences.

```
_computing_data_collection        ?
_computing_cell_refinement        ?
_computing_data_reduction         ?
_computing_structure_solution     ?
_computing_structure_refinement   'SHELXL-2013 (Sheldrick, 2013)'
_computing_molecular_graphics     ?
_computing_publication_material   ?

_refine_special_details

_refine_ls_structure_factor_coef  Fsqd
_refine_ls_matrix_type            full
_refine_ls_weighting_scheme       calc
_refine_ls_weighting_details
;
 w=1/[\s^2^(Fo^2^)+(0.0868P)^2^+7.8921P]
 where P=(Fo^2^+2Fc^2^)/3
;
_atom_sites_solution_primary      ?
_atom_sites_solution_secondary    ?
_atom_sites_solution_hydrogens    geom
_refine_ls_hydrogen_treatment     constr
_refine_ls_extinction_method      none
_refine_ls_extinction_coef        .
```

_refine_ls_number_reflns	10044
_refine_ls_number_parameters	590
_refine_ls_number_restraints	0
_refine_ls_R_factor_all	0.1274
_refine_ls_R_factor_gt	0.0796
_refine_ls_wR_factor_ref	0.2275
_refine_ls_wR_factor_gt	0.1997
_refine_ls_goodness_of_fit_ref	1.080
_refine_ls_restrained_S_all	1.080
_refine_ls_shift/su_max	0.000
_refine_ls_shift/su_mean	0.000

Hydrogen-bond geometry (Å, º)

D	—	H	···	*A*	*D*—H	H···*A*	*D*···*A*	*D*—H···*A*
N2	—	H2	···	O8	0.88	1.99	2.853(5)	168.3
N4	—	H4	···	O1	0.88	2.11	2.973(5)	165.1
N6	—	H6	···	O6	0.88	1.95	2.795(5)	161.8
N8	—	H8	···	O2	0.88	1.96	2.818(5)	165.8

References

[1] Lehn, J. M. *Science*. **1993**, 260, 1762–1763.

[2] Lehn, J. M. *Angew. Chem. Int. Ed. Engl.* **1990**, 29, 1304-1319.

[3] Schneider, H. J. *Angew. Chem. Int. Ed. Engl.* **1991**, 30, 1417-1436.

[4] Sugiyasu, K.; Shinkai, S. *Supramolecular Polymer Chemistry.* Wiley-VCH Verlag GmbH & Co. KGaA. **2012**.

[5] Van Esch J. H. *Nature*. **2010**, 466, 193-194.

6 Desiraju, G. R. *J. Am. Chem. Soc.* **2013**, 135, 9952−9967

7 Shishkin, O. V.; Zubatyuk, R. I.; Shishkina, S. V.; Dyakonenko, V. V.; Medviediev, V. V. *Phys.Chem.* **2014**, 16, 6773-6786.

[8] Desiraju, G. R. *Angew. Chern., Int. Ed. Engl.* **1995**, 34, 2311-2327.

[9] Thalladi, V. R.; Goud, B. S.; Hoy, V. J.; Allen, F. H.; Howard, J. A. K.; Desiraju, G. R. *Chem. Commun.* **1996**, 3, 401-402.

[10] Desiraju, G. R. *J. Mol. Struct.* **2003**, 656, 5–15.

[11] Lee, J. Y.; Farha, O. K.; Roberts, J.; Scheidt, K. A.; Nguyena, S. T.; Hupp, J. T. *Chem. Soc. Rev.* **2009**, 38, 1450-1459.

[12] Bailey, W. R. D.; Bradner, M. W.; Fleischman, S.; Morales, L. A.; Moulton, B.; Rodríguez-Hornedob, N.; Zaworotko, M. J. *Chem. Commun.* **2003**, 186-187.

[13] Kurth, D. G. *Sci. Technol. Adv. Mater.* **2008**, 9, 014103.

[14] Bureekaew, S.; Shimomura, S.; Kitagawa, S. *Sci. Technol. Adv. Mater.* **2008**, 9, 014108.

[15] HolLingsworth, M. D. *Science*. **2002**, 295, 5564.

[16] Kitagawa, S.; Kitaura, R.; Noro, S. *Angew. Chem. Int. Ed.* **2004**, 43, 2334-2375.

[17] Rosi, N. L.; Eddaoudi, M.; Kim, J.; O'Keeffe, M.; Yaghi, O. M. *Cryst. Eng. Com.* **2002**, 4, 401-404.

[18] Han, S. S.; Choib, S. H.; van Duin, A. C. T. *Chem. Commun.* **2010**, 46, 5713-5715.

[19] Rosi, N. L.; Eddaoudi, M.; Kim, J.; O'Keeffe, M.; Yaghi, O. M. *Cryst. Eng. Com.* **2002**, 4, 401-404.

[20] Rosi, N. L.; Eckert, J.; Eddaoudi, M.; Vodak, D. T.; Kim, J.; O'Keeffe, M.; Yaghi, O. M. *Science,* **2003**, 300, 1127.

[21] O. M. Yaghi; M. O'Keeff;, N. W. Ockwig; H. K. Chae; M. Eddaoudi; J. Kim. *Nature*. **2003**, 423, 705-714.

[22] Feng, X.; Ding, X. S.; Jiang, D. L. *Chem. Soc. Rev.* **2012**, 41, 6010.

[23] Thomas, A. *Angew. Chem., Int. Ed.* **2010**, 49, 8328.

[24] Cooper, A. I. *Adv. Mater.* **2009**, 21, 1291.

[25] Wu, D. C.; Xu, F.; Sun, B.; Fu, R. W.; He, H. K.; Matyjaszewski, K. *Chem. Rev.* **2012**, 112, 3959.

[26] Yang, W.; Greenaway, A.; Lin, X.; Matsuda, R.; Blake, A. J.; Wilson, C.; Lewis, W.; Hubberstey, P.; Kitagawa, S.; Champness, N. R.; Schröder, M. *J. Am. Chem. Soc*. **2010**, 132, 14457-14469.

[27]Jiang, J. X.; Su, F.; Niu, H.; Wood, C. D.; Campbell, N. L.; Khimyak, Y. Z.; Cooper, A. I. *Chem. Commun.* **2008**, 4, 486−488.

[28] El-Kaderi, H. M.; Hunt, J. R.; Mendoza-Cortés, J. L.; Côté, A. P.; Taylor, R. E.; O'Keeffe, M.; Yaghi, O. M. *Science*, **2007**, 316, 268.

[29] Kuhn,P.; Antonietti, M.; Thomas, A. *Angew. Chem., Int. Ed*. **2008**, 47, 3450.

[30] Uribe-Romo, F. J.; Hunt, J. R.; Furukawa, H.; Klöck, C.; O'Keeffe, M.; Yaghi, O. M. *J. Am. Chem. Soc*. **2009**, 131, 4570.

[31] Côté, A. P.; Benin, A. I.; Ockwig, N. W.; O'Keeffe, M.; Matzger, A. J.; Yaghi, O. M. *Science.* **2005**, 310, 1166-1170.

[32] Maly, K. E. *J. Mater. Chem,* **2009**, 19, 1781–1787.

[33] Long, J. R.; Yaghi, O. M. *Chem. Soc. Rev.* **2009**, 38, 1201.

[34] Vaidhyanathan, R.; Iremonger, S. S.; Shimizu, G. K. H.; Boyd, P. G.; Alavi, S.; Woo, T. K. *Science*. **2010**, 330, 650.

[35] Sumida, K.; Rogow, D. L.; Mason, J. A.; McDonald, T. M.; Bloch, E. D.; Herm, Z. R.; Bae, T.-H.; Long, J. R. *Chem. Rev.* **2012**, 112, 724.

[36] Zhang, Z.; Zaworotko, M. J. *Chem. Soc. Rev.* **2014**, 43, 5444.

[37] Xiang, Z. H.; Cao, D. P.; Lan, J. H.; Wang, W. C.; Broom, D. P. *Energy Environ. Sci.* **2010**, 3, 1469–1487.

[38] Endo, K.; Sawaki, T.; Koyanagi, M.; Kobayashi, K.; Masuda, H.; Aoyama, Y. *J. Am. Chem. Soc.* **1995**, 117, 8341.

[39] Malek, N.; Maris, T.; Perron, M.; Wuest, J. D. *Angew. Chem., Int. Ed.* **2005**, 44, 4021.

[40] Kobayashi, K.; Sato, A.; Sakamoto, S.; Yamaguchi, K. *J. Am. Chem. Soc.* **2003**, 125, 3035.

[41] Yang, W.; Li, B.; Wang, H.; Alduhaish, O.; Alfooty, K.; Zayed, M. A.; Li, P.; Arman, H. D.; Chen, B. *Cryst. Growth Des.* **2015**, 15, 2000–2004.

[42] Mukherjee, S.; Joarder, B.; Manna, B.; Desai, A.V.; Chaudhari, A. K.; Ghosh, S. K. *Scientific Reports*, **2014**, 4.

[43] Murray, L. J.; Dinca, M.; Long, J. R. *Chem. Soc. Rev.* **2009**, 38, 1294 – 1314 .

[44] Henke, S.; Schneemann, A.; Fischer, R. A. *Adv. Funct. Mater.* **2013**, 23, 5990–5996.

[45] S. Y. Ding; J. Gao; Q. Wang; Y. Zhang; W. G. Song; C. Y. Su; W. Wang. *J. Am. Chem. Soc.* **2011**, 133, 19816–19822.

[46]Thomas, A.; Kuhn, P.; Weber, J.; Titirici, M. M.; Antonietti, M. *Macromol. Rapid Commun.* **2009**, 30, 221−236.

[47] Davis, M. E. *Nature*. **2002**, 417, 813−821.

[48] McKeown, N. B.; Budd, P. M. *Macromolecules*. **2010**, 43, 5163−5176.

[49] An, J.; Farha, O. K.; Hupp, J.T.; Pohl, E.; Yeh, J. I.; Rosi, N. L. *Nat Commun*. **2012**, 3, 604

[50] Roques, N.; Mouchaham, G.; Duhayon, C.; Brandes, S.; Tachon, A.; Weber, G.; Bellat, J. P.; Sutter, J. P. *Chem. Eur. J*. **2014**, 20, 11690 – 11694

[51] Natarajan, R.; Bridgland, L.; Sirilculkajorn, A.; Lee, J. H.; Haddow, M. F.; Magro, G.; Ali, B.; Narayanan, S.; Strickland, P.; Charmant, J. P. H.; Orpen, A. G.; Mckeown, N. B.; Bezzu, C. G.; Davis, A. P. *J. Am. Chem. Soc.* **2013**, 135, 16912−16925.

[52] Zou, X. Q.; Ren, H.; Zhu, G. S. *Chem. Commun.* **2013**, 49, 3925−3936.

[53] Kumari, G.; Jayaramulu, K.; Maji, T. K.; Narayana, C. *J. Phys. Chem. A.* **2013**, 117, 11006−11012.

[54]Côté, A. P.; El-Kaderi, H. M.; Furukawa, H.; Hunt, J. R.; Yaghi, O. M. *J. Am. Chem. Soc.* **2007**, 129, 12914−12915.

[55]Chen, L.; Honsho, Y.; Seki, S.; Jiang, D. L. *J. Am. Chem. Soc.* **2010**, 132, 6742−6748.

[56]Kanoya, I.; Furuta, T.; Sakamoto, R.; Hosoe, M.; Ichikawa, M.; Itoh, K.; Fukunaga, T. *J. Appl. Phys.* **2010**, 108, 074310.

[57]Weber, J.; Thomas, A. J. *Am. Chem. Soc.* **2008**, 130, 6334−6335.

[58] R. L. Martin; M. Haranczyk. *Cryst. Growth Des.* **2013**, 13, 4208−4212.

[59] Zhu, G.; Ren, H. *Porous Organic Frameworks: Design, Synthesis and Their Advanced Applications.* Springer Heidelberg: New York, **2015**.

[60] Cooper, A. I. *Angew. Chem., Int. Ed*. **2012**, 51, 7892.

[61] Luo, X. Z.; Jia, X. J.; Deng, J. H.; Zhong, J. L.; Liu, H. J.; Wang, K. J.; Zhong, D. C. *J. Am. Chem. Soc.* **2013**, 135, 11684.

[62] Lewis, W.; Bichoutskaia, E.; Tang, C. C.; Blake, A. J.; Cao, R.; Schröder, M. *J. Am. Chem. Soc*. **2014**, 136, 12828.

[63] He, Y.; Xiang, S.; Chen, B. *J. Am. Chem. Soc*. **2011**, 133, 14570.

[64] Li, P.; He, Y.; Arman, H. D.; Krishna, R.; Wang, H.; Weng, L.; Chen, B. *Chem. Commun*. **2014**, 50, 13081.

[65] L. Stryer. *Biochemistry, 4 Ed*. W. H. Freeman and Company: New York, **1995**.

[66] Alberts, B.; Johnson, A.; Lewis, J.; Raff, M.; Roberts, K.; Walters, P. *Molecular Biology of the Cell, Fourth Edition.* Garland Science: New York and London. **2002**.

[67] C. F. Guerra; F. M. Bickelhaupt; J. G. Snijders; E. J. Baerends. *J. Am. Chem. Soc.* **2000**, 122, 4117–4128.

[68] A. J. Parker; J. Stewart; K. J. Donald; C. A. Parish. *Am. Chem. Soc.* **2012**, 134, 5165−5172.

[69] Schindler, D.; Eißmann, F.; Weber, E. *Org. Biomol. Chem.* **2009**, 7, 3549–3560.

[70] A. K. Jissy; A. Datta. *Phys. Chem. B*. **2010**, 114 (46), 15311–15318.

[72] Jiang, Q.; Zhu, J. H.; Zhang, Y. M.; Xiao, N.; Guo, Z. J. *Biometals.* **2009**, 22, 297–305.

[73] Sessler, J. L.; Lawrence, C. M.; Jayawickramarajah, J. *Chem. Soc. Rev.* **2007**, 36, 314.

[74] Ciesielski, A.; Perone, R.; Pieraccini, S.; Spada, G. P.; Samorì, P. *Chem. Commun.* **2010**,46, 4493-4495.

[75] Kochergin, P. M.; Persanova, L. V.; Aleksandrova, E. V. *Chem. Heterocycl. Compd.* **1998**, 34 (4), 480-483.

[75] D. A. McMorran; S. Pfadenhauer; P. J. Steel. *Inorg. Chem. Commun.* **2002**, 5, 449–451.

[76] H. Liu; D. Gu; G. Liu; X. Zhao; C. Chen. *Procedia Engineering*. **2011**, 18, 324 – 328.

[77] D. T. Brown; J. Eisinger; N. J. Leonard. *Am. Chem. Soc.***1968**, 90, 7302-7323.

[78] A. Raza; C. D. Dreis; R. Vince. *Bioorg. Med. Chem. Lett.* **2013**, 23, 620–623.

[79] T. Itahara. *J. Chem. Soc. Perkin Trans.* **1996**, 2, 2695-2700.

[80] N. J. Leonard; R. S. McCredie; M. W. Logue; R. L. Cundall. *Am. Chem. Soc.***1973**, 95, 2320-2324.

[81] Browne, D. T.; Eisinger, J.; Leonard, N. J. *J. Am. Chem. Soc*. **1968**, 90, 7302-7323.

[82] Itahara, T. *J. Chem. Soc., Perkin Trans. 2*. **1996**, 2695-2700.

[83] Abbas, R.; Christine D. D.; Robert, V. *Bioorganic & Medicinal Chem Lett*. **2013**, 23, 620-623.

[84] Sivakova, S.; Rowan, S. J. *Chem. Soc. Rev.* **2005**, 34, 9.

[85] Stanley, N.; Muthiah, P. T.; Luger, P.; Weber, M.; Geib, S. J. *Inorg. Chem. Commun.* **2005**, 8, 1056-1059.

[86] Joule, J. A.; Mills, K. *Heterocyclic chemistry.* Blackwell Science: Malden, MA, **2000**.

[87] Marek, R.; Brus, J.; Toušek, J.; Kovács, L.; Hocková, D. *Magn. Reson. Chem.* **2002**, 40, 353–360.

[88] L. -L. Gundersen; A. K. Bakkestuen; A. J. Aasen; H. Øverås; F. Lise. *Tetrahedron.* **1994**, 50, 9743-9756.

[89] Zhang, L.; Fan, J.; Vu, K.; Hong, K.; Le Brazidec, J. Y.; Shi, J.; Biamonte, M.; Busch, D. J.; Lough, R. E.; Grecko, R.; Ran, Y.; Sensintaffar, J. L.; Kamal, A.; Lundgren, K.; Burrows, F. J.; Mansfield, R.; Timony, G. A.; Ulm, E. H.; Kasibhatla, S. R.; Boehm, M. F. *J. Med. Chem.* **2006**, 49, 5352-5362.

[90] Lambertucci, C. A., I.; Buccioni, M.; Ben, D.D.; Kachare, D.D.; Volpini, R.; Klotz, K.-N.; Cristalli, G. *Bioorg. Med. Chem. Lett.* **2009**, 17, 2812-2822.

[91] R. Marek; J. Brus; J. Tousek; L. Kovacs; D. Hockova. *Magn. Reson. Chem*. **2002**, 40, 353–360.

[92] H. -S. M. Siah; C. H. Görbitz; L. -L. Gundersen. *J. Heterocyclic Chem.***2011**, 48, 1375-1378.

[93] Thibon, J.; Latxague, L.; Deleris, G. *J. Org. Chem.* **1997**, 62, 4635-4642.

[94] I. Ishikawa; T. Itoh; H. Takayanagi; J. Oshima; N. Kawahara; Y. Mizuno; H. Ogura. *Chem. Pharm. Bull.* **1991**, 39, 1922.

[95] G. E. Hilbert. *J. Am. Chem. Soc.* **1937**, 61,330.

[96] Z. Paryzek; B. Tabaczka. *Org. Prep. Proced. Int.* **2001**, 33(4), 400-405.

[97] Benneche, T.; Gundersen, L.-L;. Undheim, K. *Acta Chemica Scandinavica.* **1988**, B42, 384-389.

[98] H. B. Schurink; W. H. Carothers; W. L. McEwen. *Organic Syntheses, Coll.* **1943**, 2, 476.

[99] C. E. Müller; R. Hrdina; R. C. Wende; P. R. Schreiner. *Chem. Eur.* **2011**, 17, 6309-6314.

[100] T. Kitagawa; Y. Idomoto; H. Matsubara; D. Hobara; T. Kakiuchi; T. Okazaki; K. Komatsu. *Org. Chem.* **2006**, 71, 1362-1369.

[101] Q. Li; A. V. Rukavishnikov; P. A. Petukhov; T. O. Zaikova; C. Jin; J. F. W. Keana. *Org. Chem.* **2003**, 68, 4862-4869.

[102] T. Sasaki; A. Nakanishi; M. Ohno. *Chem. Pharm. Bull.* **1982**, 30, 2051-2060.

[103] T. Sasaki; A. Nakanishi; M. Ohno. *Org. Chem.* **1981**, 46, 5445-5447.

[104] C. Fleck; E. Franzmann; D. Claes; A. Rickert; W. Maison. *Synthesis*. **2013**, 45, 1452–1461.

[105] D. E. Applequist; J. D. Roberts. *Chem. Rev.* **1954**, 54, 1065-1089.

[106] Clegg, W. *Comments Inorg. Chem.* **2005**, 26, 165–182.

[107] Deschamps, J.R. *Life Sciences.* **2010**, 86, 585–589.

[108] Ooi, L. L. *Principles of X-ray crystallography*; Oxford University Press Inc: New York, **2010**.

[109] Clegg, W. *Crystal Structure Analysis Principles and Practice*; Oxford University Press Inc: New York, **2009**.

[110] Atkinson, M. B. J.; Mariappan, S. V. S.; Bucar, D. K.; Baltrusaitis, J.; Friscic, T.; Sinada, N. G.; MacGillivray, L. R. *PNAS*. **2011**, 108, 10974–10979.

[111] Luft, J. R.; Collins, R. J.; Fehrman, N. A.; Lauricella, A. M.; Veatch, C. K.; Detitta, G. T. *J Struct Biol*. **2003**, 142, 170-179.

[112] Liu, H.; Gu, D.; Liu, G.; Zhao, X.; Chen. C. *Procedia Engineering.* **2011**, 18, 324-328.

[113] Schurink, H.B. *Organic Syntheses, Coll.* **1943**, 2, 476.

[114] Dostrovsky, I.; Hughes, E. D. *J. Chem. Soc,* **1946**, 157-161.

[115] Lee, G. S.; Bashara, J. N.; Sabih, G.; Oganesyan, A.; Godjoian, G.; Duong, H. M.; Marinez, E. R.; Gutierrez, C. G. *Org. Lett.* **2004**, 6, 1705-1707.

[116] Singh, R.; Meena, J. S.; Chang, Y. C.; Wua, C. S.; Ko, F. H. *RSC Adv.* **2014**, 4, 29383–29392.

[117] Applequist, D. E.; Roberts, J. D. *Chem. Rev.* **1954**, 54, 1065-1089.

[118] Tian, J.; Ding, Y. D.; Zhou, T. Y.; Zhang, K. D.; Zhao, X.; Wang, H.; Zhang, D. W.; Liu, Y.; Li, Z. T. Chem. Eur. J. 2014, 20, 575-584.

[119] Jacobsen, Mikkel F.; Knudsen, M. M.; Gothelf, K. V. *J. Org. Chem*. **2006**, 71, 9183-9190

[120] Ding, S.; Gray, N. S.; Ding, Q.; Schultz, P. G. *Tetrahedron Lett*. **2011**, 42, 8751–8755.

[121] Bakkestuen, A. K.; Gundersen, L. L. *Tetrahedron Lett*. **2003**, 44, 3359–3362

[122] Krouzˇelka, J.; Linhart, I. *Heterocyles.* **2009**, 78, 1205–1216.

[123] Schilling, C. I.; Plietzsch, O.; Nieger, M.; Muller, T.; Bräse, S. *Eur. J. Org. Chem*. **2011**, 1743–1754.

[124] Kode, N; Chen, L. Y.; Murthy, D; Adewumi, D; Phadtare, S. *European Journal of Medicinal Chemistry*. **2007**, 42, 327-333.

[125] Leonard N. J.; McCredie R. S.; Logue M. W.; Cundall R. L. *J. Am. Chem. Soc*. **1973**, *95*, 2320-2324.

[126] Tian, J.; Ding,Y.D.; Zhou, T. Y.; Zhang, K. D. ; Zhao, X.; Wang, H. ; Zhang, D. W. ; Liu, Y.; Li, Z. T. *Chem. Eur. J.* **2014**, 20, 575 – 584.